UNIVERSITY OF CALGARY

Simulation and Modeling of Underground Coal Gasification Using Porous Medium Approach

by

Mojtaba Seifi

A THESIS

SUBMITTED TO THE FACULTY OF GRADUATE STUDIES

IN PARTIAL FULFILMENT OF THE REQUIREMENTS FOR THE

DEGREE OF DOCTOR OF PHILOSOPHY

GRADUATE PROGRAM IN CHEMICAL AND PETROLEUM ENGINEERING

CALGARY, ALBERTA

SEPTEMBER, 2014

Abstract

Increasing global demand for energy and declining fossil fuel resources continue to make coal deposits a primary source of energy. However, the process of converting coal into valuable syngas through surface gasification requires conventional mining, extraction, transportation, storage, surface processing, ash and environmental handling. Moreover, most coal deposits are located at great depth and have thin coal seams, making them either un-mineable or uneconomical using current technologies. Underground coal gasification (UCG) is an exciting alternative technique for producing syngas from coal conversion in-situ. This will eliminate the need for conventional mining and some surface facilities, increase safety, and lower capital expenditures. It is imperative that we develop accurate UCG models and simulations capable of incorporating the impacts of multi-disciplinary phenomena, in particular in the UCG process where there is no direct access to the developed underground reactors.

Small-scale models can be used to investigate the mechanisms and details of the various phenomena taking place during UCG. Most of the models in the literature apply the CFD (computational fluid dynamics) approach to predict the experimental results or explore the effects of the operational parameters on the process at lower pressures. However, the CFD models include more details, such as multi-component diffusion of the gas components and turbulent flow. Applying these models to field scale simulations can be very expensive.

The similarities between UCG and heavy oil in-situ combustion make it possible to use a thermal compositional hydrocarbon simulator to simulate the UCG process. Complex geology, various well configurations, and multi-phase flow can be efficiently simulated using models developed in the oil and gas industry. This study focuses on the adaptation of a commercial hydrocarbon simulator to model UCG processes at great depth by using applied techniques to convert the coal per gasification module. It presents assumptions and procedures to evaluate the required properties and kinetics of chemical reactions. Small-scale models are used to validate the proposed methods both quantitatively and qualitatively. In addition, large-scale numerical simulation models are used to compare the performance of different technologies. The Thulin test is modeled using a cross-sectional domain. We also explore issues and possible solutions associated with UCG modeling in tight coal seams.

Acknowledgments

Throughout the course of this work, I have worked with many people. I would like to take this opportunity to express my deepest appreciation to them. It is my pleasure to thank them for their supports and help during my PhD program at the University of Calgary.

First of all I would like to express my gratitude, regards, and sincere thanks to my Supervisor Dr. Jalal Abedi and Co-supervisor Dr. Zhangxing (John) Chen for their unconditional and outstanding support, continuous guidance during the course of my study, and providing me this opportunity to enthuse and enrich my growth as a student and researcher.

I would like to be grateful Dr. Ayodeji A. Jeje and Dr. Hassan Hassanzadeh for serving on my supervisory committee. I would also like to thank Dr. Farshid Torabi and Dr. Wenyuan Liao as members of my examining committee.

I wish to thank Mr. Lloyd Buchanan, Dr. Mohammad Reza Heydari, and Dr. David Tran from Computer Modeling Group Ltd. and also Dr. Mohammad Reza Abbaslou and Dr. Iftikhar Huq from Sherritt Technology for their valuable comments, which were really helpful throughout my study.

Financial support of NSERC/AERI (AIEES)/Foundation CMG and iCORE (AITF) Chairs Funds and the Department of Chemical and Petroleum Engineering at the University of Calgary is acknowledged.

Lastly, and most significantly, I wish to express gratitude to my parents (Maryam Ranjbar and Ashabali Seifi) and my wife (Masoumeh Mollaei) for the love, support, and encouragement they have given me throughout my PhD study.

Dedicated to my Dear

Parents & Beloved Wife

For their Love & Support

Table of Contents

List of Tables

List of Figures and Illustrations

Chapter 1 Introduction

1.1 Background

Coal is the world's most abundant and widely distributed fossil fuel and currently provides 25% of the world's total energy demand. It is used directly as a fuel in furnaces or gasified to a mixture of flammable gases composed primarily of hydrogen (H_2), carbon monoxide (CO), methane (CH_4), carbon dioxide (CO_2), and small amounts of steam (H_2O), nitrogen gas (N_2), and hydrogen sulfide (H_2S). The produced hot gas can be used as a fuel for power generation or as a chemical feedstock for various chemical products (e.g., ammonia) (Khadse et al. 2006). Depletion of hydrocarbon reserves and increasing demand for energy necessitate that coal continues to play an important role in global energy supply. In this context, gasification is a promising option for the future of coal.

Most current coal gasification technologies including entrained flow, fluidized bed, and moving bed, use a surface reactor for gasification. The main differences among these technologies relate to gas flow configuration, coal particle size, ash handling, and process conditions. An alternative method to conventional surface gasification is underground coal gasification (UCG), which eliminates the construction of special plants, piping on the surface, and transporting and stocking of raw coal and ash materials, thus significantly decreasing the capital investment. UCG also improves safety for miners and is appropriate for use in deep and thin coal deposits, which may not be considered in proven coal reserves. In addition, cavities formed as a result of UCG may have the potential to be used for CO_2 sequestration. UCG can operate at higher pressures than surface gasification. A comprehensive environmental assessment and risk analysis is required prior to beginning a UCG process, because of the possibility of land subsidence and groundwater pollution, which can be disadvantages of UCG (Perkins 2005).

In the UCG process, gasification is initiated by drilling production and injection wells into a coal seam and establishing a highly permeable pathway between them to ensure economical gas flows. Ignition takes place when the injected oxidant is forced to chemically react with the coal. A cavity is developed as a result of heterogeneous reactions that consume the char. As the cavity matures, other mechanisms, such as the thermo-mechanical failure of dry coal, sidewall scratch,

and roof collapse, play an important role in cavity growth and drive the formation of a pile of rubble at the bottom of the cavity. This pile covers the injection point and fills one to two thirds of the cavity volume. The density of the gas within the void space at the top of the rubble pile changes as a result of the temperature and concentration gradients, which implies the double-diffusive natural convective flow in this region. Combustion of a thin layer of char on the periphery of the cavity generates the heat required for further moisture evaporation, pyrolysis, and self-gasification of the char within the coal seam near the cavity wall (Perkins 2005).

The threat of a global climate change and increased energy demand have led to a growing interest in UCG in several countries such as the USA, China, Russia, Australia, UK and Canada (Shafirovich and Varma 2009). The World Energy Council's 2008 estimates place Canada tenth in the world in proven coal reserves, sharing about less than 1% of the total reserves. The Alberta Energy Resources Conservation Board (ERCB) estimates the established mineable reserves of all types of coal in Alberta at 33.4 *Gt* and total coal resources at about 2,000 *Gt*, which is almost 70% of Canada's coal reserves. The use of a UCG process in a previously unmineable coal seam at great depth increases the coal reserve and reduces the potential for groundwater contamination and surface subsidence (Richardson 2011). The Government of Alberta is currently funding a UCG pilot project at a depth greater than 1,000 *m* and a pressure of about 12 *MPa*, which is the deepest and highest pressure UCG process attempted so far.

Industry has applied several UCG technologies, based on seam depth, dip, and thickness, which result in different well configurations. As a result, linking techniques, residence time, direction of cavity growth, and accumulation of ash and rubble materials differ. The following list briefly describes some of these technologies.

- *Linked Vertical Well (LVW):* This technique is appropriate for shallow, relatively horizontal coal seams. It applies two fixed vertical wells, one as the injector and the other as the producer.
- *Linear and Parallel Controlled Retracting Injection Point (L-CRIP and P-CRIP):* These technologies are promising techniques for very deep, horizontal coal seams, which utilize a horizontal well as an injector. The L-CRIP method uses a fixed vertical well as the producer, whereas the P-CRIP technique uses a horizontal producer parallel to the injector. Both techniques burn the coal in several stages.

- *Steeply Dipping Coal Seams:* This technique is used for highly dipped coal seams. A vertical well is drilled into the coal seam to produce syngas and a slant injection well is drilled into the lower part of the seam. As ash and rubble cover the injection point, it may become necessary to drill another slant well to achieve economical injection.

Unlike surface gasifiers, lots of uncontrollable physical and chemical phenomena influence the performance of a UCG reactor. These phenomena make the process more complex than conventional surface gasification techniques. Therefore, mathematical formulation and modeling of the UCG process is crucial for evaluating its performance and understanding the details of the process. The following phenomena affect UCG reactor performance.

- Variable reactor size and shape.
- Water influx from surrounding strata, which causes a variable steam rate into the reactor.
- Mass and heat losses into surrounding formations and possible impurities within the coal layers, e.g., shale partings.
- Thermo-mechanical failure of coal and overburden materials.

1.2 UCG Models

UCG is a complicated process, which occurs in the presence of different phenomena, such as combustion, gasification, fluid flow, and rock mechanics. There are only a few measurable parameters, such as the coal and seam properties, a gas production rate, gas composition, temperature at certain locations, and operating conditions. Therefore, modeling and simulation is essential to predicting and controlling UCG processes, particularly for pilot tests at great depth. For example, the SwanHill pilot test in Alberta, Canada relies significantly on modeling predictions because there is no chance of field excavation to obtain more information regarding the size and shape of a cavity, the type of material at the bottom, and the thickness of the pyrolysis and evaporation zones.

Current UCG models are mostly based on a one-dimensional study of combustion and gasification of coal using a complex computational fluid dynamics (CFD) approach. These models were used to interpret and predict the performance of laboratory-scale experiments that were generally performed at lower pressures and oxidizing environments as well as a specific portion of field trials operating at pressures up to 5 *MPa* and shallow depths to 600 *m*. Some current UCG models assume complicated velocity equations, including the turbulent gas flow inside the cavity, and utilize chemical engineering correlations for a particle size and the porosity of the reactor. In addition, the cavity geometry and growth rate were modeled with an initially pre-assumed shape, either a tiny rectangular cube or a cylinder. Moreover, most of these studies focused on one cavity and only a few considered interactions with the overburden. These models did not consider interactions between cavities. Due to the enormous complexity and computational cost of these models as the grid numbers increase, they cannot be efficiently used to simulate large-scale field trials. Using the CRIP technology, the coal is gasified in several stages and a sequence of cavities are developed according to the applied retraction strategies. These cavities are known to influence each other thermally. For this reason, the current models are not appropriate to investigate the performance of different UCG technologies at a large scale.

A comprehensive study of complicated UCG processes requires an integrated model composed of several submodels:

- A coal submodel to investigate evaporation, pyrolysis, self-gasification and combustion of char, the effect of water influx, and heat and mass transport phenomena.
- A cavity submodel to study cavity growth mechanisms, a growth rate, cavity geometry, formation of a rubble pile at the bottom of the cavity, and fluid flow and mass transfer within the cavity.
- Gas cleaning and environmental submodels that focus on the separation of undesired gas species from the product gas, the surface treatment of the syngas for final use, and handling of the produced CO_2, H_2S, etc.

The UCG models in the literature can be divided into two main categories, global models and process models. Global models describe the overall field performance of UCG, while the process models are simple models of specific parts of the process, such as rock and coal spalling and the

effect of water influx. The global models incorporate several approaches, such as packed bed models, coal block models, and channel models.

1.2.1 Packed Bed Models

Packed bed models simulate gasification in a highly permeable porous medium with a stationary coal bed that is consumed over time. This approach is the earliest UCG model and is primarily applicable to laboratory-scale tests. Winslow (1976) and Thorsness and Grens (1978) developed one-dimensional packed bed models using finite difference discretization and an adaptive grid to ensure large resolution in the vicinity of the drying and pyrolysis fronts. They achieved good predictions of gas production, gas composition, and coal consumption from laboratory experiments on crushed coal for a feed gas with a steam to oxygen ratio of 6:1.

This approach is not feasible for field-scale gasifiers because the field scale requires 3D treatments and a much larger size, exponentially increasing the number of grid blocks and computation time. In addition, it is not clear how to incorporate cavity growth mechanisms, such as thermo-mechanical failure, into packed bed models.

1.2.2 Coal Block Models

Coal block models assume that gasification begins from one end of a semi-infinite block of wet or dry coal with a relatively lower permeability than that of the coal in the packed bed model. In addition, there are net counter-current heat and mass fluxes in which heat flows from the surface of the char into the coal. Tsang (1980) proposed a model for mass and heat transfer in a wet right cylindrical coal block to simulate experimental work performed by Forrester (1979) on sub-bituminous coal with a 15 cm diameter in an inert environment at atmospheric pressure. He increased the surface temperature from ambient to 1273 K at a rate of 3.3 K/min. Tsang (1980) investigated the location of the pyrolysis and drying fronts, onset temperatures of different volatile matter evolution, water saturation distribution in a wet zone, and the mass fluxes of different species resulting from the pyrolysis, evaporation, and self-gasification of the char.

Massaquoi and Riggs (1981) developed a one-dimensional numerical model of a wet coal slab, assuming a constant ash thickness found in previous experiments. They assumed that all of the moisture content of the coal evaporated at the drying front, no water flowed into the cavity from

the surrounding formations, the coal and char did not shrink, viscous flow was the dominant mass transfer, and the bulk gas had constant velocity, pressure, temperature and composition. They compared their results to laboratory experiments of Texas lignites conducted at atmospheric pressure and found that mass transfer from the bulk gas stream to the surface of the coal is a limiting step in carbon conversion under oxidizing conditions (Massaquoi 1983).

Hong Lae Chang (1984) developed a comprehensive numerical model to predict the gas composition and cavity growth rate. First, he used dispersion, parallel dispersion, tanks-in-series (TIS), and parallel TIS models to model the flow characteristics in field experiments of Hoe Creek No. III. It was concluded that there are two regions inside a cavity because only two-branch parallel models fit the tracer test data accurately. This was confirmed by observations from field tests, which show that there are two distinct regions inside the cavity, void space and rubble. A self-gasification model was developed to predict the temperature at the coal surface and the gas fluxes resulting from pyrolysis and self-gasification of the coal by pyrolysis products in the absence of external oxidants. Hong Lae Chang applied previous submodels to develop a cavity model to predict the growth rate and composition of the final product gas. In his approach, the cavity was divided into several compartments representing a TIS model. Each compartment was assumed to include two regions, void space and a rubble pile, representing the two branches of the parallel TIS model. The lower branch (the rubble pile) and the upper branch (void space) were modeled using plug flow and continuously stirred tank reactors, respectively. It was assumed that all of the ash particles fall down on the rubble pile. This model was used to simulate the Hoe Creek III field trial completed by the Lawrence Livermore National Laboratory.

Perkins (2005) developed a generalized model to study mass and heat transfer within wet coal. His model is basically the same as Massaquoi's model. The model considers a water influx from the surrounding strata, multi-component diffusion of gas species within the solid phase and gas boundary layer, and a random pore model to account for the change in char reactivity during conversion. He assumed that all reactions take place in a reducing environment. This model was validated by comparison with the pyrolysis of large coal particles, drying and pyrolysis of a cylindrical coal block, and simulations of coal gasification in semi-infinite coal blocks (Perkins et al. 2006).

Most of the above models are designed for use at oxidizing conditions and atmospheric pressures. However, UCG process reactions take place in a reducing environment where the gas pressure is many times higher than atmospheric pressure, especially in deep coal seams.

1.2.3 Channel Models

In channel models, a coal seam is assumed to have a cylindrical geometry with a cylindrical or rectangular channel in the middle of the seam, the diameter of which can be fixed or variable. All heterogeneous reactions take place on the channel wall. Magnani (1975) developed a one-dimensional channel model with a fixed diameter, assuming that neither axial nor radial diffusion exists, and there are constant axial convection, two reactions of char oxidation and Boudouard reactions, constant reaction rates, and only axial heat transfer in the solid phase. This model was used to investigate gas composition and temperature profile trends along the channel.

Pasha and Farouq Ali (1978) improved the shortcomings of the previous model by including radial and axial diffusion, radial and axial heat transfer in the solid phase, variable gas velocity, and a variable channel diameter. Unlike the previous model, which was simple enough to find an analytical solution, this approach must be solved numerically.

Dinsmoor et al. (1978) developed a model in which a gasifier was treated as an expanding cylindrical cavity in the coal seam and was used to explain breakthrough phenomena observed during early field trials. They concluded that UCG is not feasible in a channel configuration. Kuyper (1994) developed a two-dimensional model that used the Navier-Stokes equations to model fluid flow within a cross section of the channel. This model was used to predict the gas compositions of the Pricetown I field trial.

1.2.4 Process Model

As previously described, UCG is a complicated process that includes several mutually influential sub-processes. Therefore, many assumptions are required to simplify the development of a process model. As a result, these models can be used to enhance our understanding of specific phenomena, but cannot predict the overall performance of a UCG test.

Biezen (1996) studied double-diffusive natural convection flows, i.e., flows driven by both temperature and composition difference, in a 3D trapezoidal configuration. It was assumed that the top portion of this domain was insulated with the sidewalls colder than the bottom base. He

used the Navier-Stokes equations to obtain the gas velocities within the chamber as a function of the temperature and concentration of the gas species, in order to study the turbulent nature of the gas flow in a cavity.

1.3 Motivations and Objectives

As described in the previous section, the CFD-based models predict the cavity growth mechanism assuming a single predetermined shape for a cavity in one dimension. However, in large field trials, a sequence of cavities is created. In addition, these models consist of complex sets of momentum, mass, and energy conservation equations, making their application on a large scale prohibitively expensive.

An appropriate alternative to these models is the application of a 3D thermal, compositional porous medium simulator like those employed in heavy oil in-situ combustion processes. The 3D simulation study of a UCG process is essential for design and control, as the process takes place at great depths and only a few operational parameters, such as the syngas rate and composition, can be monitored. The use of a 3D porous medium model allows early cavity growth to be effectively controlled. The coal seam can be gasified in several stages allowing the effect of the previously created cavities to be considered in the evolution of the next cavity. Using this 3D numerical simulator, a UCG pilot test can be modeled with an emphasis on the prediction of the product gas rate, cavity shape, cavity growth rate, gas composition, gas temperature and pressure. Although the porous medium approach considers the same mass and energy conservation equations, it applies Darcy's law as the momentum equation for velocity prediction. Moreover, the porosity and permeability can be determined by accounting for the effect of rock strength and solid concentration changes. The porous medium approach can be used for various well configurations, different coal seam layering and geology, and two-phase flow. This model assumes thermal equilibrium between all fluids and solid phases. STARS (Steam, Thermal, and Advanced Processes Reservoir Simulator) software designed by Computer Modeling Group Ltd. (CMG) is used in this study.

1.4 Components and Outline of this Study

The present thesis is based on the papers published in peer-reviewed journals as well as those that are in the publication process. Each chapter consists of a separate abstract, introduction, materials, methodologies, results, discussions, conclusions, and nomenclatures, allowing them to

be considered independently. There is some unavoidable repetition between chapters, particularly in the Introduction Sections.

In the Second Chapter, *"Analytical Modeling of Underground Coal Gasification Through Application of a Channel Method"* (Seifi et al. 2010), we developed a simplified analytical channel model based on Magnani's work to investigate the combustion and gasification of pure carbon in a channel between the injection and production points. In addition to the carbon oxidation and Boudouard reactions, steam gasification and water-gas-shift reactions were included in the system to study the effect of steam on a typical UCG process. This closed-form solution was used to investigate the effect of the steam/oxygen molar ratio on the composition of the produced syngas and the length of the oxidation and reduction zones along the channel. Moreover, a sensitivity analysis was applied to the most effective operational parameters to provide a conceptual understanding of a typical UCG process. The experimental results were used to qualitatively verify the effect of some of the parameters.

In the Third Chapter, *"Numerical Simulation of Underground Coal Gasification Using the CRIP Method"* (Seifi et al. 2011), we developed a generic 3D simulation model for a typical linearly controlled retracting injection point technique. The purpose of this work is to explain the applied conservation equations and property evaluation methods in the simulation of a UCG process using the porous medium approach. The simulation results were used to investigate critical aspects of a UCG process such as the syngas composition and rate, cavity shape, and temperature profiles in different regions.

Chapter Four, *"Application of Porous Medium Approach to Simulate UCG Process"* (Seifi et al. 2014), explains the major assumptions for the adaptation of hydrocarbon reservoir simulators to simulate a UCG process. Due to the differences between the nature of coal seams and hydrocarbon porous media, it is necessary to evaluate several required physical properties such as the molecular weight of the coal, initial void porosity, initial concentration of coal in the unit, pore volume of the seam, initial coal solid density, and initial char solid density, for a hydrocarbon simulator. These properties are rarely obtained experimentally. Volume and mass balances are used to determine relationships among the measured parameters in fundamental coal analyses, i.e., proximate and elemental tests. In this way, the parameters required for porous medium simulators are determined. The proposed assumptions and property assessment

procedures are validated qualitatively and quantitatively using combustion tube tests, analytical modeling of pyrolysis, and the results of the self-gasification experiments on the vertical cylindrical coal core.

In Chapter Five, *"Reaction Rate Constants in Simulation of Underground Coal Gasification Using Porous Medium Approach"* (Seifi et al. 2014), we propose procedures for determining the reaction constants and activation energies in the form required by the porous medium simulators. Since the applied commercial simulator is not able to handle a reversible homogeneous reaction as a single rate expression, two homogeneous reactions are used, which disables the effect of the equilibrium constant. The proposed procedure allows us to include the effect of the equilibrium constant in reversible reactions. The complex pyrolysis process is modeled using a single-step-decomposition method in which only one reaction is used. A procedure is proposed to determine appropriate pyrolysis reaction kinetics with or without pyrolysis experimental results. The Arrhenius relationship and power law method are used to model heterogeneous reactions in porous medium simulators with a rate in unit bulk volume of the domain. However, the kinetics from surface gasifiers in the literature is expressed in unit specific surface area of the solid reactant. The proposed procedure converts the available kinetic data to the form used in hydrocarbon simulators to make an initial estimate of the heterogeneous reaction kinetics for the simulation. Although all of the kinetic parameters can be obtained by matching with the experimental or pilot results, these procedures are useful in situations without practical test results, to create a proper and consistent initial data set for the simulation model.

Finally, in Chapter Six, *"Large Scale Simulation of UCG Process Applying Porous Medium Approach"* (Seifi et al. 2014), the performance of three major technologies applied in the UCG industry, i.e., LVW, L-CRIP, and P-CRIP, are compared using three-dimensional large scale numerical simulation models. These models were applied using the Ardley coal formation in Alberta, Canada. We compared the sweep efficiency, composition and rate of produced syngas, shape and size of the developed cavities, and the heating value of the produced syngas of each technique. The second part of this chapter explains the Thulin test, a two-dimensional simulation of a UCG process in a tight coal seam. Issues, such as pressurization, and possible solution methods are also investigated.

Chapter 2 Analytical Modeling of Underground Coal Gasification Through Application of a Channel Method[1]

2.1 Abstract

Underground coal gasification (UCG) is a process of recovery of the energy of coal through partially combustion and gasification of coal by means of injected oxidant; and, the produced syngas is collected for processing for a variety of end uses.

In this work, an analytical model of UCG is developed by applying a channel method on one-dimensional coal seams and assuming four reactions with constant reaction rates. The process is assumed to be steady-state, so that a closed-form solution can be obtained. The model can be used to perform sensitivity analyses of operating parameters, such as the steam/oxygen ratio, the rate of oxidant injection, and the length of channel, on the composition of the species in the syngas, so that the findings can be applied to numerical simulations.

2.2 Introduction

Underground coal gasification (UCG), as a new method of utilization of the energy content of coal, has recently received a great deal of attention. It offers four potential advantages over conventional mining and the subsequent surface processing of coal: (1) the health hazard to miners is minimized, thereby improving safety; (2) the product gas may be cheaper due to the elimination of some surface plants and lower capital investment; (3) it has ecological benefits, because the land surface is left intact and the capture and storage of CO_2 is easier in this process; and, (4) it is a feasible method for exploitation of deep and thin coal seams that are not economic to mine using current mining technology (Thorsness et al. 1976; Britten et al. 1988).

The procedure to gasify the coal in-situ consists of three steps:

[1] M. Seifi, J. Abedi, and Z. Chen 2010. Analytical Modeling of Underground Coal Gasification Through Application of a Channel Method. *Energy Sources, Part A: Recovery, Utilization, and Environmental Effects* **35**: 1717-1727. DOI: 10.1080/15567036.2010.531501.

(1) The linking step, which consists of drilling an injection and production well from the surface to the coal seam and establishing a high permeability path between them.

(2) Ignition of the coal by injecting air, enriched air or a mixture of oxygen and steam through the injection well, which reacts chemically with the coal. A synthesis gas (called syngas) is produced, which is recovered through the production well and is cleaned and used either as a fuel for power generation or a chemical feedstock for various chemical products (e.g. hydrogen and ammonia). The raw product gas is composed mainly of hydrogen (H_2), carbon monoxide (CO), methane (CH_4), carbon dioxide (CO_2), and slightly of steam (H_2O), nitrogen (N_2), and hydrogen sulfide (H_2S).

(3) Once gasification operations in a section of the coal seam have finished, the third step is performed to return the environment back to its original state by flushing the cavities with steam and/or water to remove pollutants from the coal seam to prevent them from diffusing into surrounding aquifers.

A schematic of UCG is shown in **Fig. 2-1**. UCG involves a complex range of physical and chemical processes that occur over a wide range of characteristic time and length scales. The modeling of such processes is a compromise between model complexity (often assumed to give better predictive capability) versus simplicity (known to give faster computational run-times). Study of the UCG process primarily considers two aspects of modeling: the geomechanical aspect, which deals with the coal seam properties and the determination of the cavity growth and geometry, subsidence and other mechanical parts; and, the geochemistry aspect, which deals with chemical reactions, the type of products and their compositions, and pressure and temperature profiles by considering mass and heat transfer phenomena (Perkins 2005; Yang 2005).

The UCG models reported in the literature can be grouped into the four categories of coal block models, packed bed models, free channel models and process models. Coal block models consider the injection of oxidant agents on the surface of a dry/wet coal slab, in order to investigate the transport phenomena and chemical reactions kinetics. In packed bed models, a one-dimensional channel filled with crushed coal particles undergoes gasification to predict the gas composition and production. The assumption of an open channel with an exposed face of

fresh coal is the basic idea of the free channel models, in which the reactions take place on the perimeter of the channel; and, the radius of the channel can be assumed to expand during the gasification or to be constant. These free channel models are primarily used to analyze the effect of some operating conditions, such as the gasification length and the injection rate on the coal gasification. The existence of different physical and chemical processes, such as cavity growth, and water intrusion from surrounding formations into the underground reactor during UCG, requires the study of each phenomenon separately, which is the aim of process models (Sawyer et al. 1976; Perkins 2005; Khadse et al. 2006).

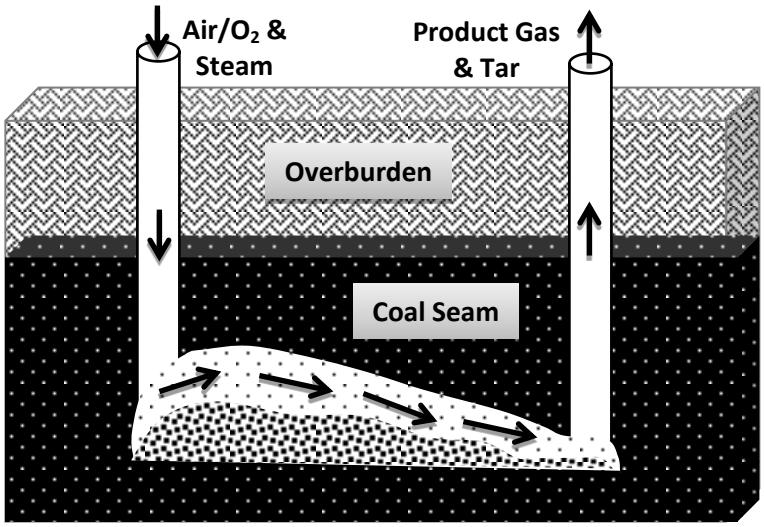

Fig. 2-1: Schematic of the UCG process

In this study, an analytical model of UCG is developed by assuming a free channel model in a one-dimensional coal seam with four reactions – three irreversible heterogeneous reactions and one reversible homogeneous reaction. Two major assumptions of the constant reaction rates and the steady-state process make the model simplified enough so that a closed-form solution can be developed. The heterogeneous reactions are assumed to take place on the wall of the channel, and the homogeneous reaction occurs in the gas phase. The developed linear model is used to investigate the effect of some critical parameters, such as the gasification agent, the inlet velocity and the length of channel, on the composition of the different species in the raw product gas. The results are physically reasonable and consistent with those reported in the literature. These results can be used to check numerical simulation outcomes and support pilot tests of UCG.

2.3 Assumptions and Formulations

As noted above, UCG is a complex process. In order to develop a model with an analytical solution, a large number of simplifications must be postulated. **Fig. 2-2a** schematically illustrates a typical coal seam channel that is to be modeled and an assumed control volume, **Fig. 2-2b**, that is used to derive the governing equations. The following set of assumptions was made in the development of the analytical model (Magnani 1973):

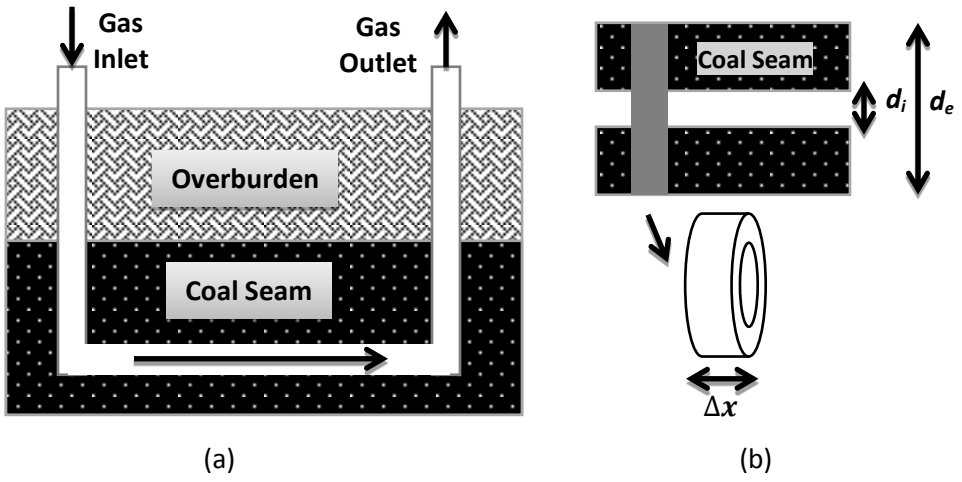

Fig. 2-2: (a) Schematic of the coal seam channel to be modeled, and (b) assumed control volume to develop the governing equations

- The coal seam and channel geometry are in a cylindrical form with constant diameters. Having a constant internal diameter for the channel in the middle of the coal seam implies that there is no regression of the channel wall as a result of heterogeneous reactions.

- The coal is assumed to be pure carbon, so that proximate and elemental analyses are not required for this model.

- Only a gas phase exists in the channel with a constant flow rate; the flow is assumed to be steady-state and in one dimension.

- Three irreversible heterogeneous reactions are assumed to take place on the coal surfaces on the channel wall; and, a reversible homogeneous reaction in the gas phase occurs, in which R_1, R_2, R_3, R_4, and R_5 are the respective reaction rates that are assumed to be of first order, with respect to the reactant gas concentrations:

$$C + O_2 \xrightarrow{R_1} CO_2 \quad (2\text{-}1)$$

$$C + CO_2 \xrightarrow{R_2} 2CO \quad (2\text{-}2)$$

$$C + H_2O \xrightarrow{R_3} CO + H_2 \quad (2\text{-}3)$$

$$CO + H_2O \xrightarrow{R_4} CO_2 + H_2 \quad (2\text{-}4)$$

$$CO_2 + H_2 \xrightarrow{R_5} CO + H_2O \quad (2\text{-}5)$$

- The reaction rates R_1, R_2, R_3, R_4, and R_5 are the average reaction rates that occur over the length of the reaction zone. These average reaction rates are based on experimental data, such as those provided by Lowry (Lowry 1963). They can also be calculated from experimental and mathematical analyses.

- Both axial and radial gas phase diffusions are neglected, and convection is the only gas transport phenomenon.

- All thermal, mechanical and chemical properties are assumed to be constant and are evaluated at axially averaged concentrations and temperatures.

- For heat transfer, a linear, one-dimensional, steady-state heat conduction equation is assumed along the axial of the cylinder in the solid phase; and, inside the gas phase, only convection heat transfer is considered. Radial heat conduction and radiation from the solid surface to the species molecules in the gas phase are neglected.

- The concentrations of all species at the inlet of the channel are assumed to be constant. Gas and solid temperatures at the inlet are fixed, but the solid temperature is assumed to be equal to or larger than the minimum temperature required to sustain the combustion. The solid surface at the outlet is considered to be adiabatic.

Applying mass and energy conservation law on both gas and solid phases in the control volume illustrated in **Fig. 2-2b** and utilizing the aforesaid assumptions, a system of seven coupled, linear, constant coefficient ordinary differential equations (ODEs) was developed to formulate the proposed model. All equations and relevant boundary conditions are summarized below.

Mass Balance Equations:

Oxygen: $$u_g \frac{dC_1}{dx} = -R_1.C_1 \quad (2\text{-}6)$$

Carbon dioxide: $$u_g \frac{dC_2}{dx} = R_1.C_1 - R_2.C_2 + R_4.C_3 - R_5.C_5 \quad (2\text{-}7)$$

Carbon monoxide: $$u_g \frac{dC_3}{dx} = 2R_2.C_2 - R_4.C_3 + R_3.C_4 + R_5.C_5 \quad (2\text{-}8)$$

Steam: $$u_g \frac{dC_4}{dx} = -R_4.C_3 - R_3.C_4 + R_5.C_5 \quad (2\text{-}9)$$

Hydrogen: $$u_g \frac{dC_5}{dx} = R_4.C_3 + R_3.C_4 - R_5.C_5 \quad (2\text{-}10)$$

Nitrogen: $$C_6 = C_t - (C_1 + C_2 + C_3 + C_4 + C_5) \quad (2\text{-}11)$$

In these equations, C_1, C_2, C_3, C_4, C_5, and C_6 are the concentrations of O_2, CO_2, CO, H_2O, H_2, and N_2, respectively, u_g is the gas phase velocity; and, C_t is the total concentration of all species inside the element volume.

Heat Transfer Equations (Appendix 2-A):

Solid phase: $$\frac{d}{dx}\left(\bar{K}_s \frac{dT_s}{dx}\right) - \frac{h.P}{A_e}(T_s - T_g) + \frac{A_i}{A_e}\sum_{j=1}^{3}(R_j.\Delta H_j.\rho_g.y_j) = 0 \quad (2\text{-}12)$$

Gas phase: $$-u_g \frac{d(\bar{\rho}_g \bar{C}_g T_g)}{dx} + \frac{h.P}{A_i}(T_s - T_g) = 0 \quad (2\text{-}13)$$

Where T_s and T_g denote the solid and gas temperature, A_i and A_e are the cross sectional area of channel and coal seam, $\bar{K}_s$ is average solid thermal conductivity, h is convective heat transfer coefficient, y_j's are the mole fraction of different species, ΔH_j's are heat of reactions, P is the perimeter of channel, and $\bar{\rho}_g$ and $\bar{C}_g$ are average density and specific heat of gas, respectively.

The required boundary conditions for the above seven differential equations are as follows:

For mass transfer equations:

$$\begin{aligned} C_1(x=0) &= C_{10} \\ C_2(x=0) &= C_{20} \\ C_3(x=0) &= C_{30} \\ C_4(x=0) &= C_{40} \\ C_5(x=0) &= C_{50} \end{aligned} \quad (2\text{-}14)$$

For heat transfer equations:

$$\begin{aligned} &T_g(x=0) = T_{g0} \\ &T_s(x=0) = T_{s0} \\ &\frac{dT_s}{dx}(x=L) = 0 \end{aligned} \tag{2-15}$$

where C_{j0}'s are the molar concentration of the species at the inlet and L is the length of channel. T_{s0} and T_{g0} denote the inlet solid and gas temperatures, respectively.

2.4. Solution of the Model

In order to facilitate the solution method and also the later analysis, the dimensionless parameters in equation (2-16) are used to convert all differential equations into the dimensionless form, as shown in equations (2-17) to (2-25):

$$x_d = \frac{x}{L}, \quad T_{gd} = \frac{T_g}{T_{g0}}, \quad T_{sd} = \frac{T_s}{T_{g0}}, \quad y_{id} = \frac{C_i}{C_{10}}, \quad y_{id0} = \frac{C_{i0}}{C_{10}}, \quad i = 1, \dots, 5 \tag{2-16}$$

Mass Transfer Equations:

Oxygen: $$\frac{dy_{1d}}{dx_d} = -\psi_1 y_{1d}, \qquad y_{1d}(x_d = 0) = 1.0 \tag{2-17}$$

Carbon dioxide: $$\frac{dy_{2d}}{dx_d} = \psi_1 y_{1d} - \psi_2 y_{2d} + \psi_4 y_{3d} - \psi_5 y_{5d}, \qquad y_{2d}(x_d = 0) = y_{2d0} \tag{2-18}$$

Carbon monoxide: $$\frac{dy_{3d}}{dx_d} = 2\psi_2 y_{2d} - \psi_4 y_{3d} + \psi_3 y_{4d} + \psi_5 y_{5d}, \qquad y_{3d}(x_d = 0) = y_{3d0} \tag{2-19}$$

Steam: $$\frac{dy_{4d}}{dx_d} = -\psi_4 y_{3d} - \psi_3 y_{4d} + \psi_5 y_{5d}, \qquad y_{4d}(x_d = 0) = y_{4d0} \tag{2-20}$$

Hydrogen: $$\frac{dy_{5d}}{dx_d} = \psi_4 y_{3d} + \psi_3 y_{4d} - \psi_5 y_{5d}, \qquad y_{5d}(x_d = 0) = y_{5d0} \tag{2-21}$$

Nitrogen: $$y_{6d} = \frac{1}{y_{10}} - \sum_{i=1}^{5} y_{id} \tag{2-22}$$

Energy Equations:

Solid phase: $$\frac{d^2 T_{sd}}{dx_d^2} - \xi\left(T_{sd} - T_{gd}\right) + \varphi(x_d) = 0 \quad , T_{sd}(0) = T_{sd0}, \quad \frac{dT_{sd}}{dx_d}(1) = 0 \tag{2-23}$$

Gas phase: $$-\frac{dT_{gd}}{dx_d}+\eta\left(T_{sd}-T_{gd}\right)=0 \qquad ,T_{gd}(x_d=0)=1 \tag{2-24}$$

where

$$\xi=\frac{hPL^2}{\bar{K}_s A_e},\quad \eta=\frac{hPL}{\bar{\rho}_g \bar{C}_g u_g A_i},\quad \psi_j=\frac{R_j L}{u_g},\qquad j=1,\dots,5$$
$$\varphi(x_d)=\frac{A_i y_{10} L^2}{\bar{K}_s A_e T_{g0}}\sum_{k=1}^{3} R_k \Delta H_k \rho_k y_{kd}(x_d) \tag{2-25}$$

All mass balance equations form a system of homogeneous, constant coefficient, first-order, linear ODEs in the form of $\overrightarrow{Y'}=[A]\vec{Y}+\vec{B}$, which can be solved by determining the eigenvalues and eigenvectors of the coefficient matrix, *A*. The final solution is the mole fraction of each species and is in the form of $\vec{Y}=\sum_{j=1}^{5}\emptyset_j e^{\lambda_j x}\vec{u}_j$, in which λ_j and $\vec{u}_j$ are the eigenvalues and corresponding eigenvectors, respectively, and $\emptyset_j$are the constant coefficients that can be obtained by applying the boundary conditions into the final solution (Appendix 2-B).

The heat transfer equations are non-homogeneous and linear ODEs; therefore, to solve them in the same procedure as for the mass transfer equations, a change of variable is required as follows:

$$\frac{dT_{sd}}{dx_d}=Z_d \tag{2-26}$$

In this case, the final solution is in the form of $\vec{Y}=\sum_{j=1}^{5}\Phi_j(x)e^{\lambda_j x}\vec{u}_j$, in which the coefficients, $\Phi_j(x)$, are functions of distance.

2.5 Results and Discussion

This model can be used to predict the compositions of the gas species through the channel that are comparable to those reported in the literature in light of trends and magnitudes. **Fig. 2-3** presents the typical composition profiles in the case of injecting an equal concentration of steam and oxygen during gasification in a cylindrical channel. As shown, oxygen and steam decreased exponentially with distance, and carbon dioxide reached a maximum and then decreased, due to Boudouard reaction. Carbon monoxide and hydrogen increase smoothly until the conversion is

completed. Nitrogen does not participate in the reactions. The decay of Nitrogen illustrated in **Fig. 2-3** is due to the change in the mole fractions of other species.

Fig. 2-4a presents the effect of the inlet gas velocity on the compositions of the gas species, where the solid lines represent the lower velocity of 15.24 *cm/sec* and the dotted lines illustrate the velocity of 45.72 *cm/sec*. The oxygen concentration did not change considerably at the outlet, because all oxygen molecules react with coal as soon as they reach the channel surface; however, as can be observed in the figure, the amount of oxygen increased at any point along the channel through increased gas velocity, which implies an increase in the oxidation zone length. The same behavior can be observed for steam, except that the increase in its mole fraction at the outlet was larger, due to a decreased contact time. At the higher velocity, the amounts of CO and H_2 decreased and the amount of CO_2 increased, because the residence time for O_2, H_2O, and CO_2 decreased with increasing the velocity, which lowers the progress of reactions (2-1), (2-2), and (2-3).

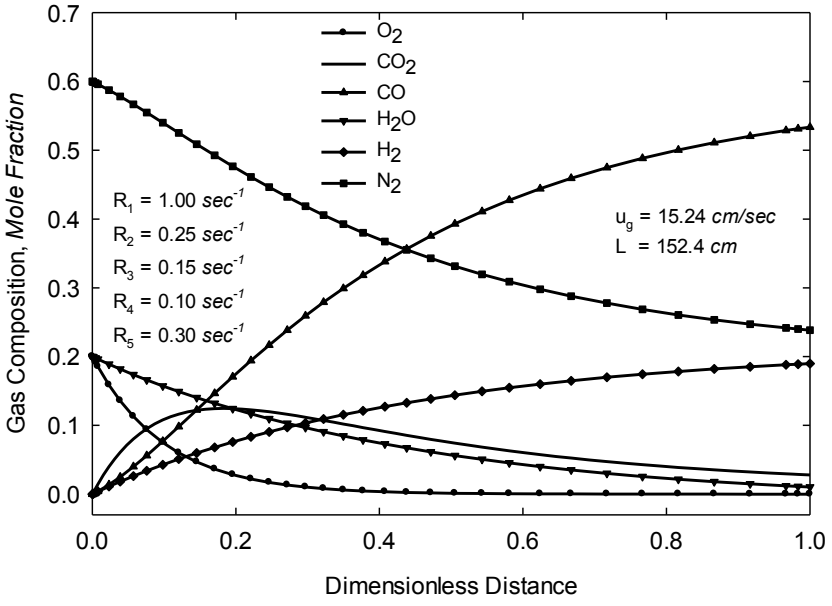

Fig. 2-3: Typical composition profiles through the channel by injecting equal mole fractions of O_2 and H_2O

Fig. 2-4b presents the effect of the channel length on the composition profiles: The solid lines stand for the short channel, 152.4 *cm*; and, the dotted lines represent the long channel, 304.8 *cm*. This length is an indicator of the well spacing in real fields. As can be seen, because of the increase in the residence time in longer channels, a slight increase in the amount of H_2, a

considerable increase in the CO content and a slight decrease in the CO_2 concentration of the product syngas can be observed. Due to the greater consumption of H_2O and O_2 in the long channel, the concentration of these species at each point through the channel was smaller than the short channel.

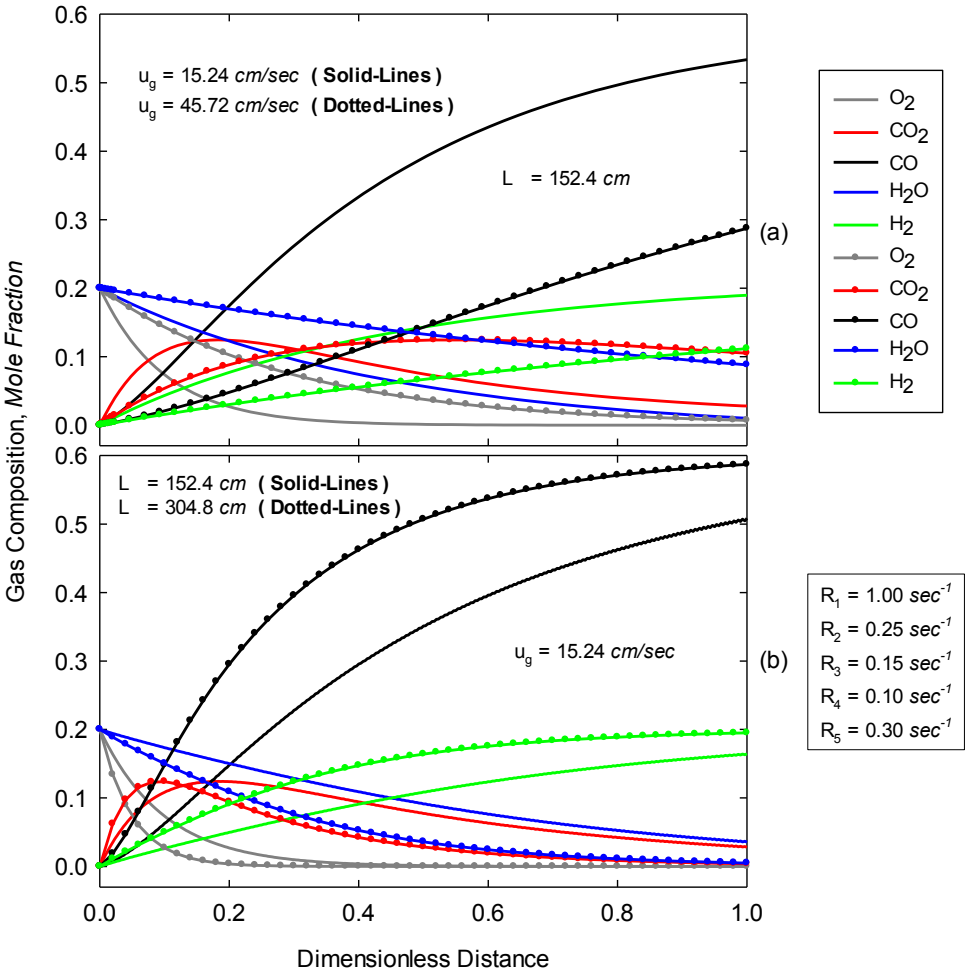

Fig. 2-4: (a) Effect of the inlet gas velocity on the compositions of the gas species, and (b) effect of the channel length on the compositions of the gas species

A critical factor influencing the success of a gasification project is the selection of an appropriate gasification agent. As reported in the literature, most applied oxidants in UCG are normal air, enriched air and a mixture of steam and air. Using the developed linear model, a sensitivity analysis was done on the mole fraction ratio of steam/oxygen in the injected gas, by assuming a constant value of 0.2 for the mole fraction of oxygen in the gasification agent. **Fig. 2-5a** presents the results of analysis. The results show the ratio of 2 as the most favorable value,

due to the largest amount of CO and H_2 in the raw product gas, which conforms to the literature. This value is confirmed by the optimal interval of 1.8 to 2.2 (V/V) reported by Yang as a result of channel gasification experiment, shown in **Fig. 2-7b**, because in this interval the effective gas reaches the maximum (Yang 2008).

Fig. 2-5b illustrates the typical gas and solid dimensionless temperatures through the channel. Despite the heat generated by the oxidation reaction, the solid temperature decreased with distance, due to the other two endothermic reactions. The gas temperature increased monotonically with distance, due to the increased heat gained by the gas caused by the convective heat transfer. Finally, both solid and gas temperatures reached an equal value – the thermal equilibrium value.

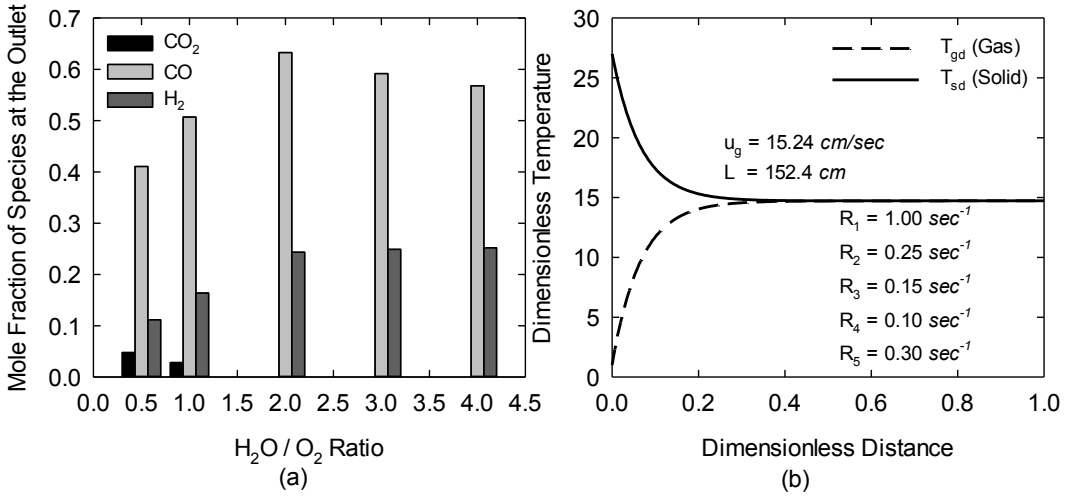

Fig. 2-5: (a) Results of the sensitivity analysis on the steam/oxygen ratio, and (b) gas and solid temperature profiles through the channel

The amount of carbon consumed at any point of the channel provides a relative index of the gasification effectiveness. Using the composition of the gas at each point, the amount of consumed carbon can be calculated, because all CO_2 and CO contained in the product gas are proportional to the amount of carbon consumed (Magnani 1973). **Fig. 2-6a** presents the effect of the oxygen concentration in the inlet on the amount of the carbon consumed up to each point in the channel. As shown in the figure, increasing the O_2 concentration increased the amount of the carbon consumed.

The cumulative heat released per unit weight of the injected gas is a quantity that indicates the total heat generated and absorbed within the channel up to any point. Its slope defines the domination of exothermic or endothermic reactions (Magnani 1973). **Fig. 2-6b** illustrates the effect of the oxygen concentration in the inlet on the cumulative heat released through the channel. Early in the process, the exothermic reaction dominated; and, the effect of the endothermic reactions increased as the distance inside the channel increased, until both took almost the same role in the process as the gas and solid temperatures became equal.

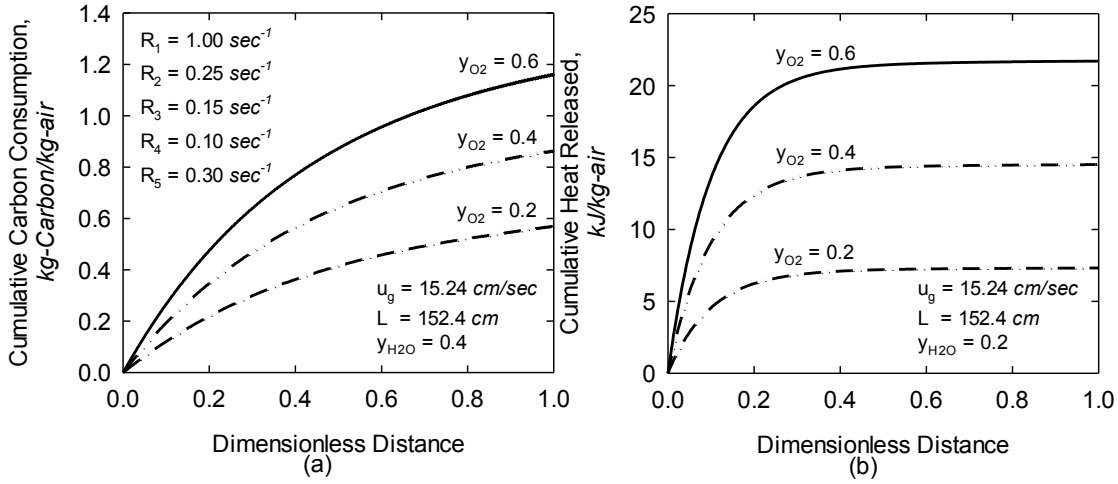

Fig. 2-6: (a) Effect of the oxygen concentration on the cumulative carbon consumption, and (b) effect of the oxygen concentration on the cumulative heat released

Fig. 2-7a illustrates the calculated dry basis heating value of the produced syngas using composition of the carbon monoxide and hydrogen versus the gas velocity. As can be seen, increasing the gas velocity reduces the heating value of the produced gas because of the lower residence time which deteriorates the progress of reactions (2-1), (2-2), and (2-3). This is confirmed qualitatively by the results of the pilot project experiment of UCG accomplished by Yang et al. depicted in **Fig. 2-8** (Yang et al. 2003). As shown in this figure, the average heating value of the produced gas declines as increasing the average flow capacity.

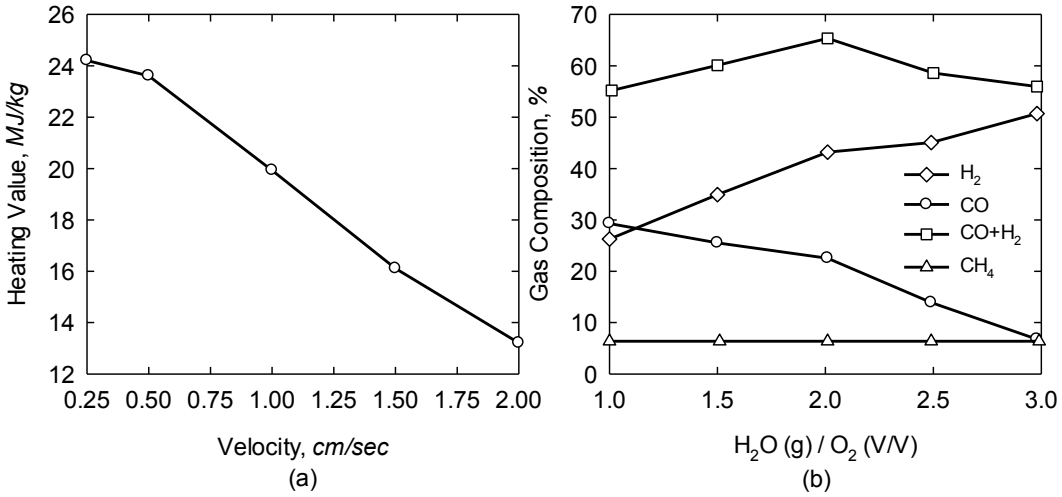

Fig. 2-7: (a) Heating value of produced gas from the model at different gas velocity, and (b) Composition of different gas species at varying value of steam-oxygen ratio obtained from experiment (Yang 2008)

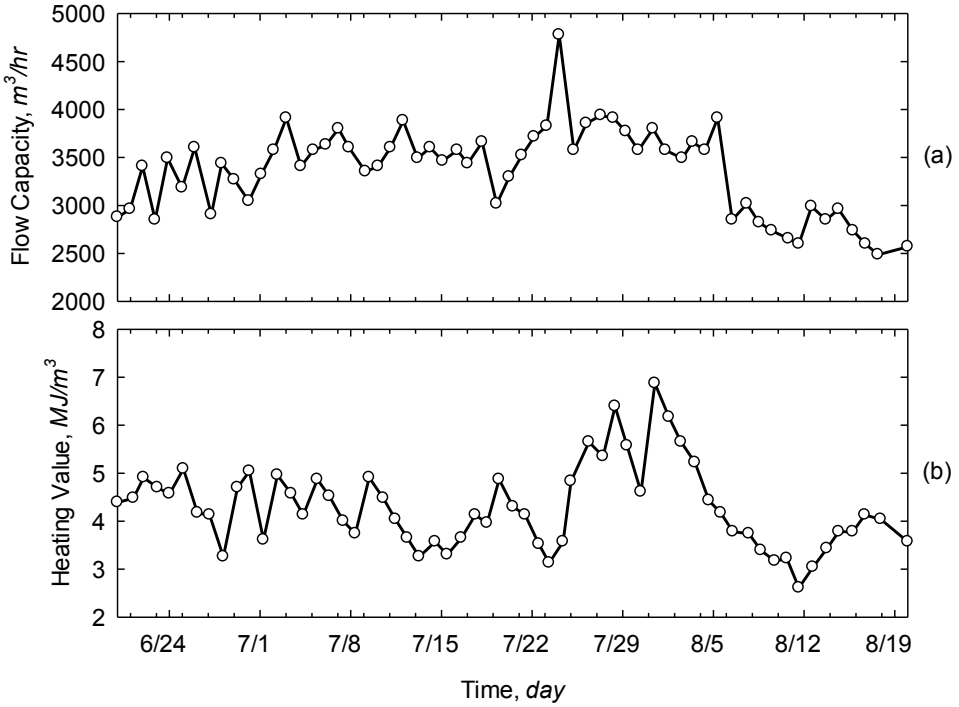

Fig. 2-8: Flow capacity (a) and heating value (b) of produced gas from experiment gasifier (Yang et al. 2003)

2.6 Conclusions

A linear simplified analytical model of UCG has been developed that can be used to predict the composition of gas species and also the temperature profiles within the channel. This model was used to perform sensitivity analyses on the input variables, such as the steam/oxygen ratio in the injected gas, the injection velocity, and the channel length. The optimal value of 2 was observed for the H_2O/O_2 mole fraction ratio, and results also show that the longer channel provided a better condition for chemical reactions through increased residence time. However, in real cases, there should be a compromise between the linkage condition and the well spacing. A larger velocity reduced the contact time and, consequently, decreased the activity of the reactions. The model and sensitivity analysis can be used to check the validity and accuracy of numerical simulations and pilot tests for UCG qualitatively.

2.7 Appendix 2-A: Derivation of Equation (2-12)

Equation (2-12) is the energy conservation in solid phase in steady state condition as described by equation (2-A.1); there is no accumulation of energy within solid phase. It is assumed that heterogeneous reactions take place on the periphery of the channel and the generated heat will distribute within the solid phase rather than being directly transferred to the gas phase. Moreover, the endothermic reactions absorb the required energy from solid phase only.

$$\begin{aligned}&[Heat\ conducted\ into\ solid\ element]\\ &-[Heat\ loss\ by\ convection\ to\ gas\ phase]\\ &+[Heat\ of\ reactions\ on\ the\ surface]\\ &=[Heat\ conducted\ out\ of\ solid\ element]\end{aligned} \tag{2-A.1}$$

Applying Fick's and Newton's cooling laws, equation (2-A.1) can be written as equation (2-A.2). $A_i\Delta x$ is the volume of the gas in the portion of channel within the control volume. y_j is the mole fraction of gas component j in the gas phase. $P\Delta x$ is the area of the channel exposed to the solid phase within the control volume and the convective heat loss from solid phase to gas phase happens through this surface.

$$\left(-\overline{K_s}A_e\frac{dT_s}{dx}\right)_x - hP\Delta x\left(T_s - T_g\right) + \sum_{j=1}^{3}\left(\rho_g A_i \Delta x y_j R_j \Delta H_j\right) = \left(-\overline{K_s}A_e\frac{dT_s}{dx}\right)_{x+\Delta x} \tag{2-A.2}$$

Since A_e and A_i are constant, both sides of the equation (2-A.2) can be divided by $A_e.\Delta x$, equation (2-A.3). The first term of equation (2-A.3) is the derivative of conductive heat flux with respect to space, equation (2-A.4).

$$\frac{(\overline{K_s}\frac{dT_s}{dx})_{x+\Delta x} - \left(\overline{K_s}\frac{dT_s}{dx}\right)_x}{\Delta x} - \frac{hP}{A_e}(T_s - T_g) + \frac{A_i}{A_e}\sum_{j=1}^{3}(\rho_g y_j R_j \Delta H_j) = 0 \quad \text{(2-A.3)}$$

$$\frac{d}{dx}\left(\overline{K_s}\frac{dT_s}{dx}\right) - \frac{hP}{A_e}(T_s - T_g) + \frac{A_i}{A_e}\sum_{j=1}^{3}(\rho_g y_j R_j \Delta H_j) = 0 \quad \text{(2-A.4)}$$

2.8 Appendix 2-B: Solution of the ODE Equations

Equations (2-17) to (2-21) can be written in a matrix form as shown in equation (2-B.1) which implies a system of homogeneous, constant coefficient, coupled, and first-order linear ODEs. In order to solve this system of ODEs, the eigenvalues, λ_j, and their corresponding eigenvectors, $\overrightarrow{u_j}$, of the coefficient matrix, [A], should be determined. However, since the coefficient matrix has variable entries depending on the rate of reactions, channel length, and the gas velocity, the final closed-form solution for mole fraction of the gas components cannot be determined prior to setting the values of these parameters. On the other hand, for the specific values of $\psi_j$the solution of the system can be determined in the form of $\overrightarrow{Y'} = \sum_{j=1}^{j=5}\phi_j e^{\lambda_j x}\overrightarrow{u_j}$ in which constant coefficients ϕ_j can be obtained by applying the boundary conditions.

$$\overrightarrow{Y'} = [A]\vec{Y} + \vec{B} \quad \text{(2-B.1)}$$

where

$$\overrightarrow{Y'} = \begin{Bmatrix} y'_{1d} \\ y'_{2d} \\ y'_{3d} \\ y'_{4d} \\ y'_{5d} \end{Bmatrix}, \quad [A] = \begin{bmatrix} -\psi_1 & 0 & 0 & 0 & 0 \\ \psi_1 & -\psi_2 & \psi_4 & 0 & -\psi_5 \\ 0 & 2\psi_2 & -\psi_4 & \psi_3 & \psi_5 \\ 0 & 0 & -\psi_4 & -\psi_3 & \psi_5 \\ 0 & 0 & \psi_4 & \psi_3 & -\psi_5 \end{bmatrix}, \quad \vec{Y} = \begin{Bmatrix} y_{1d} \\ y_{2d} \\ y_{3d} \\ y_{4d} \\ y_{5d} \end{Bmatrix}, \quad \vec{B} = \begin{Bmatrix} 0 \\ 0 \\ 0 \\ 0 \\ 0 \end{Bmatrix}, \quad \psi_j = \frac{R_j L}{u_g}$$

Chapter 3 Numerical Simulation of Underground Coal Gasification Using the CRIP Method[2]

3.1 Abstract

A three-dimensional simulation of the Underground coal gasification (UCG) process is studied in terms of the heat and mass transport phenomena and chemical kinetics in a coal seam during coal combustion by applying the controlled retracting injection point (CRIP) technique. The STARS module of the Computer Modeling Group software (CMG) is used in this study. The gas species flow rate, cavity shapes, and temperature profile in the coal seam during gasification are investigated. The main motivation behind this study is to provide a simulation methodology by using a comprehensive porous media flow approach to understand the critical aspects of the UCG process.

Keywords Cavity, Chemical Reaction Kinetics, CRIP, Pyrolysis, Underground Coal Gasification,

3.2 Introduction

Coal as one of the fossil fuels currently provides 25 % of the total energy demand of the world. It is being used either directly as a fuel in the furnaces or being gasified to a mixture of flammable gases that are mostly composed of H_2, CO, CH_4, CO_2, and slightly of H_2O, N_2, and H_2S. The product gas can be used either as a fuel for power generation or a chemical feedstock for various chemical products (e.g., hydrogen and ammonia) (Perkins 2005).

Most current technologies of coal gasification such as entrained flow, fluidized bed, and moving bed use a surface reactor for gasification. The main differences between these technologies relate to the gas flow configuration, coal particle size, ash handling, and process conditions. An alternative for surface gasifier is an underground coal gasifier that eliminates the need for mining and can be used in deep or steeply dipping, unmineable coal seam. It also lowers

[2] M. Seifi, Z. Chen, and J. Abedi 2011. Numerical Simulation of Underground Coal Gasification Using the CRIP Method. *The Canadian Journal of Chemical Engineering* **89**: 1528-1535.

the capital investment by eliminating the need for specialized coal processing (transporting and stocking) and gasification reactors. UCG has other advantages such as increased work safety, no surface disposal of ash, low dust, and noise pollution. It can be operated at high pressure to increase the reaction activity and improve the efficiency of the process. A comprehensive environmental assessment and risk analysis is required prior to embarking the UCG process because of possibility of land subsidence and ground water pollution, the UCG disadvantages (Lowry 1963; Perkins 2005; Khadse et al. 2006).

Several field designs have been operated in order to make UCG functional regarding different operating aspects such as a linking technique, avoiding heat and gas loss into adjacent formation, producing constant high quality gas, minimizing the inhibitor effect of ash, and reducing the environmental effects (Perkins 2005). **Fig. 3-1** illustrates the most applied field designs of the UCG process. Linked vertical wells (LVW) require drilling two vertical wells as the producer and injector and establishing a linking channel between them using various technologies, including hydraulic fracturing, explosive fracture, reverse combustion, and directionally drilling. In the gasification of steeply dipping coal seams, the injector is drilled at an angle in a lower part of the coal seam and the producer is drilled vertically in an upper part. Also, in order to access fresh coal and minimize the effect of deposited ash dregs over the injection point, a series of injection wells are drilled at an angle over the course of the UCG process. Another technique, the controlled retracting injection point (CRIP) is the most favorable technique of gasification of coal in-situ. In the CRIP process, the production well is drilled vertically, and the injector is drilled horizontally close enough to the producer to have considerable flow connection. When the linking channel is established, the coal is ignited at the end of the horizontal well and a cavity is initiated. Once the coal near this cavity is burnt up, the injection point is retracted to a new location to access fresh coal and begin the next cavity. This procedure carries on until the majority of coal between the wells is consumed (Perkins 2005; Yang 2005; Burton et al. 2008).

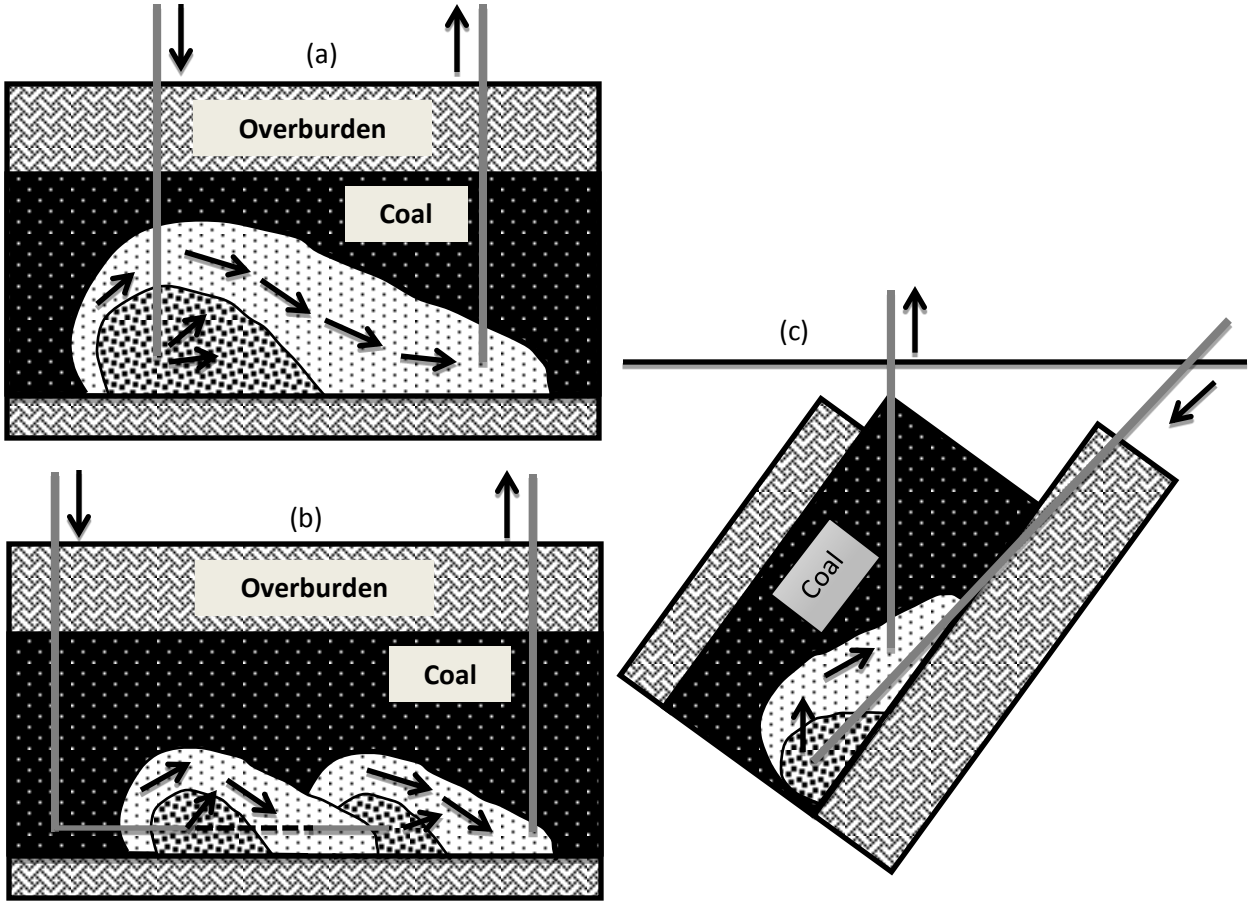

Fig. 3-1: Schematics of most applied field designs of UCG (a) Linked vertical wells, LVW, (b) Controlled retracting injection point, CRIP, and (c) Steeply dipping coal seams

In this work, three-dimensional numerical simulation of the UCG process is studied by using the CRIP technique and a porous media flow approach as in hydrocarbon reservoir simulation. The STARS module of the Computer Modeling Group software (CMG) is used in this study. The major approach is to apply heat and mass transport phenomena in conjunction with chemical reactions in order to investigate the cavity shapes, temperature variation, product gas composition, and flow rates that are the critical aspects of the UCG process.

The modeling of the UCG process has mostly been done by using the computational fluid dynamics (CFD) approach (Shirsat 1989; Burton et al. 2008). They used complicated velocity equations, included the turbulent gas flow inside a cavity, and utilized chemical engineering correlations for particle sizes, the porosity of a reactor, and an equilibrium controlled formulation for reversible reactions. A porous medium approach, which is based on mass conservation,

Darcy's law, and energy conservation and accounts for the change in porosity and permeability due to the rock strength change, is more appropriate for the description of UCG. Furthermore, in this approach the reversible reactions are replaced with two irreversible reactions with effective kinetics mechanisms. The focus of this work is to establish this porous medium approach for the description of UCG and show that the findings from this approach are in agreement with those in the literature using the CFD approach.

3.3 Model Formulation and Properties

3.3.1 Model Structure

The modeling of UCG can generally be divided into two categories: the geomechanics part that deals with cavity shapes, cavity growth mechanisms, subsidence, and other mechanical aspects and the geochemistry part that deals with the fluid flow, product gas composition and heating value, chemical reactions, and heat and mass transport phenomena. Therefore, the modeling of the UCG process is very complex and involves comprehensive simulation of coupled fluid, chemical, thermal transport, and mechanical deformation processes (Shirsat 1989). In our model, the cavity growth is caused by char combustion and gasification reactions. Thus the rate of cavity growth depends on the progress rate of these reactions. Other types of mechanisms such as thermo-mechanical failure, rock spalling, sidewall regression, and bulk collapse of coal need to be included in the future work as a separate module in addition to the STARS module of the CMG software (Britten and Thorsness 1988).

In this study, a rectangular coal seam with dimensions of 25 *m* length, 12.5 *m* width, and 9 *m* height is used. It is divided into 99 intervals in the *x*-direction, 49 intervals in the *y*-direction, and 35 layers in the *z*-direction numbered downwards. A vertical well located at one extremity of the seam and in the middle of width is considered as the production well. It is extended from the top layer to layer 31 and perforated at the last layer. The injection well is placed horizontally at layer 31 from block 2 to 84 in the *x*-direction and in the same block as the producer in the *y*-direction. The injector is initially perforated at the toe which is 3 *m* away from the producer. All boundaries of the seam domain are considered to be no flow boundary. Despite of increasing the runtime of simulation, the grid blocks have been taken to have a very small size ($0.25m \times 0.25m \times 0.25m$) so that the temperature gradient will be more distinguishable and also because STARS

uses the average temperature of each block to calculate the chemical reaction constants, having small blocks increases the accuracy of the reaction rates. **Fig. 3-2** delineates the structure of the applied coal seam. Decreasing the grid size to $(0.15m \times 0.15m \times 0.15m)$ did not change the results significantly, except increasing the grid numbers and runtime. Consequently, the cubical grid blocks with the size of 0.25 *m* were considered as the optimum size.

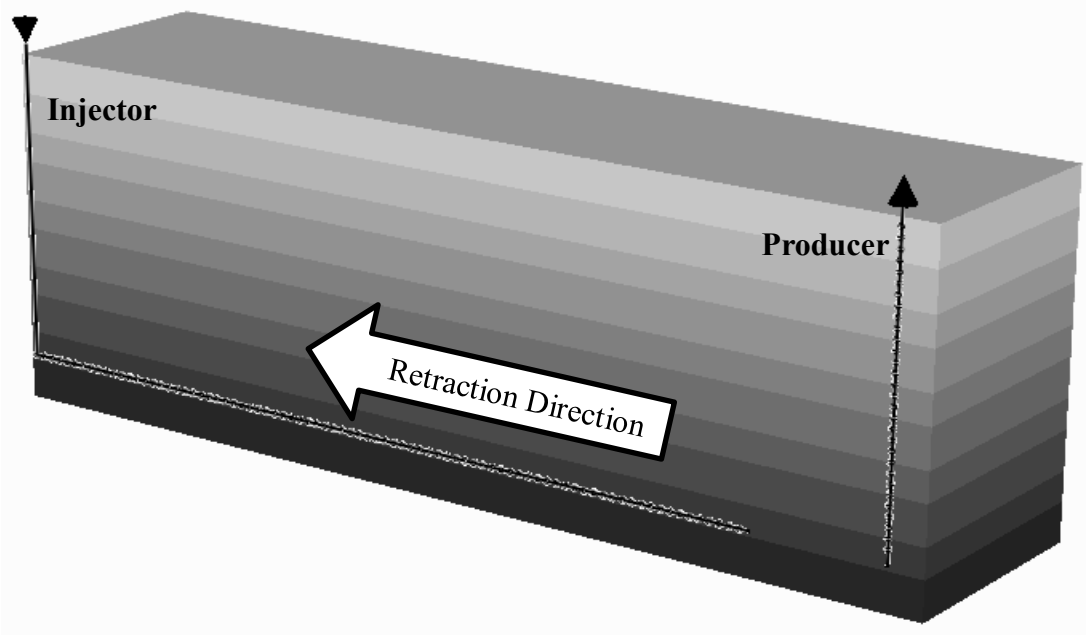

Fig. 3-2: Geological structure of the applied coal seam model

3.3.2 Conservation Equations

For investigation of the reactive behavior of coal gasification, the momentum balance law for determination of the flow velocity, the mass conservation law for composition prediction, and the energy conservation law for temperature profile prediction are generally considered. In the model, the momentum conservation is approximated by Darcy's law due to the porous medium approach used, and all conservation equations are defined in three-dimensional space as follows. The radiation effect between incandescent coal surfaces and gas molecules is ignored in heat transport phenomenon.

The momentum balance equation for j^{th} phase is (z-axis is downwards)

$$\overrightarrow{v_j} = -\frac{k_j}{\mu_j}\left(\overrightarrow{\nabla p} - \rho_j g\overrightarrow{\nabla Z}\right) \tag{3-1}$$

The mass balance equation for flowing component *i* in block *L* is (CMG: STARS Technical Manual 2009)

$$\begin{aligned}\sum_{l=1}^{n_b}\sum_{j=1}^{n_p}\phi_f D_{ij}\rho_j\Delta y_{ij} + \sum_{l=1}^{n_b}\sum_{j=1}^{n_p}T_j\rho_j y_{ij}\Delta\Phi_j + V_{bL}\sum_{m=1}^{n_r}(S'_{mi} - S_{mi})\,r_m + \sum_{j=1}^{n_p}\rho_j q_{jk}y_{ij} \\ + \delta_{iw}\sum_{l=1}^{n_{aqb}}\rho_w q_{aq_{wl}} \\ = \left(\frac{V_{bL}}{\Delta t}\right)\left(\left(\phi_f\sum_{j=1}^{n_p}(\rho_j S_j y_{ij})\right)^{(n+1)} - \left(\phi_f\sum_{j=1}^{n_p}(\rho_j S_j y_{ij})\right)^{(n)}\right)\end{aligned} \tag{3-2}$$

The first and second expressions are flowing terms, diffusion and convection, respectively. The mass transfer caused by chemical reactions during the process is illustrated by the third term. The fourth and fifth terms account for the external injection of component *i* via an injection well or an aquifer influx, respectively. The only term on the right-hand side describes the accumulation of component *i* in a gird block with the bulk volume of V_{bL}. The phase *j* transmissibility, T_j, is defined as

$$T_j = \left(\frac{A}{\Delta l}\right)^{eff} k^{eff}\left(\frac{k_{rj}}{\mu_j . R_j}\right), \quad j = 1, \dots, n_p \tag{3-3}$$

Which is a function of the effective permeability, viscosity, cross sectional area, and node spacing.

The conservation equation of solid component *i* in block *L* is (CMG: STARS Technical Manual 2009)

$$V_{bL}\sum_{m=1}^{n_r}(S'_{mi} - S_{mi})r_m = \left(\frac{V_{bL}}{\Delta t}\right)\left((\phi_v c_i)^{(n+1)} - (\phi_v c_i)^{(n)}\right) \tag{3-4}$$

Equation (3-4) describes the variation of concentration of solid component *i* with time which is only caused by chemical reactions. The left-hand side describes the consumption rate of solid component *i* during the gasification and the right-hand side is the accumulation term. In our model, two solid components of original coal and char in dry-ash-free basis are considered.

The energy conservation equation is (CMG: STARS Technical Manual 2009)

$$\sum_{l=1}^{n_b}\sum_{j=1}^{n_p} T_j\rho_j H_j \Delta\Phi_j + \sum_{l=1}^{n_b} K_l \Delta T_l + V_{bL}\sum_{m=1}^{n_r} H_{rm} r_m + \sum_{j=1}^{n_p} \rho_j H_j q_{jk} + \sum_{l=1}^{n_{aqb}}\sum_{j=1}^{n_p}\left(\rho_j H_j q_{aq_{jl}} + K_l \Delta T_l\right) + \sum_{f=1}^{n_f}\left(HL_f + HL_{vf} + HL_{cf}\right) = \left(\frac{V_{bL}}{\Delta t}\right)\left(\zeta^{(n+1)} - \zeta^{(n)}\right) \quad (3\text{-}5)$$

Energy transfer by convection and conduction mechanisms are illustrated by the first and second terms, respectively. The third term accounts for the reaction source/sink term and the last term describes the well source/sink for energy. In the model, neither well term for solid nor heat loss is considered. The accumulation term of energy is included on the right-hand side in which ξ is defined as

$$\zeta = \phi_f \sum_{j=1}^{n_p} \rho_j S_j U_j + \phi_v c_S U_S + (1-\phi_v) U_r \quad (3\text{-}6)$$

3.3.3 Chemical Processes

During in-situ combustion of coal different processes of vaporization (drying), pyrolysis, and combustion and gasification of char take place. **Fig. 3-3** illustrates different chemical regions of gasification of coal in-situ. In the drying zone, surface water in the wet coal is vaporized at temperatures above the saturation temperature of seam water at a specified pressure, which makes the coal more porous. The dried coal undergoes the pyrolysis process upon more heating in the next phase. During pyrolysis, coal loses about 40 to 50 % of its dry weight as low molecular-weight gases, chemical water, light hydrocarbons and heavy tars and after evolving the volatile matters, a more permeable solid substance called char will be combusted and gasified by the injected oxidant agents and exhausted gases from the previous steps (Campbell 1976; Merrick 1983).

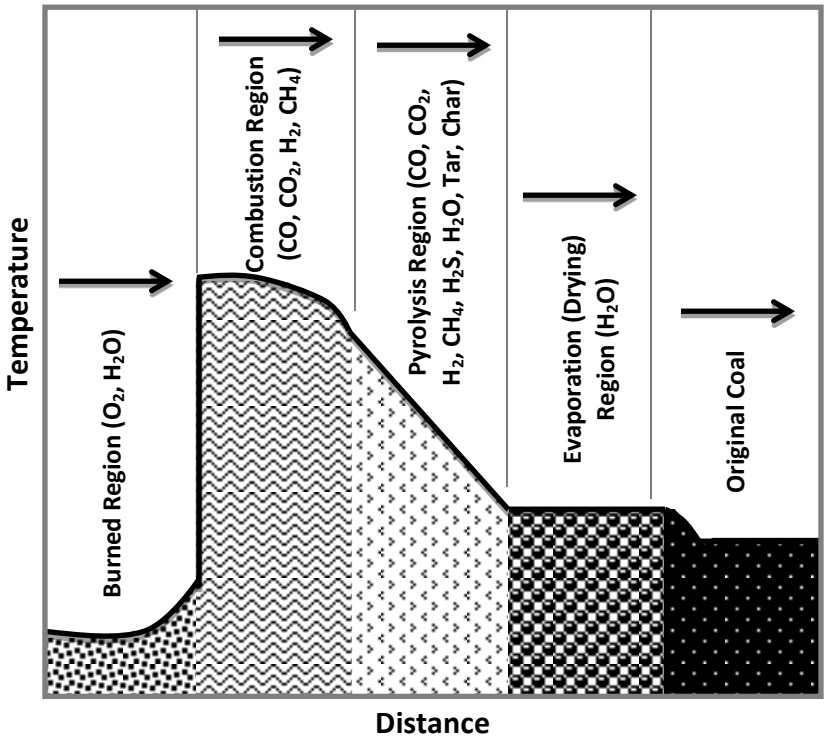

Fig. 3-3: Thermal wave propagation through coal seam during in-situ gasification which demonstrates the different regions

The pyrolysis process is a complex thermal decomposition process at the typical temperature range of 400-900 $°C$ which results in a series of reactions releasing volatile matters from the porous coal matrix and changes the chemical and physical structure of the coal. Several kinetic models of coal pyrolysis such as the consecutive decomposition, multi-step consecutive-competitive model, simultaneous independent reaction model for each species, and single step decomposition (or overall first order reaction model) have been proposed in the literature (Tsang 1980; Perkins 2005). In this study, the latter model is applied to describe the pyrolysis process. It is assumed that the dried coal is decomposed to CO, CO_2, H_2, CH_4, and char as shown in reactions (3-7) and (3-8). For simplicity, the char is assumed to be pure carbon. Thus the effect of ash dreg residuals in the porous medium will be eliminated in this model.

$$\boldsymbol{Coal(daf) \rightarrow Char\ (C) + Volatile\_Matter + Ash + Chemical\_Water} \qquad (3\text{-}7)$$

$$\boldsymbol{Volatile\_Matter} \rightarrow \alpha_1\boldsymbol{CO} + \alpha_2\boldsymbol{CO_2} + \alpha_3\boldsymbol{H_2} + \alpha_4\boldsymbol{CH_4} \quad (3\text{-}8)$$

The stoichiometry coefficients have been calculated by using material balance on each element in the reaction and applying the elemental analysis of sub-bituminous coal under study as shown in **Table 3-1**. Thus the final form of the pyrolysis reaction used in the model is

$$\boldsymbol{Coal(daf)} \rightarrow 4.63\boldsymbol{Char} + 0.12\boldsymbol{CO} + 0.18\boldsymbol{CO_2} + 0.43\boldsymbol{H_2} + 0.79\boldsymbol{CH_4}$$
$$\Delta H^0_{298} \approx 0.0 \quad (3\text{-}9)$$

The kinetics of the volatile matter releasing is described during the pyrolysis process in the model by a first order reaction on the concentration of coal for which the rate varies with temperature according to an Arrhenius relationship below where the values of 1.9E+17 day^{-1} and 180.0 *kJ/mol* are used for the pre-exponential factor, κ_0, and activation energy, E, respectively (Merrick 1983; Vargas and Perimutter 1985; Ma et al. 1991; Nourozieh et al. 2010)

$$\kappa = \kappa_0 \exp(-\frac{E}{R\bar{T}}) \quad (3\text{-}10)$$

Table 3-1: Coal analysis results

Ultimate Analysis (*wt%, ar*)		**Proximate Analysis (*wt%, ar*)**	
Moisture	0.89	Moisture	4.72
Ash	9.66	Ash	9.29
H	3.55	Volatile matter	30.46
C	73.76	Fixed carbon	55.54
N	1.07		
S	0.43		
O	10.64		
Total	**100.00**	**Total**	**100.00**

A set of heterogeneous reactions between char and gas species mostly on the surface of cavities and homogeneous reactions among gas species inside the cavities take place. The rate of progress of these heterogeneous reactions determines the rate of consumption of carbon and cavity growth, and these homogeneous reactions play the main role in the ultimate composition of the product syngas, particularly the water-gas shift and methane steam reforming reactions. The most important reactions are summarized as follows (Thorsness and Rozsa 1976; Perkins 2005; Nourozieh et al. 2010):

$$C + O_2 \rightarrow CO_2 \qquad \Delta H^o_{298} = -393kJ/gmol \qquad (3\text{-}11)$$

$$C + H_2O \rightarrow H_2 + CO \qquad \Delta H^o_{298} = +131kJ/gmol \qquad (3\text{-}12)$$

$$C + CO_2 \rightarrow 2CO \qquad \Delta H^o_{298} = +172kJ/gmol \qquad (3\text{-}13)$$

$$C + 2H_2 \rightarrow CH_4 \qquad \Delta H^o_{298} = -75kJ/gmol \qquad (3\text{-}14)$$

$$CO + \frac{1}{2}O_2 \rightarrow CO_2 \qquad \Delta H^o_{298} = -283kJ/gmol \qquad (3\text{-}15)$$

$$CO + H_2O \leftrightarrow CO_2 + H_2 \qquad \Delta H^o_{298} = -41kJ/gmol \qquad (3\text{-}16)$$

$$CH_4 + H_2O \leftrightarrow CO + 3H_2 \qquad \Delta H^o_{298} = +206kJ/gmol \qquad (3\text{-}17)$$

Except reaction (3-14) which is more effective at high pressures, other reactions are more common for the surface coal gasifiers and shallow UCG processes.

In order to model these reactions that appear as the source/sink terms in the conservation equations, all are treated as first order reactions based on the concentration of the reactants and using the power law as shown in equation (3-18), and the temperature dependent rates are described by the Arrhenius correlation. Reversible reactions are divided into two separate forward and backward reactions when introduced into the STARS simulator. The relevant frequency factors, κ_m, and activation energies, E_m, for these reactions are summarized in **Table 3-2**. These are effective kinetic parameters that include the intrinsic kinetics and gas-film diffusion resistance (Nourozieh et al. 2010).

$$r_m = \kappa_m \prod_{i=1}^{i=n_c} C_i^{\,n_{im}} \qquad (3\text{-}18)$$

Table 3-2: Kinetics parameters of heterogeneous and homogeneous reactions

Reaction No *(m)*	Reaction Name	E_m *(kJ/gmol)*	κ_m (Variable)
3-11	Coal Combustion	100	1.80E+06
3-12	Steam Gasification	156	4.70E+07
3-13	Boudouard	249	6.40E+09
3-14	Hydrogen Gasification	200	1.50E+14
3-15	Carbon-Monoxide Oxidation	247	6.48E+03
3-16	Forward Water Shift	126	2.40E+05
3-16	Reverse Water Shift	126	2.40E+03
3-17	Forward Methane Steam Reforming	30	2.70E+07
3-17	Reverse Methane Steam Reforming	30	2.70E+08

3.3.4 Model Properties

In the UCG process, the porosity of a block can be divided into two categories: void porosity, ϕ_v, which is defined as the volume fraction of solid and fluid in the block and fluid porosity, ϕ_f, which is the volume fraction of the fluids. Both porosities vary with time as the solid components in the block are consumed. In the model, these parameters are calculated using equations (3-19) and (3-20).

$$\phi_v = \phi_{vr}\left(1 + C_p(P - P_r) - C_T(T - T_r)\right) \tag{3-19}$$

$$\phi_f = \phi_v\left(1 - \sum_{i=1}^{n_s}\left(\frac{c_{si}}{\rho_{si}}\right)\right) \tag{3-20}$$

Permeability is a strong function of the porosity, especially in the case of the UCG process with a high amount of solid consumption; the large change in the void porosity causes a considerable change in the permeability. Large permeability at the same operating conditions makes an easy production of gas species and reduces the contact time for reactions. In this model, the permeability variation is described in exponential form as shown in equation (3-21).

$$K = K_0.exp\left[K_{mul}.\left(\frac{\phi_f - \phi_{f0}}{1 - \phi_{f0}}\right)\right] \tag{3-21}$$

Here, K_0 and ϕ_{f0} are the initial permeability and fluid porosity, respectively, and K_{mul} is a multiplier which is taken to be 4 for all directions (CMG: STARS Technical Manual 2009).

Solid and gas heat properties such as heat capacity and thermal conductivity are considered to be constant as shown in **Table 3-3**, except the heat capacities of gas species that are calculated by using equation (3-22) with the related constant coefficients summarized in **Table 3-4** (Reid et al. Apendix A 1987; CMG: STARS Technical Manual 2009).

$$C_{P_i}(T) = \alpha_i + \beta_i T + \gamma_i T^2 + \xi_i T^3 \tag{3-22}$$

Table 3-3: Thermal properties of solids and fluids

Char Heat Capacity, *J/(gmol-°C)*	17
Coal Heat Capacity, *J/(gmol-°C)*	17
Rock Heat Capacity, *J/(m^3-°C)*	3.0E+06
Solid Thermal Conductivity, *J/(m-day-°C)*	4.5E+05
Rock Thermal Conductivity, *J/(m-day-°C)*	2.0E+05
Water Thermal Conductivity, *J/(m-day-°C)*	48384
Gas Thermal Conductivity, *J/(m-day-°C)*	4000

Table 3-4: Values of coefficients for gas species heat capacity correlation

Coefficients	O_2	CO_2	H_2	CO	CH_4
α, *J/gmol-C*	28.106	19.795	27.14	30.869	19.251
β, *J/gmol-C^2*	-3.68E-06	7.34E-02	9.27E-03	-1.29E-02	5.21E-02
γ, *J/gmol-C^3*	1.75E-05	5.60E-05	-1.38E-05	2.79E-05	1.20E-05
ξ, *J/gmol-C^4*	-1.07E-08	1.72E-08	7.65E-09	-1.27E-08	-1.13E-08

The initial properties of the coal seam required for the modeling purpose are summarized in **Table 3-5**. In this model, the equal-molar mixture of steam and oxygen is used as oxidant agents. The runtime for this model is about 3 *days* for 50 *days* of simulation.

Table 3-5: Initial properties of the coal seam required for the modeling purpose

Porosity , *fraction* (Coal + Initial Fluid)	0.95
Absolute Permeability, *md*	1.0
Coal Concentration, *gmol/m^3-of-pore-volume*	1.27E+04
Water Saturation	0.7
Temperature, *°C*	60
Pressure, *MPa*	11.5
Fluid in Porous Media	CH_4
Coal Density, *kg/m^3*	1200
Char Density, *kg/m^3*	1740

3.4 Results and Discussion

As mentioned earlier, the main goal of this study is to introduce a numerical methodology to simulate the UCG process by using the STARS module of the CMG software in terms of a porous media flow approach. The findings, especially the temperature profile, cavity shape, and compositions of gas species are comparable qualitatively with those reported in the literature. The cavity shape can be investigated by using the values of char/coal concentrations and fluid porosity. **Figs. 3-4** and **3-5** illustrate the profiles of the char concentration and fluid porosity at the end of simulation of 50 *days*. At the early time of simulation when the injection point is

much closer to the perforated interval of the producer, the cavities are smaller and not completely clean from char, because the injection point is retracted after a small time interval in order to prevent the high temperature combustion front to reach the production well. Around each injection point a cavity is developed, and based on the injection time at the same point the size of the cavities is becoming larger as receding from the production well. In the innermost section of each cavity the concentration of the char is zero and the amount of fluid porosity is the maximum value, only the incombustible solid components remaining; their values are increasing towards the boundaries of the coal seam so that an elliptic shape cavity is generally formed. Having zero concentration of char outside of the elliptic shape indicates that the pyrolysis front has not reached this section, the original coal remained intact, and the fluid porosity in this part has its lowest value which determines no coal consumption. **Fig. 3-6** shows each cavity in the three-dimensional view based on the fluid porosity range of 60-95%. **Fig. 3-7** demonstrates the elliptic shape which includes the whole affected volume of the coal seam by the combustion and gasification processes after a 50 *days* run of simulation.

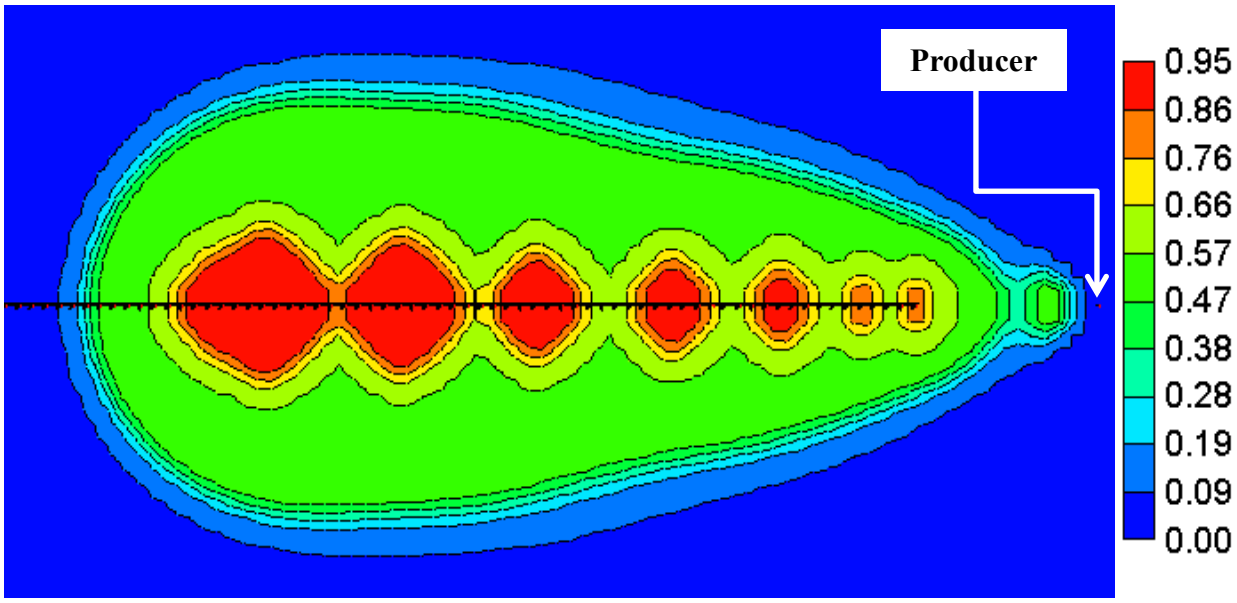

Fig. 3-4: Fluid porosity variation at the end of a 50 *days* run, x-y cross section

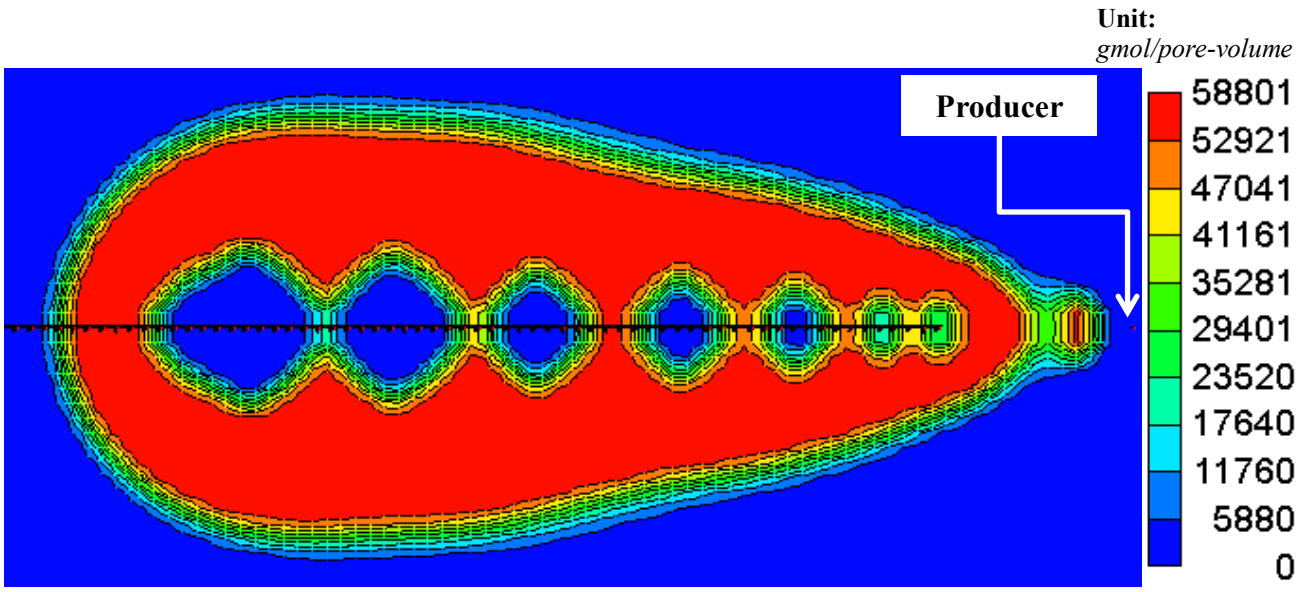

Fig. ȝ-5: Char concentration variation at the end of 50 *days* run, x-y cross section

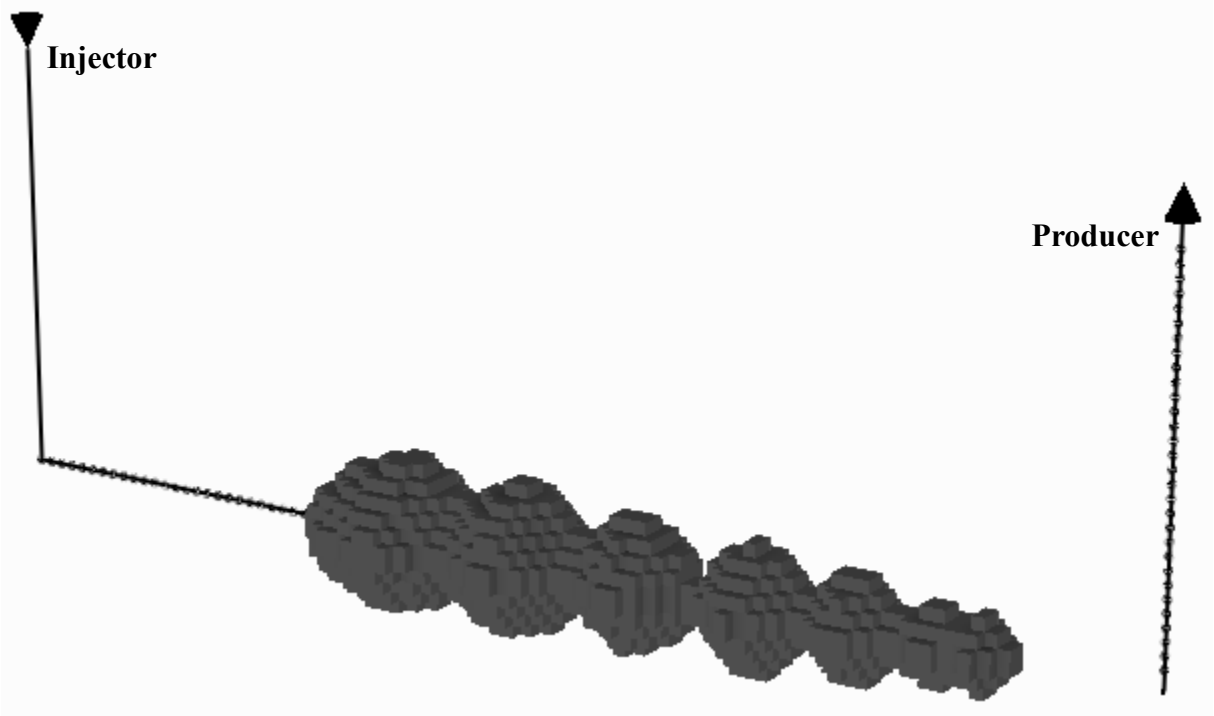

Fig. ȝ-6: Three-dimensional view of created cavities after 50 *days* of simulation

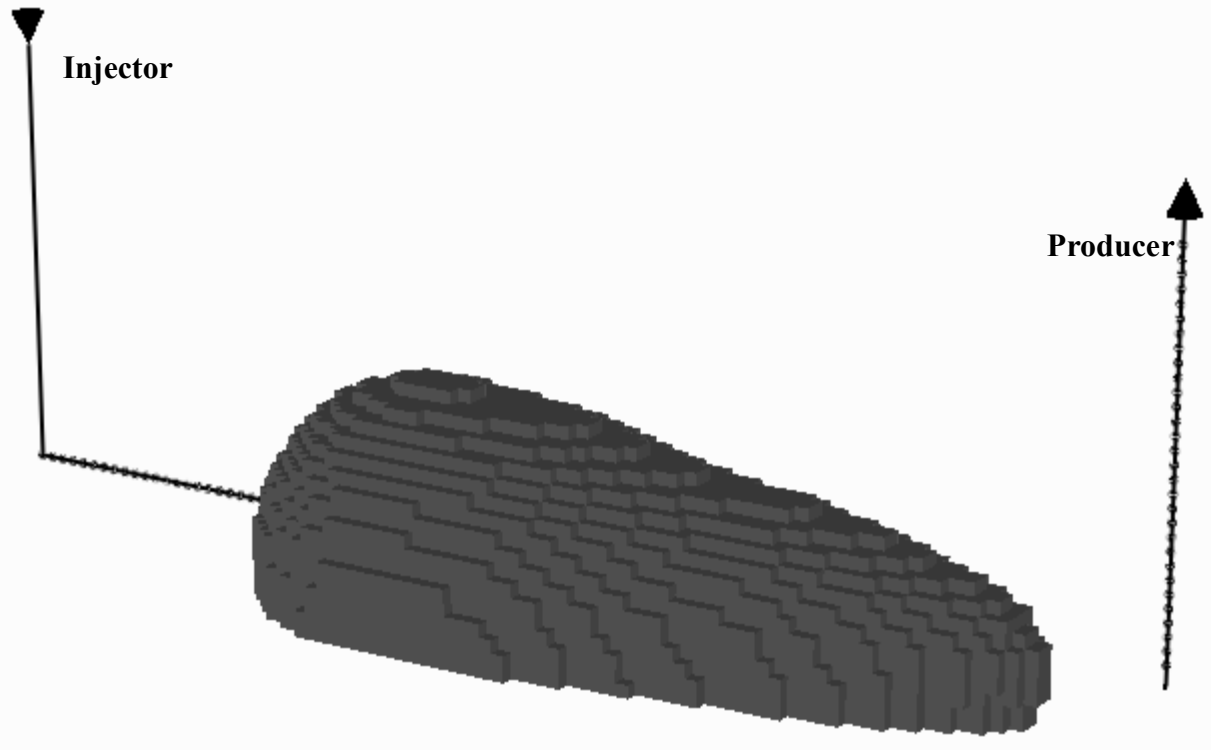

Fig. 3-7: Three-dimensional view of the elliptic form of the whole cavities after 50 *days* of simulation

Fig. 3-8 shows the flow rate of the different gas species during the 50 *days* run of simulation. As seen, except at the early time which includes the ignition process and generating heat to establish the combustion front, the production rate of all species behaves steady-state and this result conforms to those reported in the literature. Each hump indicates the formation of new cavity in which in addition to access of fresh coal, the intensity of reactions increases due to a lower effect of gas film resistance and more availability of oxidant agents. The more production of CH_4 at the early time is because of the original existence of the methane in the porous medium, and pyrolysis is the main source of the methane production at the late time. For an appropriately designed gasification reactor, the production of oxygen should be zero because having a large amount of oxygen production may cause explosion in the producer. In this model, all oxygen is consumed during the gasification.

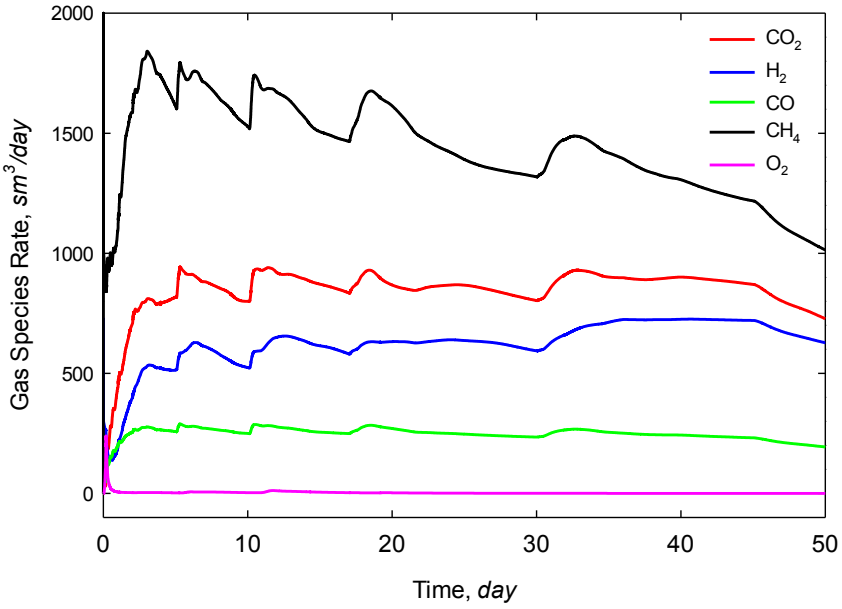

Fig. 3-8: Flow rates of different gas species during 50 *days* of simulation

The UCG process is composed of three chemical regions of drying, pyrolysis, and combustion and gasification. **Fig. 3-9** illustrates these regions qualitatively and quantitatively based on the temperature distribution. As seen, the most inner part with a temperature of around 995 $°C$ resembles the combustion front where the main chemical reactions of the UCG process take place. The second region with a temperature range of 250-800 $°C$ describes the pyrolysis region. Regions 3 and 4 illustrate the drying and original coal parts, respectively. **Fig. 3-10** shows the temperature profile for three different times along the well spacing in layer 31 where the injector is located. The width of plots increases with time, which indicates the increase of gasification length. The maximum temperature decreases with time due to more heat propagation through the coal seam and increasing of the length of the pyrolysis region. Two humps on each plot determine the combustion fronts on both sides of the cavity, which implies that the heterogeneous reactions take place on the sidewall of cavities and there is no spalling of char from the roof of the cavity as expected because the geomechanical mechanisms have not been included in the model.

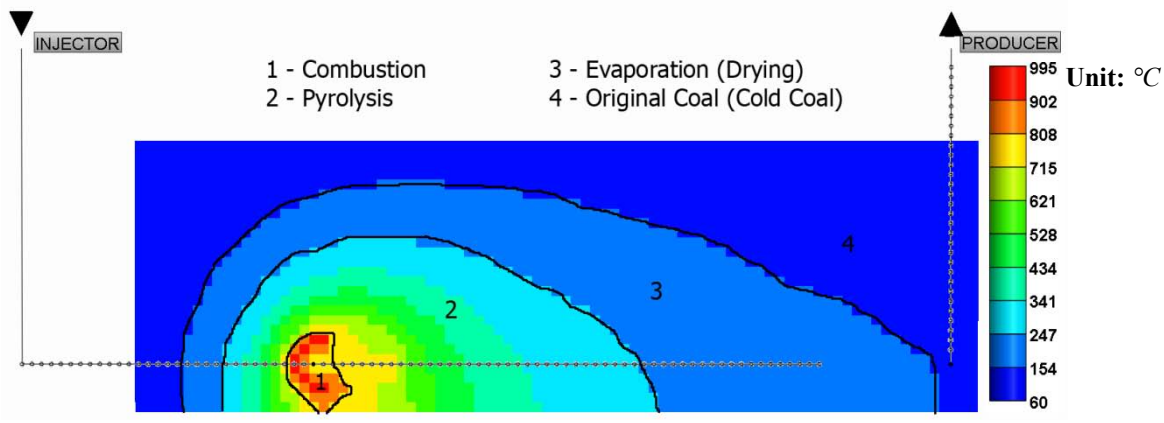

Fig. 3-9: Different chemical regions based on temperature profile

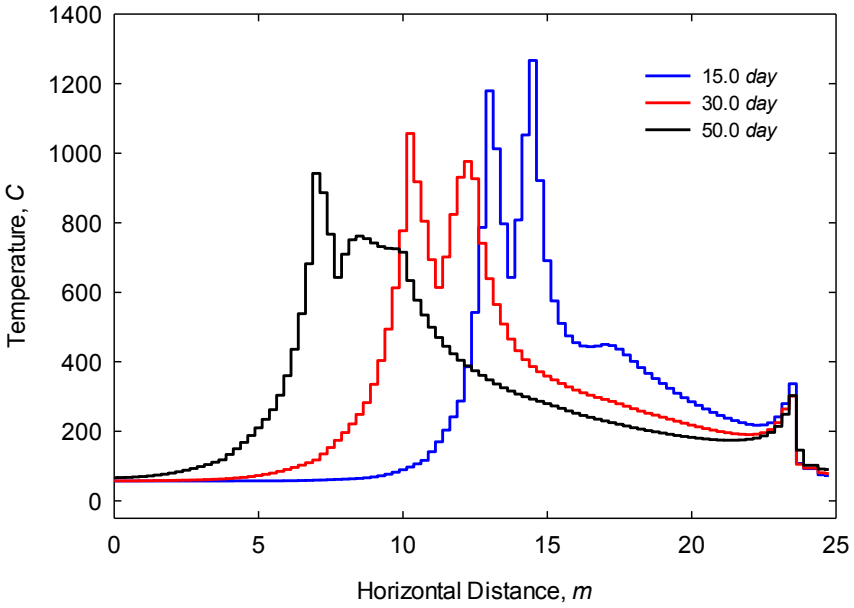

Fig. 3-10: Temperature variation along the length of the coal seam at different times

Figs. 3-11 and **3-12** depict the typical vertical solid concentration variation profiles at different times during the growth of the sixth cavity. As shown in **Fig. 3-11**, each char concentration plot begins from the zero value, indicating the consumption of produced char inside the cavity, and then gradually increases due to the pyrolysis process. It goes through a peak during maximum possible pyrolysis and then declines as the required temperature for pyrolysis decreases. Eventually, it reaches the zero value wherein, due to the lack of enough heat for pyrolysis, the

coal remains unaffected. The width of the char plots increases with time, which indicates that the combustion front (left side of the figure) moves slower than the pyrolysis front (right side of the figure), because heat conduction is faster than the mass transfer and in-situ reactions in this process.

Fig. 3-12 confirms the observations of **Fig. 3-11**. In this figure, each plot begins from the zero value of the coal concentration in which the coal is completely converted into char and then begins to increase after the corresponding maximum possible char concentration until reaching the initial concentration of coal where there is no char.

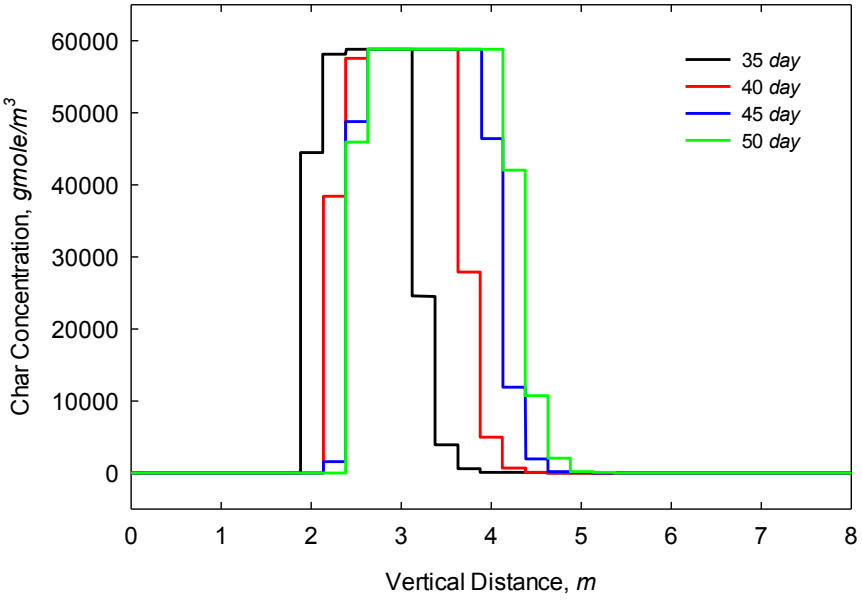

Fig. 3-11: Vertical char concentration profile in the sixth cavity at different times

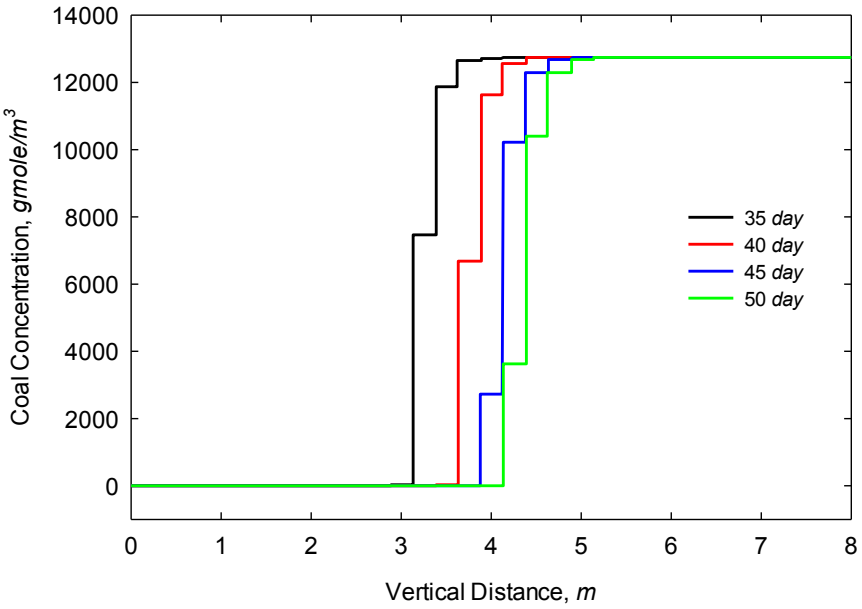

Fig. 3-12: Vertical coal concentration profile in the sixth cavity at different times

3.5 Conclusions

Three-dimensional numerical simulation of the UCG process has been performed by applying the CRIP technique in terms of a porous media flow approach. Despite of assuming constant thermal properties for solid components and water and also predicting the pyrolysis process with one reaction, the findings are physically reasonable and in consistent with those in the literature in the light of the syngas flow rate, cavity shape, and temperature profile. Addition of ash as a separate solid whose concentration changes during the gasification may improve the accuracy of the intensity of reactions and results. Including the condensation of steam and tar and also involving N_2, H_2S, C_2H_6, C_3H_8, and C_2H_4 in the released volatile matter during pyrolysis can predict the composition of species more accurately. A geomechanical module for UCG, including the modeling of spalling of rock and coal, is being developed by our group. With an appropriate coupling of the model developed in this paper and the geomechanical module, the UCG process can more accurately be simulated by using the porous medium approach, which will appear in a subsequent paper.

3.6 Nomenclature

C_i = Molar concentration of component *i*, mol/m^3

C_P = Compressibility, MPa^{-1}

C_T = Thermal compressibility, $°C^{-1}$

D_{ij} = Molecular diffusion coefficient of component *i* in phase *j*, m^2/sec

E = Activation energy, *kJ/mol*

G = Gravity, $9.81\ m/sec^2$

H_j = Enthalpy of phase *j*, *kJ/kg*

H_{rl} = Enthalpy of reaction *l*, *kJ/kg*

k = Absolute permeability, *md*

k_0 = Initial absolute permeability, *md*

HL_{cf} = Constant heat transfer model, *kJ/gmol*

HL_f = Conductive heat transfer rate to adjacent formations, *kJ/gmol*

HL_{vf} = Heat transfer rate calculated from a convective model, *kJ/gmol*

P = Fluid phase pressure, *MPa*

P_r = Reference pressure, *MPa*

q_{jk} = Injection/production flow rate of phase *j* in layer *k* of well, m^3/day

r_l = Rate of reaction *l*, day^{-1}

S_{il} = Stoichiometry coefficient of component *i* in the reactants of reaction *l*

S'_{il} = Stoichiometry coefficient of component *i* in the products of reaction *l*

S_j = Saturation of phase *j*, *fraction*

T = Temperature, *°C*

T_j = Transmissibility term of phase *j*, $T_j = (\frac{A}{\Delta l})(\frac{k_j}{\mu_j})$

T_r = Reference temperature, *°C*

U_j = Internal energy of phase *j*, *kJ/gmol*

V = Grid block volume, m^3

y_{ij} = Mole fraction of component *i* in phase *j*, *fraction*

Z = Depth, *m*

Greek Letters

κ = Reaction constant, day^{-1}

κ_0 = Pre-exponential factor (frequency factor), day^{-1}

μ_g = Gas viscosity, *cp*

ϕ_f = Fluid porosity, *fraction*

ϕ_v = Void porosity, *fraction*

ρ_j = Density of phase *j = g, w, solid component*, kg/m^3

Φ_j = Fluid potential, *MPa*

δ_{iw} = Mole fraction of component *i* in aquifer influx, *fraction*

Chapter 4 Application of Porous Medium Approach to Simulate UCG Process[3]

4.1 Abstract

Underground coal gasification (UCG) is a promising technique where coal is converted into valuable syngas in underground reactors developed in coal seams. This method is of paramount interest due to its lower cost, the ability to access coal at greater depths, and the utilization of oil and gas technologies and previously drilled wells to reach the coal seams. In this study, the main assumptions of a porous medium approach for the simulation of the UCG process are explained in detail. Moreover, the formula and procedure to obtain the required parameters through hydrocarbon reservoir simulators are presented. The proposed method is evaluated with three case studies. Computer Modelling Group's STARS software is used in this study.

Keywords Hydrocarbon Simulator, Modeling, Porous Medium, Pyrolysis, Self-gasification

4.2 Introduction

Underground coal gasification (UCG) is a technique for the utilization of coal reserves, particularly at great depths where mining is not economical. UCG is an in situ process that converts solid fuel to synthetic gas (syngas) in the presence of steam and oxygen. This process has only a modest environmental impact and produces an easily transportable product. The intended uses of this syngas include the production of electrical power and chemicals (Shirsat 1989; Yonggang et al. 2009).

UCG involves the gasification of coal in the seam by injecting oxidants through an injection well and extracting the syngas through a production well. The configuration of these wells implies different technologies, such as linked vertical wells, steeply dipping seams, linear controlled retracting injection point (CRIP), and parallel CRIP.

[3] M. Seifi, J. Abedi, and Z. Chen 2014. Application of Porous Medium Approach to Simulate UCG Process. *Fuel Journal* **116**: 191-200.

Due to the low permeability nature of the coal seams, the injection and production wells are linked by a channel, which can be developed with several proven techniques, such as reverse combustion, hydraulic fracturing, and directional drilling. Coal is then ignited around the injection point, producing a cavity as coal is combusted and gasified. In the area between the internal cavity surface and the original coal, several phenomena take place that control the heat and mass fluxes within the solid porous coal around the cavity. These phenomena include a gas film on the internal surface of the cavity, an ash layer on the cavity surface, pyrolysis, self-gasification, vaporization of the moisture content, and possible water inflow.

As shown in **Fig. 4-1**, the cavity itself can be divided into two parts: first, rubble material at the bottom of the cavity around the injection point, which may include ash, dry char and coal spalling and collapsing from the top of the cavity, and overburden materials; and second, void space on the top of the rubble materials, containing a gas mixture. In this void space, the temperature and concentration of the gas mixture may vary over time. As a result, there is a double-diffusive, turbulence-free convection flow that controls the transportation of the gaseous reactants from the bulk of the gas to the surface of the cavity (Massaquoi 1981; Perkins 2005; Yonggang et al. 2009).

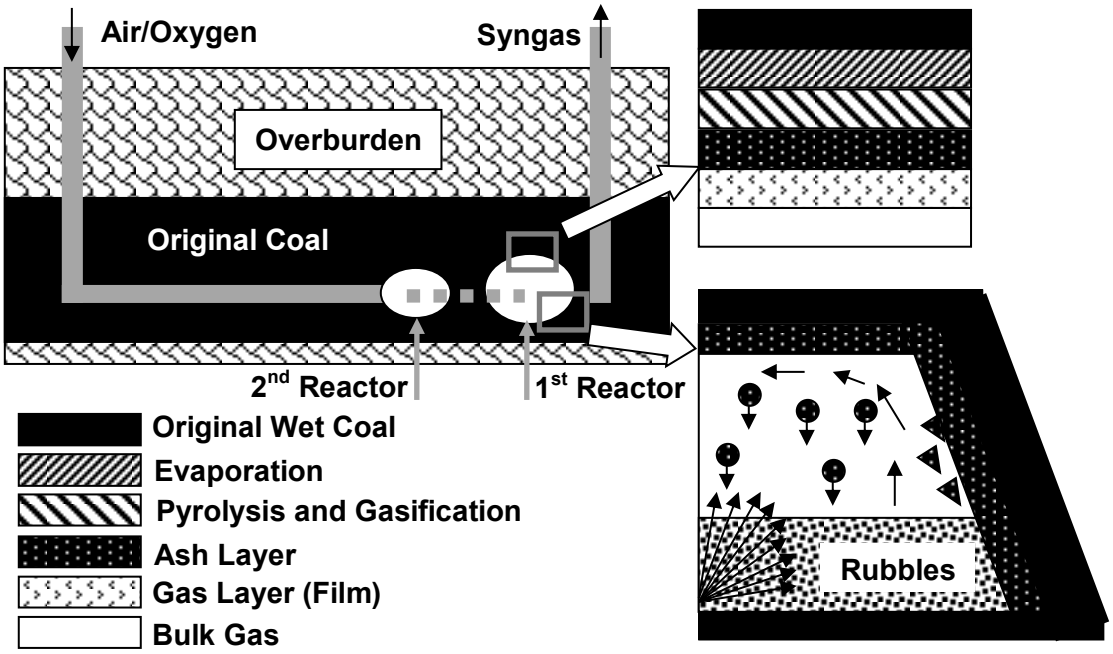

Fig. 4-1: Schematic of linear CRIP and underground cavities with relevant phenomena

UCG is a complex process; its modeling is crucial in order to understand the details of the process and the effect of different operating parameters on the objective parameters, such as the quality, rate and composition of the produced syngas, and the growth rate and shape of the developed cavity. For decades, researchers have been developing models to investigate specific aspects of this process. These models include the channel model, the packed bed model, the coal block model, and the process model.

Channel models assume a cylindrical coal seam with a channel in the middle with either a circular or rectangular cross section. The diameter of the internal channel can be fixed or variable. These models can be used to investigate the composition of the produced gas and the cavity growth rate through heterogeneous reactions. Packed bed models consider coal as a highly permeable dry or wet porous medium. These models are useful in the prediction of the composition of the product gas. In coal block models, wet or dry coal is assumed to have very low permeability in a one-dimensional (1D) semi-infinite domain. One side of this block is exposed to a mixture of gas mimicking the bulk gas mixture within the cavity and is ignited. This allows for the prediction of the rate of pyrolysis, the fire front advancement, and the temperature profile inside the coal ahead of the fire front. Process models are very simplified models used to investigate the effects of specific phenomena, such as water influx, spalling, and flow properties inside the cavity (Magnani 1973; Winslow 1977; Massaquoi 1981; Britten and Thorsness 1988; Batenburg 1992; Biezen 1996; Yang 2005; Pekins 2005).

All the current models in the literature are, however, small scale models and need to satisfy certain assumptions on the shape of the cavity, such as cylindrical or rectangular. In these models, the effects of different well configurations, coal seam geology and layering cannot be investigated, and large-scale simulation cannot be performed. Therefore, the application of hydrocarbon reservoir simulators for modeling of the UCG process has been proposed previously by the authors (Seifi et al. 2011).

Since oil and gas reservoirs have a different nature than that of coal seams, the major assumptions for the utilization of these porous medium based simulators for the UCG process are explained in this paper. A procedure and formulas are proposed to obtain the required information for the model from basic elemental and proximate analyses of coal and ash. The assumptions and procedure are evaluated with three case studies. The first case is the qualitative

evaluation of the model according to a heavy oil in situ combustion tube test. Case two matches the results of an analytical method for modeling of the pyrolysis process using this proposed method. Finally, case three is the simulation of the self-gasification experiment. The agreement between the results of the proposed simulation model and the analytical and experimental results confirms the validity of this method.

4.3 Simulation Domain Structure

The existence of a rock structure in hydrocarbon reservoirs is the major difference between coal seams and hydrocarbon reservoirs, particularly those of heavy oil. In coal seams, there is a large volume of very low porous coal that is composed of moisture, flammable material, and ash minerals. Since ash remains nearly intact at the end of the UCG process, it can be assumed that ash forms the rock structure of a porous medium simulation model. The moisture content of coal, therefore, resembles the initial water saturation of a hydrocarbon reservoir model; and, the flammable material is similar to the model's solid heavy oil content, which will undergo pyrolysis, gasification and combustion processes. **Fig. 4-2** illustrates this concept.

All the moisture content of coal is separated from the solid phase; hence, the flammable portion of the coal is assumed to be dry coal. With this approach, there is no evaporation phenomenon, which takes place in real field cases. Thus, to offset this deficiency, the evaporation of the water phase is considered in the proposed model. In addition, the pore volume is initially assumed to be filled with the moisture content of coal and gas, i.e., mostly methane (CH_4). Moreover, since ash is separated from the other solid materials to construct the rock network of the model, the solid fuel is considered to be on dry-ash-free (*daf*) basis.

Another approach is the assumption that the initial pore volume is only filled with gas and that the solid flammable material includes the moisture content of coal as well, i.e., wet coal. In this case, the moisture content must be released by an evaporation reaction in which wet coal is converted into steam and dry coal. The usual evaporation-condensation of water must be included as in the first approach.

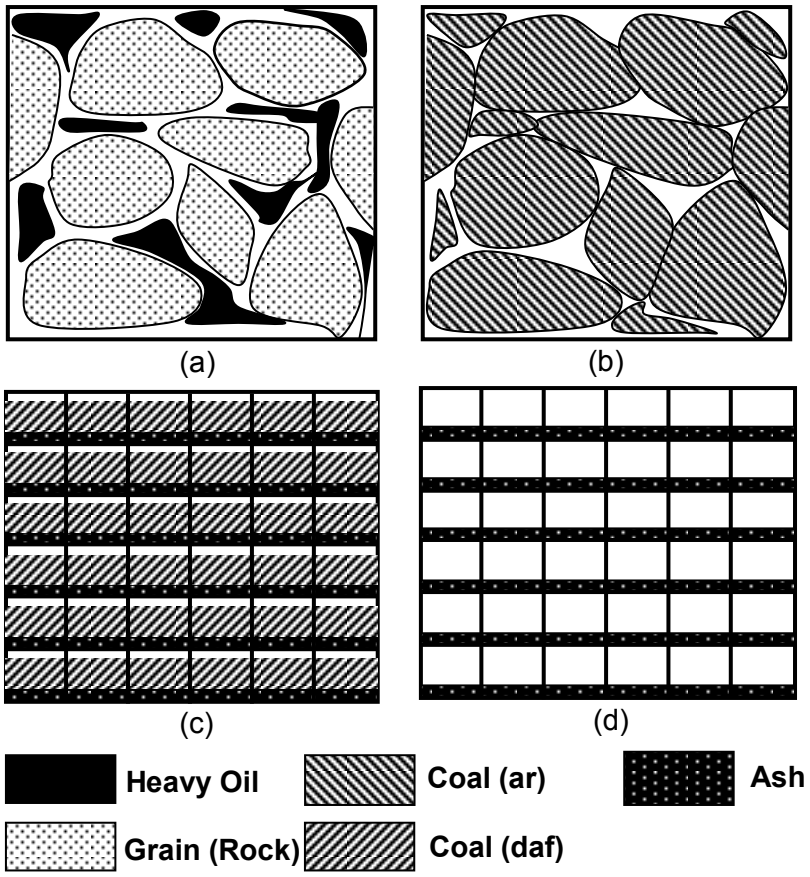

Fig. 4-2: Schematic of domain structures: (a) heavy oil reservoir, (b) coal seam, and (c) and (d) a coal seam in the simulation model before and after gasification and combustion, respectively

4.4 Seam Physical Properties

Due to the differences between the natures of coal seams and hydrocarbon porous media, there are several required physical parameters needed for simulation that have rarely been obtained experimentally; therefore, they must be calculated from the coal proximate and ultimate analyses based on the following approach. Some of these important parameters are the coal's molecular weight, the initial void porosity, and the initial concentration of coal in the unit pore volume of the seam, the initial coal solid density, and the initial char density. For simplicity, char is assumed to be a pure carbon, such as graphite, because char is the product of the pyrolysis process and consists of mostly carbon, depending on the rank of coal.

Using material and volume balances, a set of relationships has been developed to relate the results of the coal analysis tests and the required parameters for the simulation model. In this

procedure, it is assumed that the ash solid density, the water density at the initial coal seam conditions and the wet coal bulk density are known. The ash density can be obtained from elemental and ash analysis tests. Moreover, it is assumed that the initial pore volume is filled entirely with the coal moisture content. The latter assumption may introduce a very small inaccuracy due to the initial existence of gas, but due to very low initial porosity of the coal seam, it does not have a significant effect on the estimation of the properties. Equations (4-1) to (4-5) can be used to calculate the above properties.

$$MW_{daf\_coal} = \frac{100MW_C}{x_c} \tag{4-1}$$

$$\emptyset_V^o = 1 - \frac{x_{ash} \cdot \rho_{wc}^o}{\rho_a^o} \tag{4-2}$$

$$C_S^o = \frac{1000\rho_{wc}^o(1 - x_{H2O} - x_{ash})}{\emptyset_V^o . MW_{daf\_coal}} \tag{4-3}$$

$$\emptyset_f^o = \frac{\rho_{wc}^o . x_{H2O}}{\rho_{wat}^o} \tag{4-4}$$

$$\rho_{daf\_coal}^o = \left(\frac{\emptyset_V^o}{\emptyset_V^o - \emptyset_f^o}\right)\left(\frac{C_S^o . MW_{daf\_coal}}{1000}\right) \tag{4-5}$$

In cases where partings are dispersed in the coal and cannot be considered as a separate parting layer, the determination of the initial fluid porosity from experiments is necessary. The difference of this fluid porosity and the one calculated from equation (4-4) can then be deducted from the initial void porosity obtained with equation (4-2), which implies the addition of this amount to the rock volume. The initial coal content and coal solid density can then be recalculated with equations (4-3) and (4-5).

4.5 Fluid Properties

Generally, the coal pore volume is initially filled with water and gas, which is mostly composed of CH_4. During the simulation process, other gas components, such as carbon oxides, and hydrogen (H_2), are also introduced to the proposed model. Therefore, in addition to the initial properties of water and gas, some physical and thermal properties of other components must be entered into the model.

4.6 Case Studies

4.6.1 Case 1: Combustion Tube Test

The combustion tube test is an important test in the heavy oil in situ combustion process. The fuel type, the air requirement, the maximum temperature during the combustion process, and the rate of advance of the fire front can be obtained from this experiment. This information can be used either for pilot design or large-scale simulation. Due to the similarity of UCG to the heavy oil in situ combustion process, a 1D horizontal model has been developed using the above assumptions, in order to investigate the physical behavior of the model and generate the combustion tube results qualitatively. The domain was discretized into 100 grid blocks sized $5 \times 1 \times 1\ cm$. Oxygen (O_2) was injected into the first block, and syngas was produced from the last block. In order to initiate the ignition of coal, the injection block was heated for one day, and O_2 was then injected at a rate of 0.3 sm^3/day.

In this model, six gas components (H_2, O_2, CH_4, water (H_2O), carbon dioxide (CO_2), and carbon monoxide (CO) and two solid components (dry-ash-free coal and char) have been considered. The initial pressure and temperature were assumed to be 11.5 *MPa* and 60 *°C*, respectively, which are typical values of Alberta's coal seams at great depths. **Table 4-1** summarizes the results of the ultimate and proximate analysis of the coal used for this model. **Table 4-2** shows the applied eight first-order Arrhenius-type reactions in this model. They are the common reactions in a UCG process. The reaction kinetics was obtained from the literature (Green and Willhite 1998; Perkins 2005).

Table 4-1: Coal analysis results

Proximate Analysis (*ar, wt%*)		**Ultimate Analysis (*daf, wt%*)**	
Moisture	4.72	H	5.56
Ash	9.28	C	73.49
Volatile Matter	30.46	N	1.54
Fixed Carbon	55.54	S	0.52
		O	18.89
Total	**100.00**	**Total**	**100.00**

Table 4-2: Applied reactions in simulation model of Case 1 (Seifi et al. 2011)

Reaction Name	Reaction Formula	A_0	E_a, *kJ/mol*
Carbon Oxidation	$C + O_2 \rightarrow CO_2$	1.80E+06	100
Steam Gasification	$C + H_2O \rightarrow H_2 + CO$	4.70E+07	156
Boudouard	$C + CO_2 \rightarrow 2CO$	3.20E+10	249
Methanation	$C + 2H_2 \rightarrow CH_4$	1.56E+08	200
Pyrolysis	$daf_{coal} \rightarrow C, CO, CO_2, H_2, CH_4$	1.90E+14	180
Carbon Monoxide (CO) Oxidation	$CO + 0.5O_2 \rightarrow CO_2$	9.68E+12	247
Water-Gas Shift	$CO + H_2O \leftrightarrow CO_2 + H_2$	2.40E+05	12.6
Steam-Methane Reforming	$CH_4 + H_2O \leftrightarrow CO + 3H_2$	2.70E+07	30

Fig. 4-3 illustrates the typical temperature and solid concentration profiles. The temperature increased from the injection temperature to the oxidation temperature and then leveled off to the pyrolysis temperature, due to endothermic reactions. At the end, the temperature tended to be the original temperature of the seam. This temperature profile corresponds to the behavior of the heavy oil in situ combustion test. Before the maximum temperature, all the produced char was consumed by heterogeneous reactions; and, the char concentration then increased to the maximum level, where complete pyrolysis occurred. The reduction of the char concentration at a temperature around 500 $°C$ indicates the occurrence of partial pyrolysis. Beyond this point, the coal concentration increased to the initial value.

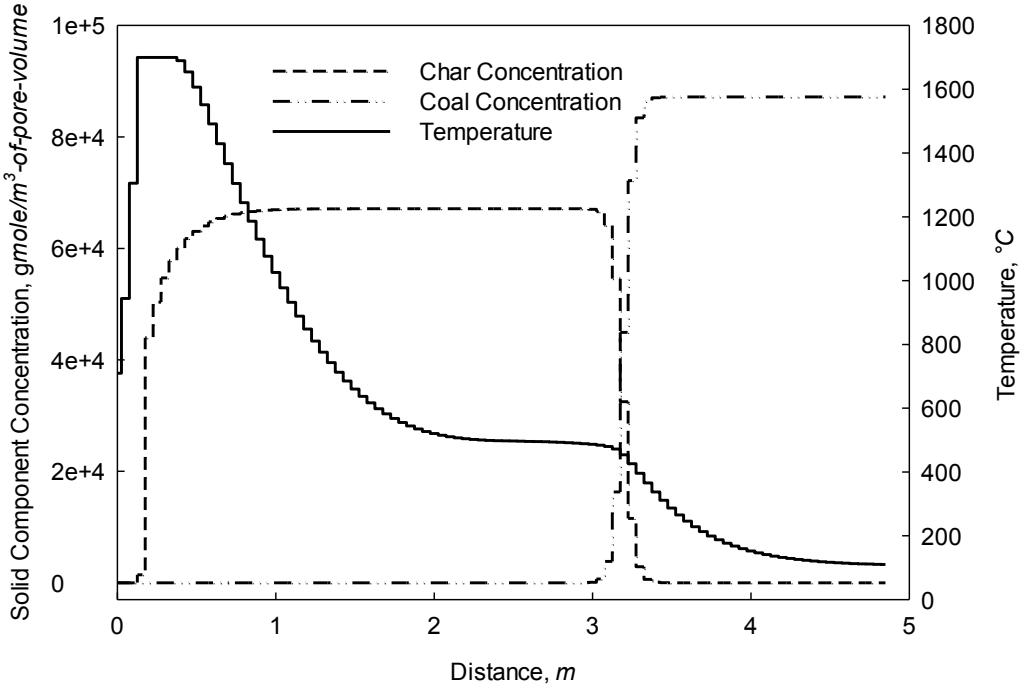

Fig. 4-3: Temperature and solid component concentration profiles at 2.5 *days*

As shown in **Fig. 4-4**, the mole fraction of CO_2 increased to a maximum at the highest temperature, due to the oxidation reaction, and then declined to zero, due to the Boudouard reaction. Carbon dioxide was also produced as a result of the pyrolysis process ahead of the fire front.

The volume-weighted thermal conductivity of the system was calculated according to equation (4-6). The drastic change in the combined thermal conductivity is an indication of variation in the solid content of the domain. When there was only ash as the solid component, the thermal conductivity began from a very small value, since the medium was filled with gas with lower thermal conductivity. The thermal conductivity increased to an intermediate value, when char also existed in the system. Finally, it reached a maximum value, corresponding to the original seam with the highest solid content.

$$k_{mix} = \emptyset_f.\left(k_w.S_w + k_g.S_g\right) + (1 - \emptyset_v).k_r + \left(\emptyset_v - \emptyset_f\right).k_s \tag{4-6}$$

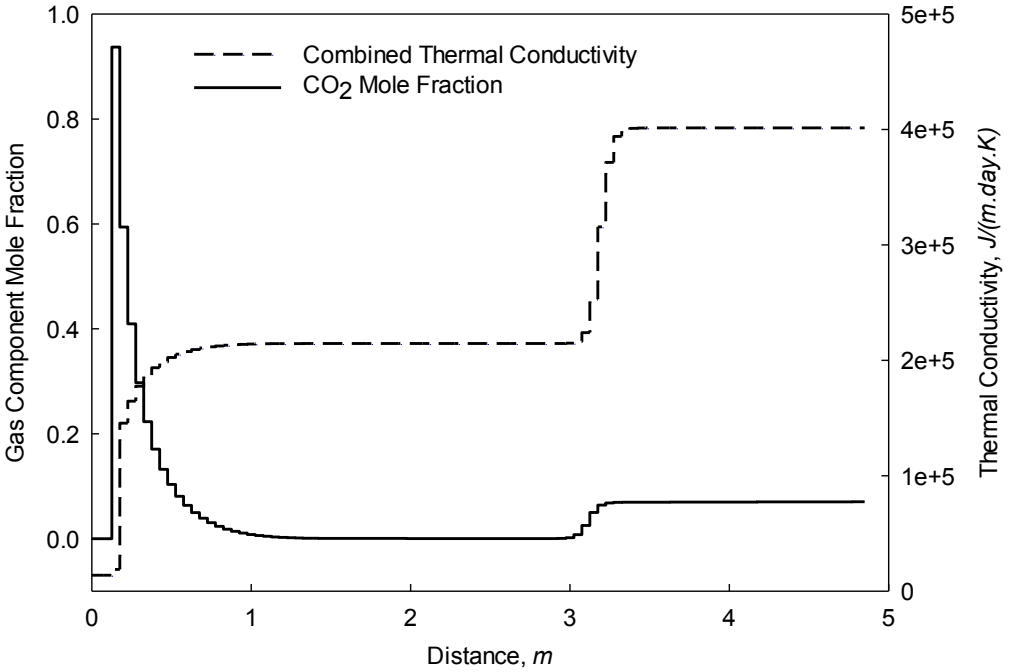

Fig. 4-4: Carbon dioxide and porous medium thermal conductivity at 2.5 *days*

The rate of advance of the fire front can be determined from the location of the maximum temperature and the maximum mole fraction of CO_2, as shown in **Figs. 4-5** and **4-6**, as these two parameters have their highest value at the location of the oxidation reaction. For the current configuration, the fire front advancement rate was approximately 15 *cm/day*.

Fig. 4-7 shows the coal concentration profiles at various times. The sharp increase in the coal concentration indicates the location of the pyrolysis front. Therefore, the rate of the pyrolysis front can be obtained from the coal concentration profile. For the current configuration, it was approximately 1 *m/day*.

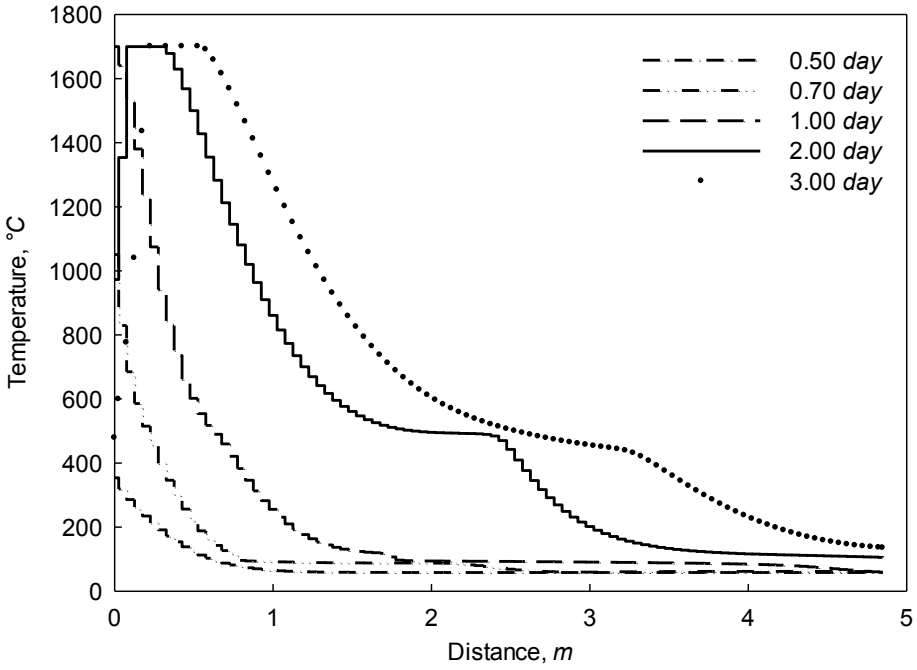

Fig. 4-5: Temperature profile at different times

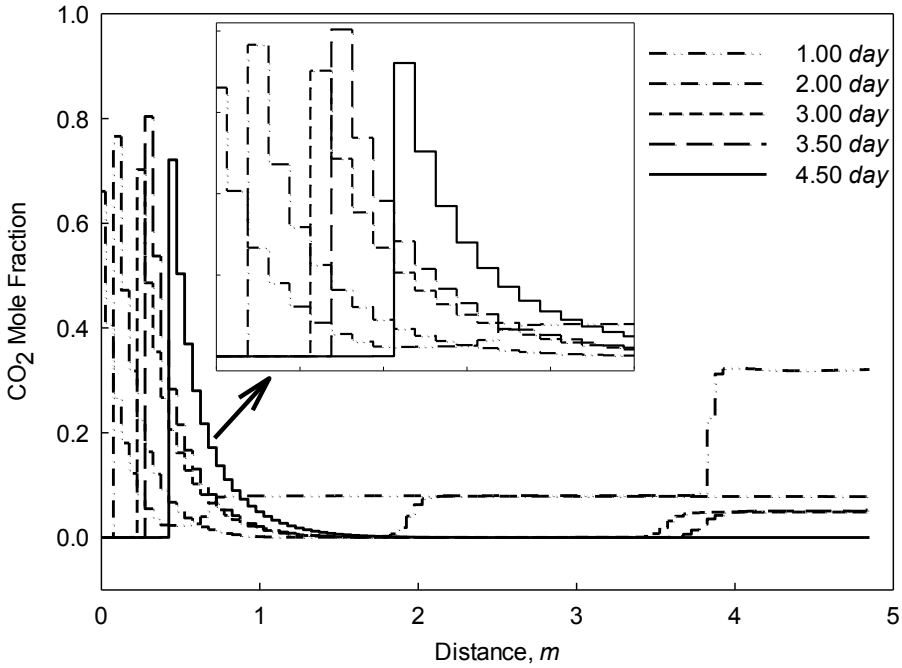

Fig. 4-6: Carbon dioxide mole fraction profile at different times

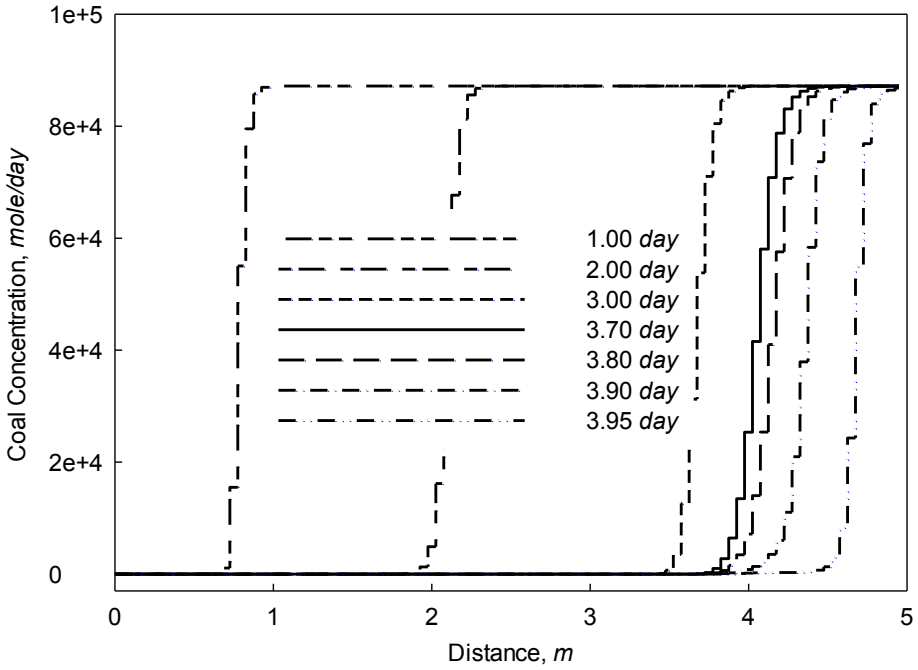

Fig. 4-7: Coal concentration profile at different times

4.6.2 Case 2: Simulation of Pyrolysis Process

The pyrolysis process is a complex thermal decomposition of coal in the absence of oxygen in the temperature range of 350 to 900 °*C*. During this process, coal is converted into low-molecular-weight gases, light hydrocarbons, and char. Each volatile matter is released from coal at different temperature ranges and rates. They also begin to evolve at different temperatures. Moreover, some species, such as CO_2 and CH_4, undergo several maximum rates of evolution, due to the cracking and carbonate decomposition reactions.

There are two widely applied methods to model pyrolysis. In the single-step decomposition method, the evolution of all species is modeled with only a single reaction. With the method of simultaneous-independent reactions for each species, it is assumed that the reactions are of the first order and Arrhenius type, the heating rate is constant, and the integral of the exponent term is approximated by equation (4-7). Therefore, the rate of evolution and cumulative amount of the i^{th} volatile matter released by time t can be obtained analytically by equations (4-8) and (4-9), respectively (Tsang 1980, Appendix 4-A).

$$\int_0^T exp\left(-\frac{E_{ai}}{RT}\right) dT \cong \left(\frac{RT^2}{E_{ai}}\right) exp\left(-\frac{E_{ai}}{RT}\right) \tag{4-7}$$

$$\frac{dm_i}{dT} = m_i^*.\frac{A_{0i}R}{\beta E_{ai}} exp\left(-\frac{E_{ai}}{RT}\right)\left(2T + \frac{E_{ai}}{R}\right).exp\left(-\frac{A_{0i}RT^2}{\beta E_{ai}} exp\left(-\frac{E_{ai}}{RT}\right)\right) \tag{4-8}$$

$$m_i = m_i^*.\left[1 - exp\left(-\frac{A_{0i}RT^2}{\beta E_{ai}} exp\left(-\frac{E_{ai}}{RT}\right)\right)\right] \tag{4-9}$$

In this section, the development of a simulation model for the modeling of the pyrolysis process using the two previously described methods and the matching of the results of the analytical method are presented. The simulation model included two blocks. The first block sized $5 \times 1 \times 1\ cm$ contained coal and a heater. The second block did not have coal, due to the temperature gradient effect. An injector was placed in the first block to inject nitrogen (N_2) as the carrier gas at a rate of 0.3 sm^3/day, and a producer was placed in the second block. Nine gas components – H_2O, CO, H_2, CO_2, CH_4, ethane (C_2H_6), propane (C_3H_8), ethylene (C_2H_4), and tar – were assumed to evolve during the pyrolysis process. Therefore, there were nine reactions in the model. The heating rate of 10 $°C/min$ was used for the analytical model. The properties of these components and relevant reactions are summarized in **Table 4-3** (Tsang 1980).

Table 4-3: Properties of components and pyrolysis reactions for Case 2 (analytical model)

Component	m_i^* gr i/gr coal	A_{0i} 1/sec	E_{ai} kJ/mol	MW_i gr/mol
CO	0.034300	1766	111.11	28.01
CO_2	0.066830	403.1	88.43	44.01
CH_4	0.028700	7.322E+04	135.61	16.043
C_2H_6	0.005310	1.667E+06	139.84	30.07
C_3H_8	0.002784	7.333E+06	146.54	44.097
C_2H_4	0.001540	2.333E+06	139.84	28.054
H_2	0.006670	20	93.37	2.016
H_2O	0.112370	0.11469	31.09	18.015
Tar	0.037890	0.11469	31.09	600

In this model, the reaction material balance must be honored; hence, nine pseudo-solid species have been defined with the same molecular weight as each volatile matter, so that in each

reaction this pseudo-solid species was converted into the corresponding volatile matter (CMG: STARS Technical Manual 2012).

Fig. 4-8 illustrates the variation of temperature in the first block of the simulation model and the experimental test. In this experiment, the heating rate and initial temperature were assumed to be 10 *°C/min* and 25 *°C*, respectively. The temperature was matched by changing the rate of heat injection, i.e., the heater rate. In the late part of the experiment, the solid content in the domain decreased, and the convection heat transfer played a dominant role; therefore, there was a poor temperature match.

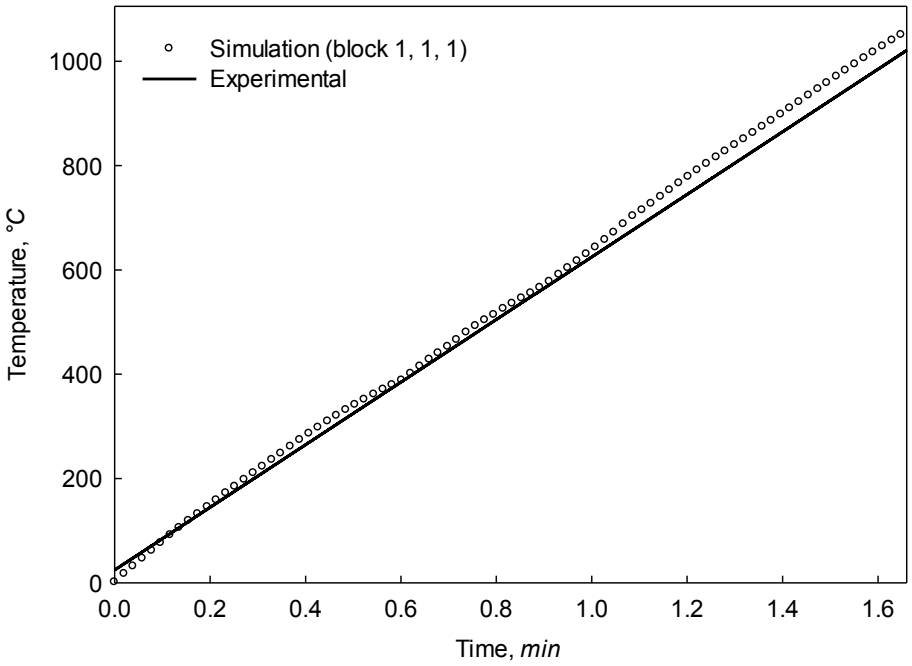

Fig. 4-8: Temperature comparison of the first block of the simulation model and the analytical model

The rate of evolution and cumulative released amount of each species are shown in **Figs. 4-9** and **4-10**. As can be seen, there was a good match between the simulation (dots) and analytical (solid lines) results. Moreover, this simulation model was able to precisely capture the onset of the evolution, the temperature range, and the maximum rate of evolution.

In the next step, pyrolysis was simulated using the single-step decomposition model for the same data set as listed in **Table 4-3**. The pyrolysis reaction was obtained using the elemental

balance, coal analysis results, and the ultimate recovery of gaseous species during pyrolysis process from Tables II-2 and II-3 of Tsang (1980):

$$\boldsymbol{coal(daf)} \rightarrow 0.583598\boldsymbol{C} + 0.029229\boldsymbol{CO} + 0.036245\boldsymbol{CO_2} + 0.042700\boldsymbol{CH_4}$$
$$+ 0.004215\boldsymbol{C_2H_6} + 0.001507\boldsymbol{C_3H_8} + 0.001310\boldsymbol{C_2H_4} + 0.078971\boldsymbol{H_2}$$
$$+ 0.148884\boldsymbol{H_2O} + 0.001502\boldsymbol{Tar}$$

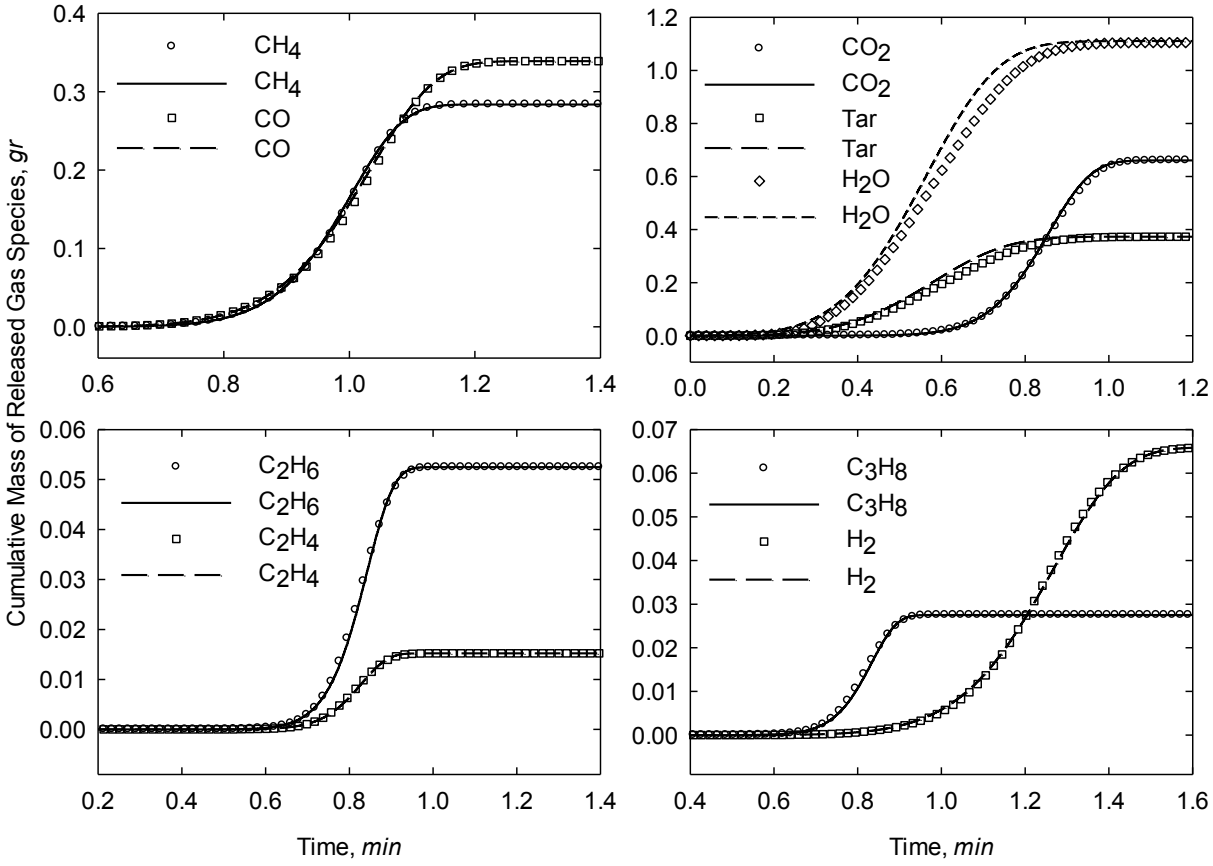

Fig. 4-9: Comparison of cumulative mass of produced gas species during pyrolysis process for analytical (lines) and simulation (symbols) results using simultaneous-independent reactions model

Fig. 4-11 shows a very good match for temperature. However, as can be seen in **Figs. 4-12** and **4-13**, the cumulative amount of the species and the rate of evolution did not match with the analytical model. Moreover, all species began to evolve at the same temperature and range of temperatures. This is due to the use of only single activation energy for the evolution of all volatile matters during the complex pyrolysis process.

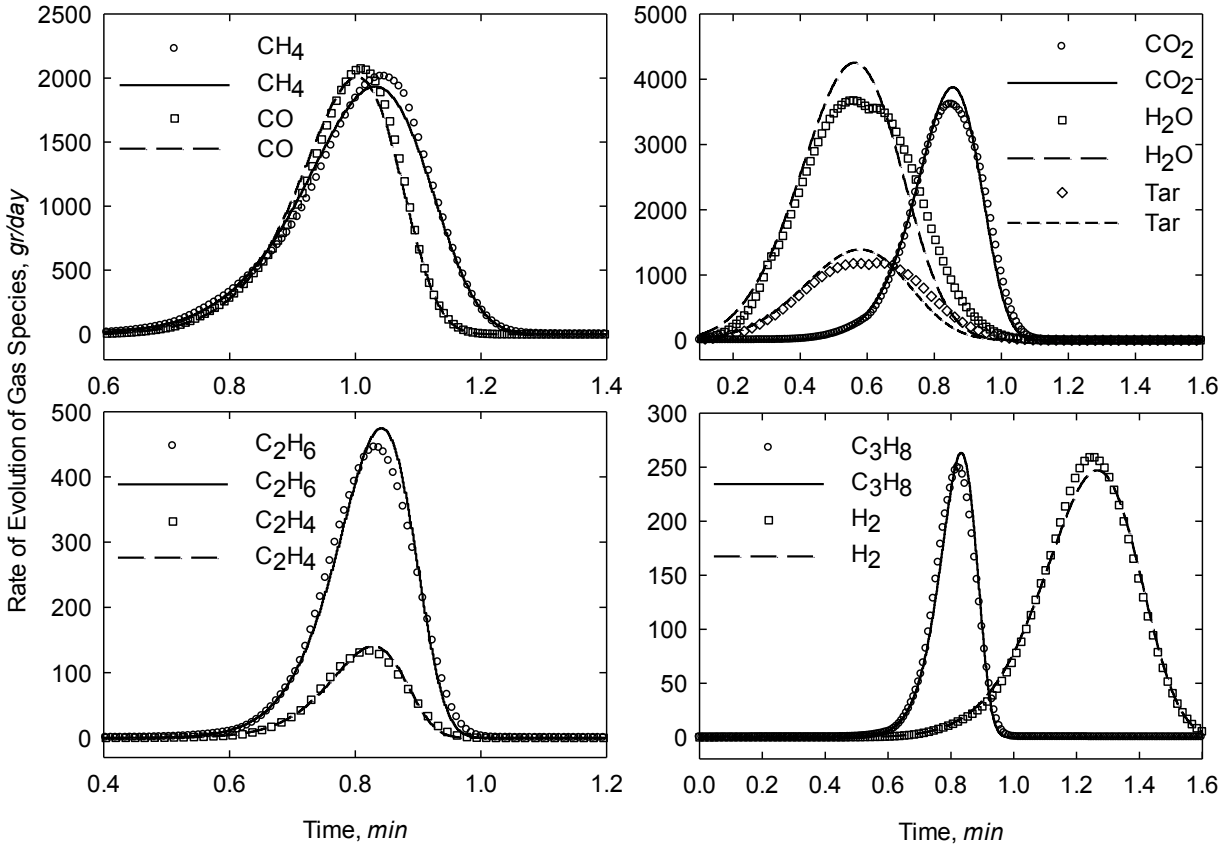

Fig. 4-10: Comparison of rate of evolution of gas species during pyrolysis process for analytical (lines) and simulation (symbols) results using simultaneous-independent reactions model

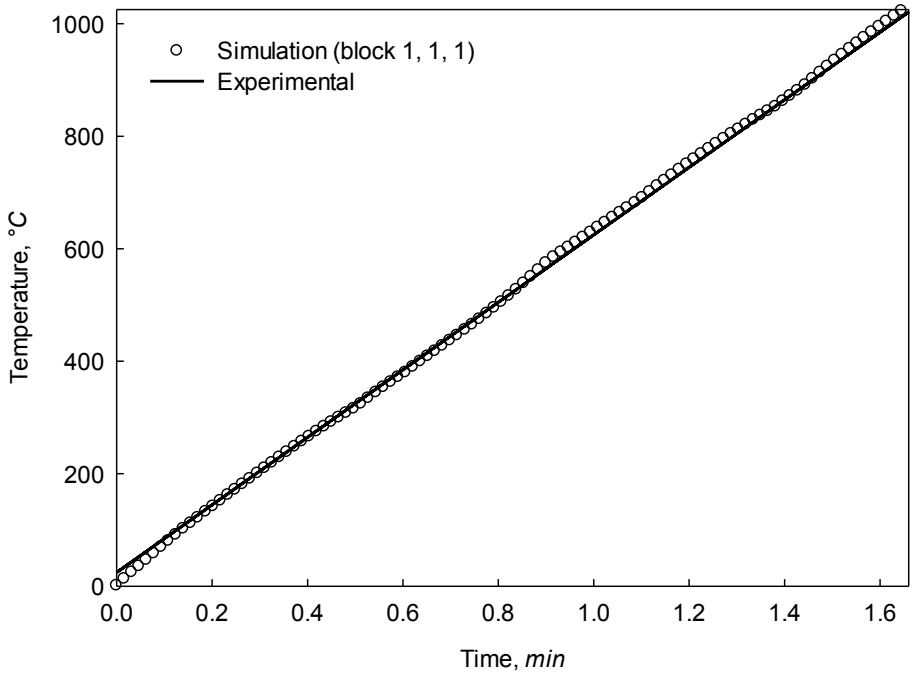

Fig. 4-11: Temperature comparison in the first block of the simulation model (single-step decomposition) and the analytical model

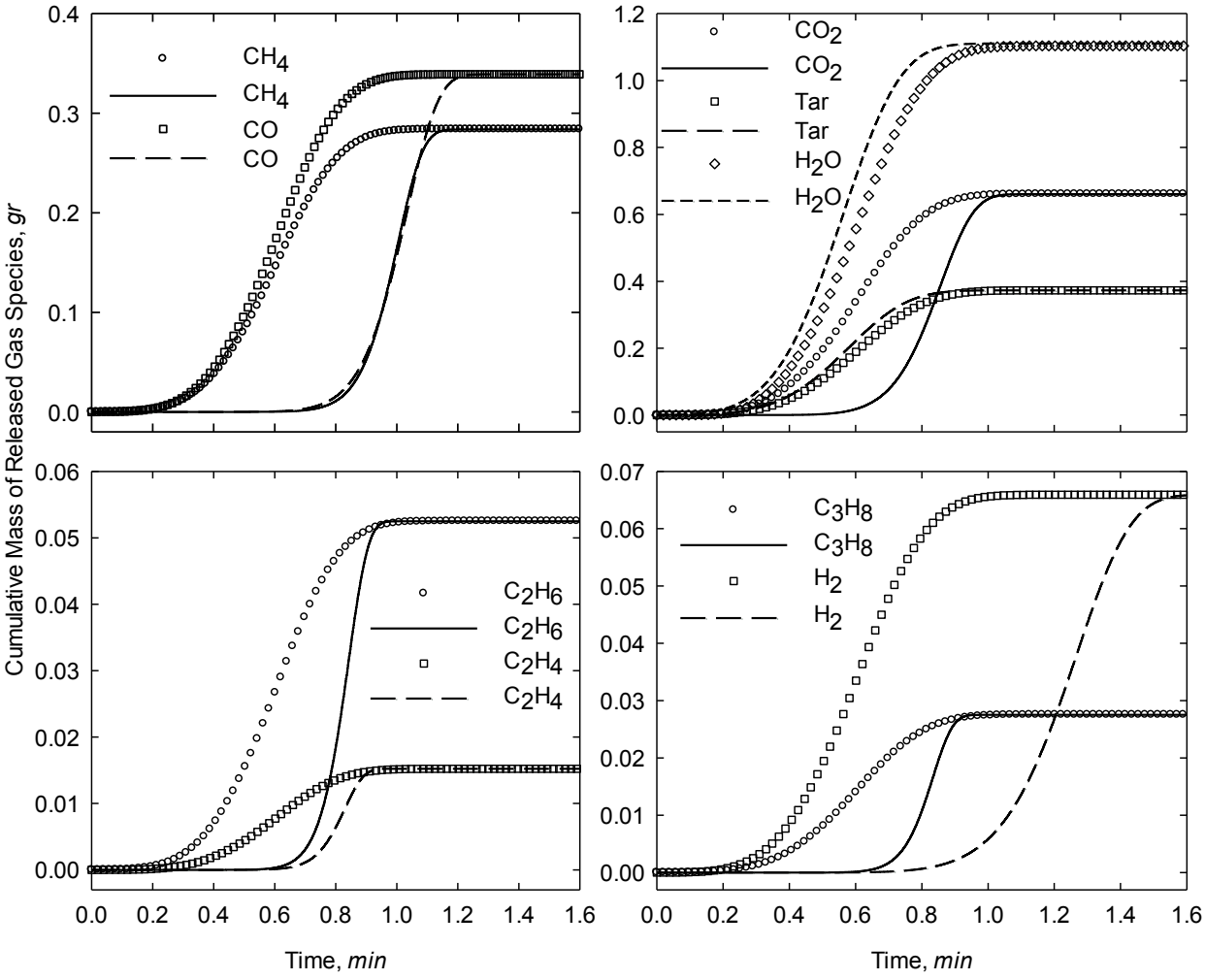

Fig. 4-12: Comparison of cumulative produced gas species during pyrolysis process for analytical (lines) and simulation (symbols) results applying single-step decomposition model

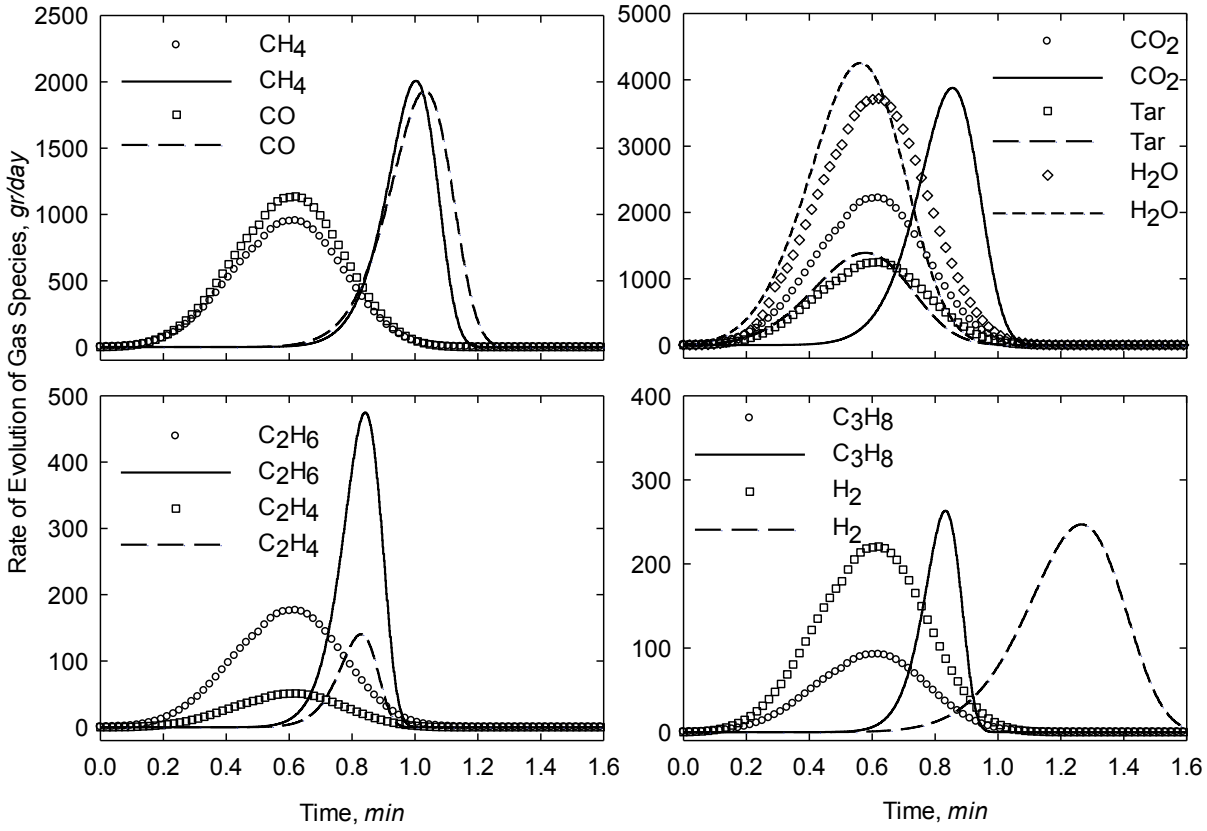

Fig. 4-13: Comparison of rate of produced gas species during pyrolysis process for analytical (lines) and simulation (symbols) results applying single-step decomposition model

4.6.3 Case 3: Simulation of Self-Gasification Experiment

In this section, a description of the simulation of the self-gasification experiment is provided. As shown in **Fig. 4-14**, the external surface of a vertical cylindrical coal core with a diameter of 20 *cm* and a height of 15 *cm* was heated at a heating rate of 0.05 *°C/sec* at the atmospheric pressure. As a result of the heat conduction, the moisture content of the coal evaporated, and pyrolysis took place within the coal. Thus, the heat flowed from the outer surface into the center of the coal; and, there was a mass flux towards outside of the coal. Therefore, both the drying and pyrolysis fronts advanced towards the center of the core. N_2 was used as the carrier gas to sweep away the volatile matter. In this experiment, the temperature was recorded at different locations and times (Forrester 1979; Tsang 1980).

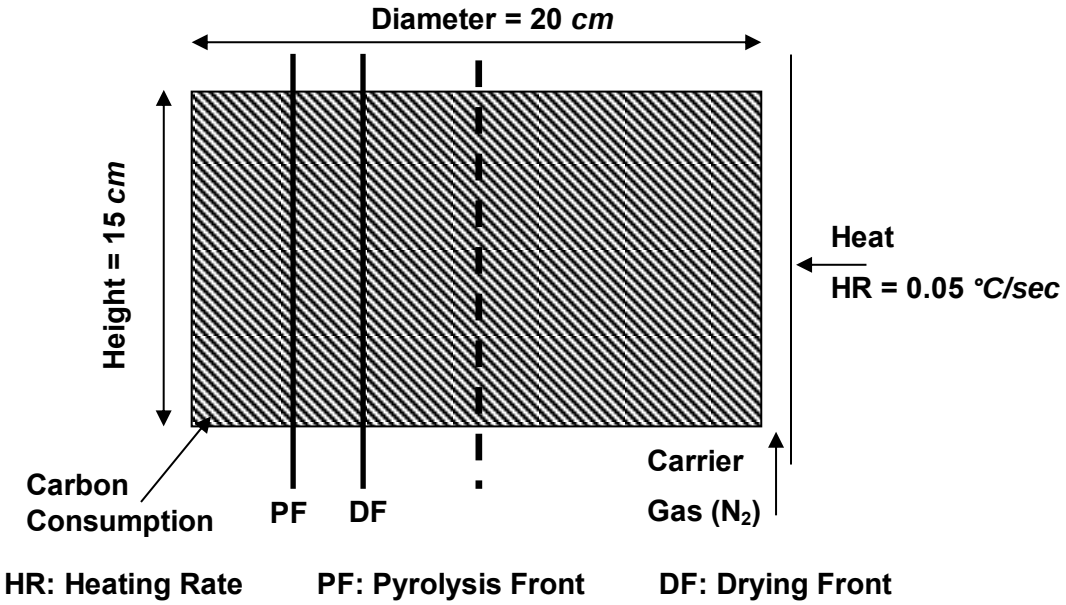

Fig. 4-14: Schematic of the experiment of coal self-gasification

To simulate this experiment, a cylindrical model with the same dimensions was developed in Computer Modelling Group Inc.'s STARS simulation software. The producer and injector were placed in the most outer block. A heater was used in this block to provide the heat requirement. Pyrolysis was modeled by the simultaneous-independent reactions method. Steam gasification, Boudouard, methanation, and water-gas-shift reactions were applied in this model, according to **Table 4-2**. The temperature was matched by changing the heat injection rate of the heater.

Fig. 4-15 illustrates the temperature profiles from the center of core to its surface at different times based on surface temperature. As can be seen, there was a good agreement between the simulation and experimental results. Since this experiment was conducted at the atmospheric pressure, the saturation temperature of water was about 100 °*C*. Thus, the deviation of the temperature from 100 °*C* is an indication of the location of the vaporization front, which moves towards the center of the core.

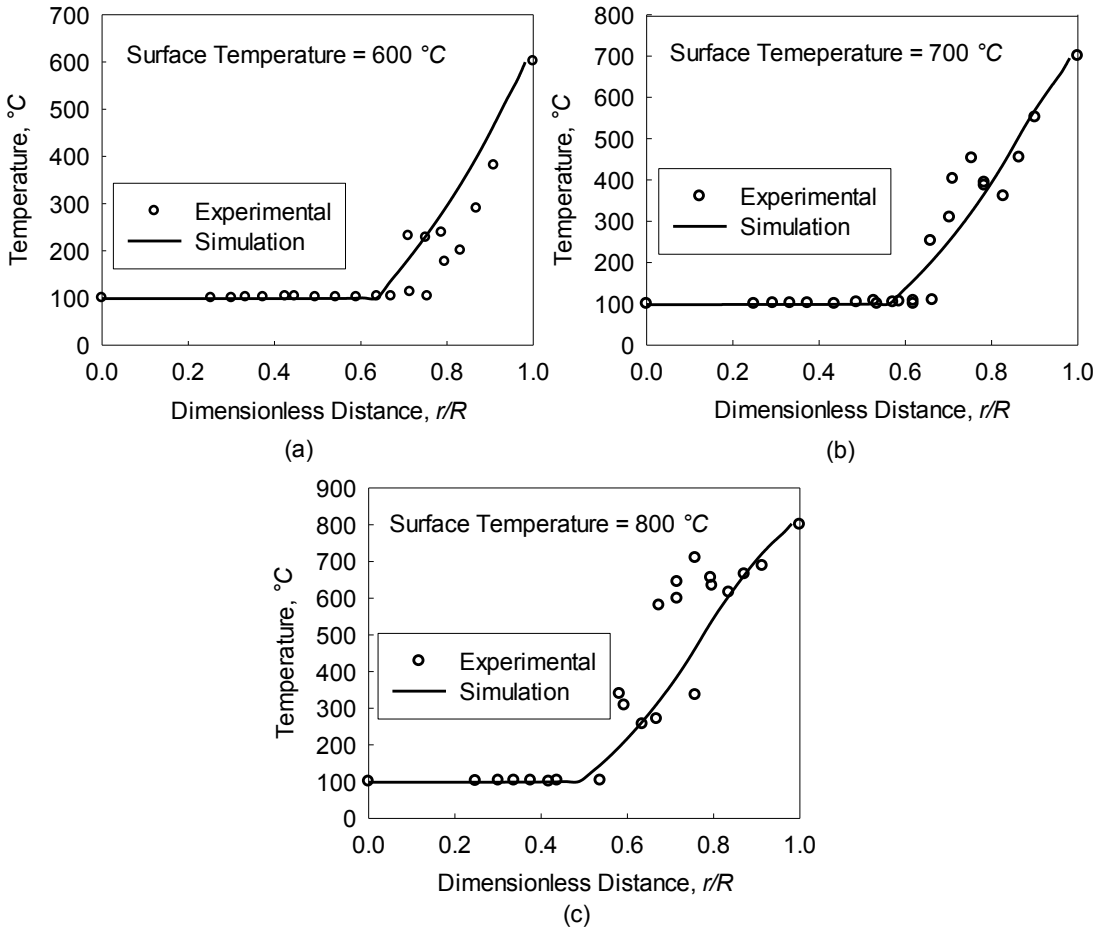

Fig. 4-15: Temperature profile at times when the surface temperature was: (a) 600 °C, (b) 700 °C, and (c) 800 °C

Temperature increased from the drying front towards the surface where the heater was located. In this region, the pyrolysis process took place. Since pyrolysis was modeled using the simultaneous-independent reactions method, each species has its own evolution onset temperature. Therefore, the pyrolysis front can be investigated according to the evolution of each species, as shown in **Fig. 4-16**. The tar front at time 3.5 *hours* was faster than that of the other species, which indicates that the activation energy for tar was less than the others and caused the early evolution of tar, although its frequency factor was significantly smaller. On the other hand, the hydrogen front was the slowest one, due to its larger activation energy and small frequency factor for hydrogen evolution, which implies that hydrogen evolved at a higher temperature. The pyrolysis front for light hydrocarbon gases and carbon oxides were almost at the same order of magnitude; hence, these species began to evolve at approximately the same temperature.

Fig. 4-17 shows the variation of permeability and porosity with temperature from the center of core towards its surface at different times. As can be seen, the porosity and permeability increased from the location of the drying front towards the surface of the core. The sharp changes in these parameters were an indication of partial and complete pyrolysis regions, as this was where they obtained their highest values. However, due to the existence of char and hot volatile matter, heterogeneous reactions, such as steam gasification and Boudouard reactions, become active close to the surface of the core. This process is called self-gasification, in which char is gasified by the species released during the pyrolysis and vaporization processes. Self-gasification causes an increase in the porosity and permeability of the core near its surface where solid materials, such as carbon, are consumed. Therefore, the highest porosity and permeability during self-gasification is on the surface of the core.

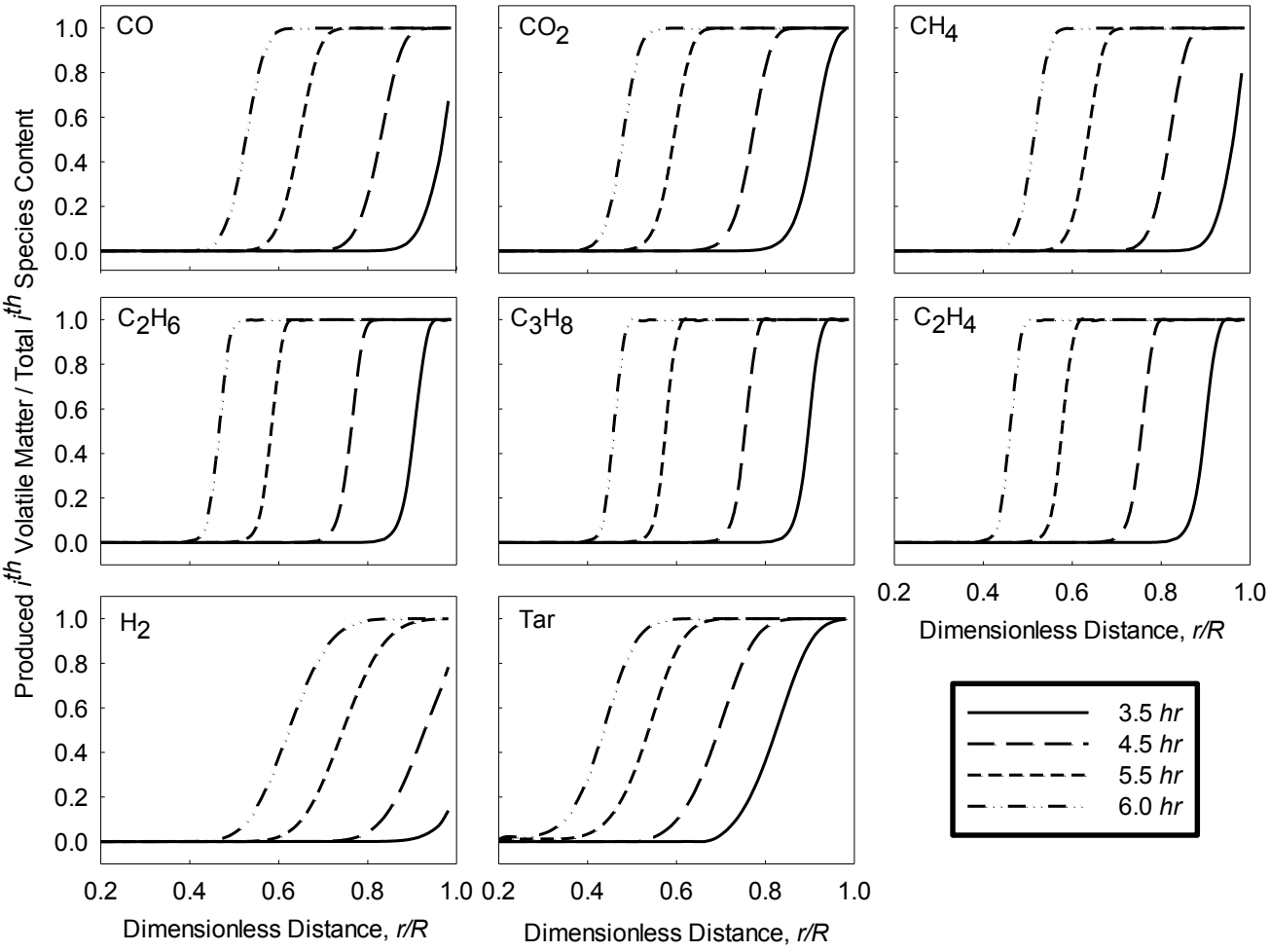

Fig. 4-16: Profile of the fraction of the cumulative evolved species from coal

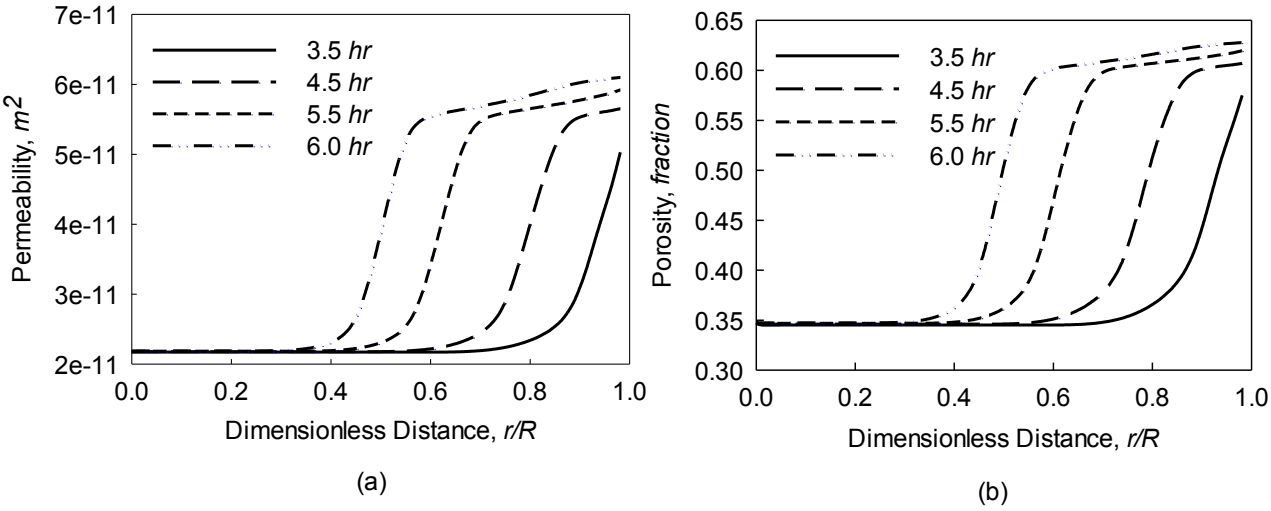

Fig. 4-17: Profiles of (a) permeability, and (b) porosity at different times

4.7 Conclusions

This paper proposed a procedure to obtain the physical properties of the solid materials required by porous medium simulators from the basic elemental and proximate analyses of coal. This procedure and relevant assumptions and proposed workflow to build the structure of the domain were evaluated through the simulation of three processes, i.e., the combustion tube test, pyrolysis, and self-gasification. The acceptable agreement of the results of the simulation, the analytical method and the experiment emphasized the reliability of the proposed procedure and assumptions. Moreover, it can be concluded that the developed numerical simulation model for the pyrolysis process can be used to match the experimental data to obtain the kinetics of the evolution of each species. This is important for cases where cracking and carbonate decomposition phenomena are significant, because the analytical model does not consider these reactions. In addition, in spite of the greater accuracy of the simultaneous-independent reactions method compared to the single-step decomposition method for modeling of the pyrolysis process, the former method can be very expensive in large-scale simulations of the UCG process using the porous medium approach, due to the requirement of a large number of components and reactions in the simulation model.

4.8 Nomenclature

A_0 = Frequency factor, *variable unit*

A_{0i} = Frequency factor of evolution of i^{th} species, *1/sec*

C_S^o = Initial coal concentration (daf basis), *mol/m³ pore volume*

E_a = Activation energy, *kJ/mol*

E_{ai} = Activation energy of evolution of i^{th} species

k_g = Thermal conductivity of gas mixture, *J/m-day-K*

k_r = Thermal conductivity of rock (ash), *J/m-day-K*

k_s = Thermal conductivity of solid fuel (char and coal), *J/m-day-K*

k_w = Thermal conductivity of water, *J/m-day-K*

m_i = Cumulative amount of i^{th} volatile matter released by time *t*, *gr*

m_i^* = Initial amount of i^{th} volatile matter can be released during pyrolysis, *gr*

MW_C = Carbon (char) molecular weight, *kg/mol*

MW_{daf_coal} = Dry-ash-free (daf) coal molecular weight, *gr/mol*

MW_i = Molecular weight of species *i*, *gr/mol*

R = Gas constant, *8.314 J/mol-K*

T = Temperature, *K*

x_{ash} = Mass percentage of coal ash content

x_{H2O} = Mass percentage of coal moisture content

Greek Letters

β = Heating rate, *°C/min*

ρ_a^o = Initial ash solid density, *kg/m³*

ρ_{wat}^o = Water density at coal seam initial condition, *kg/m³*

ρ_{wc}^o = Initial wet coal bulk density, *kg/m³*

$\emptyset_f$ = Fluid porosity

$\emptyset_f^o$ = Initial fluid porosity

$\emptyset_v$ = Void porosity of the system

$\emptyset_V^o$ = Initial void porosity

4.9 Appendix 4-A: Analytical Modeling of Pyrolysis Process Using Simultaneous-Independent-Reactions Method

Simultaneous independent reactions method assumes a separate reaction for evolving of the individual species from coal during pyrolysis process, equation (4-A.1). It also assumes that the coal is heated linearly during pyrolysis process with the heating rate of β, $T = \beta t + T_o$, and the rate of evolution of each species is proportional to the remaining amount of the species in the coal, $m_i^* - m_i$, where m_i^* is the maximum amount of species *i* that can be evolved from coal during pyrolysis and m_i is the cumulative amount of species *i* released by time *t*, first-order reactions. The proportionality parameter is Arrhenius type reaction constant, equation (4-A.2).

$$coal \rightarrow VM_i \tag{4-A.1}$$

$$\frac{dm_i}{dt} = A_{0i} exp\left[-\frac{E_{ai}}{RT}\right](m_i^* - m_i) \tag{4-A.2}$$

Since $\frac{dT}{dt} = \beta$, equation (4-A.2) can be rewritten as equation (4-A.3) which can be integrated as shown in equations (4-A.4) and (4-A.5).

$$\frac{dm_i}{dT} = \frac{A_{0i}}{\beta} exp\left[-\frac{E_{ai}}{RT}\right](m_i^* - m_i) \tag{4-A.3}$$

$$\int_0^{m_i} \frac{d\omega_i}{\omega_i^* - \omega_i} = \frac{A_{0i}}{\beta} \int_{T_0}^{T} exp\left[-\frac{E_{ai}}{R\theta}\right] d\theta \tag{4-A.4}$$

$$ln\left(\frac{m_i^*}{m_i^* - m_i}\right) = \frac{A_{0i}}{\beta} \int_{T_0}^{T} exp\left[-\frac{E_{ai}}{R\theta}\right] d\theta \tag{4-A.5}$$

Applying the estimation of (4-A.6) for the right hand side integral of equation (4-A.5) will obtain the cumulative amount of volatile matter *i* released from coal during pyrolysis process by time *t* at temperature *T*, equation (4-A.7).

$$\int_{T_0}^{T} exp\left[-\frac{E_{ai}}{R\theta}\right] d\theta \cong \left(\frac{RT^2}{E_{ai}}\right) exp\left[-\frac{E_{ai}}{RT}\right] \tag{4-A.6}$$

$$m_i = m_i^*.\left[1 - exp\left(-\frac{A_{0i}RT^2}{\beta E_{ai}} exp\left(-\frac{E_{ai}}{RT}\right)\right)\right] \tag{4-A.7}$$

The rate of evolution of individual species can be obtained by taking the derivative of equation (4-A.7) with respect to temperature and multiplying by the heating rate, β, equation (4-A.8).

$$\frac{dm_i}{dt} = m_i^*.\frac{A_{0i}R}{E_{ai}} exp\left(-\frac{E_{ai}}{RT}\right)\left(2T + \frac{E_{ai}}{R}\right).exp\left(-\frac{A_{0i}RT^2}{\beta E_{ai}} exp\left(-\frac{E_{ai}}{RT}\right)\right) \tag{4-A.8}$$

4.10 Appendix 4-B: Supplementary Material (Porous Medium Model – Governing Equations)

For investigation of the geochemistry behavior of coal gasification, the momentum balance law for determination of the flow velocity, the mass conservation law for composition prediction, and the energy conservation law for temperature profile prediction are generally considered. In the model, the momentum conservation is approximated by Darcy's law due to the porous medium approach used, and all conservation equations are defined in three-dimensional spaces as follows. The radiation effect between incandescent coal surfaces and gas molecules is ignored in the heat transport phenomenon.

The momentum balance equation is (CMG: STARS Technical Manual 2009)

$$\overrightarrow{v_g} = -\frac{k_g}{\mu_g}\left(\overrightarrow{\nabla p} - \rho_g g \overrightarrow{\nabla Z}\right) \tag{4-B.1}$$

The mass balance equation for flowing component *i* is (CMG: STARS Technical Manual 2009)

$$\overbrace{\sum_{l=1}^{n_b}\sum_{j=1}^{n_p}\phi_f D_{ij}\rho_j \Delta y_{ij}}^{(A)} + \overbrace{\sum_{l=1}^{n_b}\sum_{j=1}^{n_p} T_j \rho_j y_{ij} \Delta\Phi_j}^{(B)} + \overbrace{V_{bi}\sum_{m=1}^{n_r}(S'_{mi} - S_{mi})}^{(C)} r_m + \underbrace{\sum_{j=1}^{n_p}\rho_j q_{jk} y_{ij}}_{(D)} + \underbrace{\delta_{iw}\sum_{l=1}^{n_{aqb}}\rho_w q_{aq_{wl}}}_{(E)} = \underbrace{\left(\frac{V_{bi}}{\Delta t}\right)\left(\left(\phi_f \sum_{j=1}^{n_p}(\rho_j S_j y_{ij})\right)^{(n+1)} - \left(\phi_f \sum_{j=1}^{n_p}(\rho_j S_j y_{ij})\right)^{(n)}\right)}_{(F)} \tag{4-B.2}$$

Equation (4-B.2) is the mass balance equation for component *i* that is written for each block. Expressions (A) and (B) are diffusion and convection flowing terms, respectively, for all phases and surrounding grid blocks. The mass variation of component *i* caused by the chemical reactions during the process, is illustrated by the term (C). Term (D) accounts for the molar rate of injection or production of component *i* through all phases, wellbore term, in k^{th} perforation of well. The rate of mass exchange of component *i* between aquifer and reservoir is considered in term (E). The difference term on the right-hand side describes the change in accumulation of component *i* in the gird block with the bulk volume of V_{bi} during the time interval of Δt. The transmissibility of phase *j*, T_j, is defined as

$$T_j = T\left(\frac{k_{rj}}{\mu_j . R_j}\right), \quad T = \left(\frac{A}{\Delta l}\right)^{eff} k^{eff}, \quad j = 1, \dots, n_p \tag{4-B.3}$$

and is a function of the effective permeability, viscosity, node spacing (distance between center of adjacent grid blocks), cross sectional area, and phase resistivity.

D_{ij} is the diffusion of the component *i* in phase *j* and is defined as a product of geometric factors and component dispersion coefficients as in equation (4-B.4). The effective dispersion coefficients at the interface are the geometric means of the dispersion coefficients of the two blocks.

$$D_{ij} = \left(\frac{A}{\Delta l}\right)^{eff} D_{ij}^{eff}, \quad j = 1, \dots, n_p \tag{4-B.4}$$

The conservation equation of the solid (non-flowing) component i is (CMG: STARS Technical Manual 2009)

$$V_{bi}\sum_{m=1}^{n_r}(S'_{mi}-S_{mi})r_m=\left(\frac{V_{bi}}{\Delta t}\right)\left((\phi_v c_i)^{(n+1)}-(\phi_v c_i)^{(n)}\right) \tag{4-B.5}$$

Equation (4-B.5) describes the variation in the concentration of solid component i with time which is only caused by chemical reactions. The left-hand side describes the consumption rate of solid component i by chemical reactions, gasification and combustion, and the right-hand side is the change in the accumulation of solid component i during time Δt.

The energy conservation equation is (CMG: STARS Technical Manual 2009)

$$\overbrace{\sum_{l=1}^{n_b}\sum_{j=1}^{n_p}T_j\rho_j H_j\Delta\Phi_j}^{(A)}+\overbrace{\sum_{l=1}^{n_b}K_l\Delta T_l}^{(B)}+\overbrace{V_{bi}\sum_{m=1}^{n_r}H_{rm}r_m}^{(C)}+\overbrace{\sum_{j=1}^{n_p}\rho_j H_j q_{jk}}^{(D)}+\underbrace{\sum_{l=1}^{n_{aqb}}\sum_{j=1}^{n_p}\left(\rho_j H_j q_{aq_{jl}}+K_l\Delta T_l\right)}_{(E)}+\underbrace{\sum_{f=1}^{n_f}\left(HL_f+HL_{cf}\right)}_{(F)}=\underbrace{\left(\frac{V_{bi}}{\Delta t}\right)\left(\zeta^{(n+1)}-\zeta^{(n)}\right)}_{(G)} \tag{4-B.6}$$

where K is the thermal transmissibility at the interface between two adjacent blocks and defined as $K=\left(\frac{A}{\Delta l}\right)^{eff}\lambda^{eff}$. The effective thermal conductivity at the interface is the harmonic average of the two blocks, that is, the resistance to heat conduction is in a series.

Energy transfer by convection and conduction mechanisms are illustrated by terms (A) and (B), respectively. Term (C) accounts for heat of reaction as a sink/source in energy equation. The energy transferred by injected or produced fluid through k^{th} perforation of well located in the block is considered in term (D). The last term, (E), is the amount of energy transferred from/to aquifer either as conductive or convective form. Heat loss to the surrounding formations as conduction or convection is handled through term (E). The variation of accumulation term of energy is included on the right-hand side, (G), in which ζ is defined as

$$\zeta=\phi_f\sum_{j=1}^{n_p}\rho_j S_j U_j+\phi_v c_S U_S+(1-\phi_v)U_r \tag{4-B.7}$$

Chapter 5 Reaction Rate Constants in Simulation of Underground Coal Gasification Using Porous Medium Approach[4]

5.1 Abstract

Underground coal gasification (UCG) is an emerging energy technology for a cleaner type of coal extraction method. It avoids current coal mining challenges such as drastic changes to landscapes, high machinery costs, elevated risks to personnel, and post-extraction transport. UCG has a huge potential to provide a clean coal energy source by implementing carbon capture and storage techniques as part of the process. In order to support mitigation strategies for clean coal production and policy development, much research needs to be completed. One component of this information is the need to understand what happens when the coal burns and a subsurface cavity is formed. This paper looks at the efforts to enhance reliable prediction of the size and shape of the cavities. Reactions are one of the most important mechanisms that control the rate of the growth of the cavities. Therefore, modeling the reactions and precise prediction of reaction kinetics can influence the accuracy of a UCG process.

The produced syngas composition during UCG is closely linked to the reactions that take place in this process, the permeability of the coal seam, and the temperature distribution. Since the combination of reactions can influence the distributions of the heat and gas components in the coal seam during UCG or even extinguish the combustion, accurate modeling of the reactions is crucial, particularly when all phenomena affecting the reaction rate are considered in a single set of kinetics. In this study, procedures are proposed to estimate the frequency factor and activation energy of the pyrolysis reaction using a single-step decomposition method, the kinetics of the endothermic direction of homogeneous reversible reactions, and the frequency factor of heterogeneous reactions from experiments or literature data. The estimated kinetics is more appropriate for simulation of the UCG process using the porous medium approach.

[4] M. Seifi, Z. Chen, and J. Abedi 2014. Reaction Rate Constants in Simulation of Underground Coal Gasification Using Porous Medium Approach. *Mitigation and Adaptation Strategies for Global Change*. DOI 10.1007/s11027-014-9582-3.

Computer Modelling Group's CMG-STARS (Steam, Thermal, and Advanced Processes Reservoir Simulator) software is used in this study.

Keywords Chemical Reactions, Kinetics, Porous Medium, Pyrolysis, UCG

5.2 Introduction

Global climate change has been attributed to the increased production of greenhouse gas (GHG) emissions. The production of oil and gas, and the use of these products contribute to the volume of GHG emissions measured. In situ coal gasification or underground coal gasification (UCG) is attracting considerable attention as a viable process for the production of 'clean' fuel from coal. Both climate change legislations, and the desire to extract coal from very deep seams is promoting the need for a better understanding of the UCG process. UCG is a complex process that includes turbulent and Darcy fluid flows, free and forced natural convection flows, heterogeneous and homogeneous combustion and gasification reactions, and spalling and collapsing of char and coal materials (Seifi et al. 2013). Industry has a need for robust UCG modeling in order to facilitate the necessary understanding of the fundamentals of the process and, consequently, the design of pilot tests. Pyrolysis is a critical process in UCG, as it produces char for heterogeneous reactions. The reactions of char (carbon) with oxygen (O_2), carbon dioxide (CO_2), steam, and hydrogen (H_2) are the main sources of heat generation and consumption in coal conversion processes, precise modeling and parameter selection for these reactions is important. Moreover, homogeneous reactions in the gas phase can significantly impact the composition of produced syngas (Perkins 2005).

The reactivity of coal and char with gaseous species at different pressures, temperatures, and environment conditions has been studied by numerous researchers. For modeling the rate of heterogeneous reactions in UCG, a variety of expressions have been applied, such as the Arrhenius type, modified Arrhenius relationship, power law, and Langmuir-Hinshelwood approach. The pyrolysis process has been modeled mostly using single-step decomposition or simultaneous independent reactions methods (Dutta and Wen 1977; Tomita et al. 1977; Tsang 1980; Massaquoi 1981; Monson et al. 1995; Bryden and Ragland 1996; Roberts and Harris 2000; Yang 2004; Perkins 2005; Seifi et al. 2011).

In general, most models in the literature have applied the correlations and modeling approaches of surface gasifiers to the UCG process; for example, computational fluid dynamics models have been applied in the simulation of the flow within a cavity and the utilization of porosity correlations based on particle size. The porous medium approach, on the other hand, uses thermal compositional oil and gas simulators to simulate the UCG process (Tsang 1980; Perkins 2005; Nourozieh et al. 2010; Seifi et al. 2013).

Due to the different nature of the processes of in situ heavy oil combustion and coal gasification, there are variations in the implementation of the reactions in the corresponding models. In the simulation of the UCG process utilizing hydrocarbon reservoir simulators, all reactions are treated as the first order and the Arrhenius type, implying that only one set of kinetic parameters (the frequency factor which is constant multiplier of Arrhenius relationship, also called pre-exponential factor, and activation energy) mimics the effect of all phenomena, such as bulk diffusion, gas film, intraparticle diffusion, and intrinsic reactivity (CMG: STARS Technical Manual 2013). Therefore, the correct values of the parameters and reliable reaction kinetics are obtained using experimental tests and literature data. This is of paramount importance for cases where there is no experimental analysis of kinetics or results of a pilot test to match the simulation results. Moreover, hydrocarbon reservoir simulators do not directly account for the equilibrium state of the reversible reactions. In addition, the porous medium approach models the pyrolysis process as a single reaction (Seifi et al. 2013). It takes into consideration the rate of the heterogeneous reactions per bulk volume of the whole domain, with the literature data available based on the surface area of the solid materials.

In this study, procedures are proposed to obtain the frequency factor and activation energy for the pyrolysis reaction using the weight loss rate test on coal, the conversion of frequency factor data from the literature into simulator format for heterogeneous reactions, and a method that considers the equilibrium constant in the homogeneous reversible reactions. The proposed methods have been investigated through numerical simulation using the porous medium approach. STARS (Steam, Thermal, and Advanced Processes Reservoir Simulator) software of Computer Modelling Group is used in this study. The use of these models supports the economical and environmental decision making related to recovery and production of these energy sources.

STARS is a 3D thermal, multi-phase, compositional porous medium simulator capable of handling different types of well patterns, various geological layering, variable porosity, and permeability due to change in pressure, temperature, solid phase concentration, and rock compaction/dilation. It is based on the fundamental principles of mass and energy conservation, applying Darcy's law as the momentum equation. The STARS simulator assumes a thermal equilibrium between all of the fluid and solid phases and uses the power law to model the reaction rates with the Arrhenius relationship. Various enhanced oil recovery processes, such as heavy oil *in-situ* combustion, steam injection, steam-solvent injection, chemical flooding, and gas injection can be simulated using STARS on both the lab and field scales.

5.3 Reactions in the Porous Medium Model

Most models in the literature operate on the assumption that the original coal has a low permeability and that almost all gaseous materials produced away from the cavity will diffuse towards the cavity, **Fig. 5-1**. Consequently, the models assume the existence of various chemical regions from the surface of the cavity into the coal seam. The surface of the cavity is comprised of a layer of gaseous film and then an ash layer with a temperature that is lesser than the flame temperature and higher than the injection temperature. Beneath the ash layer is a pyrolysis region with an intermediate temperature that extends into the coal seam. The fire front, which exists somewhere between the ash zone and the pyrolysis region, generates the heat required for the process. Most of the heat diffuses towards the drying front to pyrolyze the dry coal and evaporate the moisture in the original coal. In **Fig. 5-1**, the coal has been completely pyrolyzed on the left side of the pyrolysis region, due to higher temperature, and the proportion of pyrolyzed coal decreases towards the drying zone. Alternatively, in porous medium models, the original coal seam is assumed to be permeable enough for the produced gas species away from the cavity to be transported towards the production well where the pressure is lower. The permeability increases around the cavity primarily as a result of the consumption of solid components. Additionally, higher injection pressure increases the pressure around the cavity and causes the gas components to migrate towards the production well.

Common reactions in the UCG process take place either as homogeneous reactions in the gas phase or heterogamous reactions on the surface of the solids (coal or char), **Table 5-1**. The general form of the j^{th} reaction, as shown in equation (5-1), can be written in the algebraic form

of $\sum_{i=1}^{i=n_c}(v'_{ij} - \nu_{ij})M_i = 0$, which implies negative and positive stoichiometric coefficients for reactants and products, respectively, for computational purposes. The porous medium approach computes the rate of the j^{th} reaction, r_j, using equation (5-2), and then applies $\sum_{j=1}^{j=n_r}(v'_{ij} - \nu_{ij}).r_j$ to the material balance equation of the i^{th} species and $\sum_{j=1}^{j=n_r}\Delta H_j.r_j$ to the energy balance equation as sink/source terms (CMG: STARS Technical Manual 2013).

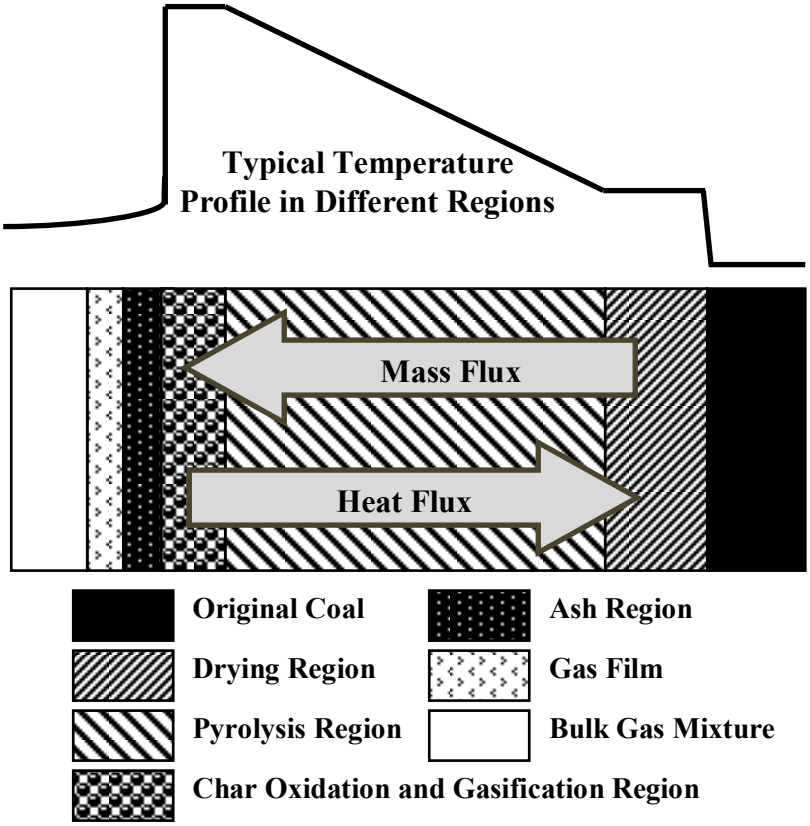

Fig. 5-1: Conceptual diagram of various regions in a typical underground coal gasification process. Temperature, coal chemical and physical properties, water content, and types of reactions vary in different regions

$$\sum_{i=1}^{i=n_c} \nu_{ij} M_i \rightarrow \sum_{i=1}^{i=n_c} v'_{ij} M_i \tag{5-1}$$

$$r_j\left(\frac{gmol\ of\ first\ reactant}{day.m^3\ of\ bulk\ volume}\right) = A_{0j} exp\left(\frac{-E_{aj}}{RT}\right)\prod_{i=1}^{i=n_c}\gamma_i{}^{e_{ij}} \tag{5-2}$$

Where ν and ν' are the stoichiometric coefficients of reactants and products, respectively. M represents the component's name. r is the rate of reaction in *gmol/day-m*^{3}. ΔH is the heat of

reaction in *J/gmol*. A_0 and E_a are the frequency factor (variable unit) and the activation energy in *J/gmol*, respectively. n_c, n_r, and e are the number of components, the number of reactions in the system, and the reaction order, respectively. T is the temperature in *K*. R is the universal gas constant, 8.314 *J/gmol-K*. Subscripts *i* and *j* stand for i^{th} component and j^{th} reaction.

γ_i in equation (5-2) can be the partial pressure of the gaseous reactants or the concentration of the reactants (gaseous or solid components) per bulk volume of the grid block. The reaction constant is based on the Arrhenius relationship. The temperature in the exponential term is the average temperature of the grid block. The stoichiometric coefficients and hence the heat of reaction should be modified so that the stoichiometric coefficient of the first reactant becomes one.

Table 5-1: List of most common reactions involved in an underground coal gasification process

	Reaction Name	Reaction Formulation
Heterogeneous	Pyrolysis	$Coal(daf) \rightarrow Char, CO, CO_2, H_2, CH_4, \ldots$
	Oxidation	$C + O_2 \rightarrow CO_2$
	Boudouard	$C + CO_2 \rightarrow 2CO$
	Methanation	$C + 2H_2 \rightarrow CH_4$
	Steam Gasification	$C + H_2O \rightarrow H_2 + CO$
Homogeneous	Forward Water-Gas Shift	$CO + H_2O \rightarrow CO_2 + H_2$
	Backward Water-Gas Shift	$CO_2 + H_2 \rightarrow CO + H_2O$
	Carbon-Monoxide Oxidation	$CO + 0.5O_2 \rightarrow CO_2$
	Forward Methane-Steam Reforming	$CH_4 + H_2O \rightarrow CO + 3H_2$
	Backward Methane-Steam Reforming	$CO + 3H_2 \rightarrow CH_4 + H_2O$

The concentrations of the i^{th} gaseous and solid components are calculated using equations (5-3) and (5-4), respectively, which are functions of gas saturation, gas density, compositions of gas and solid phases, and fluid and void porosities. In porous medium simulators, void porosity is defined as a fraction of bulk volume which is filled with fluids and flammable solid materials; whereas fluid porosity is defined as a fraction of bulk volume which is only filled with fluids. The void and fluid porosities can be obtained from equations (5-5) and (5-6). In a UCG process, fluid porosity is influenced by rock expansion/compaction and concentration of solid

components; however, its variation resulted from compressibility effect of rock and solid components is significantly small compared to the addition of pore space due to the consumption of solid materials. Thus the isothermal and isobaric rock expansion coefficients are assumed to be zero. As a result, the void porosity remains constant with time, and the fluid porosity can only change with the consumption of solid components.

$$C_i = \phi_f . \rho_g . S_g . y_i \tag{5-3}$$

$$C_i = \phi_v . c_i \tag{5-4}$$

$$\phi_v = \phi_{ref} . exp\left(C_p\left(p - p_{ref}\right) - C_T\left(T - T_{ref}\right)\right) \tag{5-5}$$

$$\phi_f = \phi_v \left(1 - \sum_{i=1}^{i=n_s} \frac{c_i}{\rho_i}\right) \tag{5-6}$$

where c_i, C_i, C_p,and C_T are pore volume concentration of solid component *i* in *gmol/m*^{3}, bulk volume concentration of gaseous species *i* in *gmol/m*^{3}, isothermal expansion coefficient in *1/kPa*, and isobaric expansion coefficient in *1/K*, respectively. p, p_{ref}, and T_{ref} are pressure in *kPa*, reference pressure in *kPa*, and reference temperature in *K*. ρ_i, ρ_g, S_g, and y_i are solid density of solid component *i* in *gmol/m*^{3}, gas phase density in *gmol/m*^{3}, gas phase saturation, and mole fraction of component *i* in gas phase, respectively. ϕ_f, ϕ_{ref}, and ϕ_v are fluid porosity, reference void porosity at P_{ref} and T_{ref}, and void porosity. n_s is the number of solid components in the system.

The volume constraint of $V_b = V_v + V_r$ on a grid block in the porous medium model implies that, due to a change in the void volume, V_v, either the bulk volume, V_b, or rock volume, V_r, has to change (CMG: STARS Technical Manual 2013). In UCG simulation using the porous medium approach, since the ash content of coal mimics the rock network of the domain and the ash compressibility is assumed to be zero, the rock volume remains constant. As a result, variation of the void volume changes the bulk volume of the grid block. This is important for cases that include a geomechanics model, such as dilation. For simplicity, it is assumed that the void volume, which is the summation of the flammable solid (dry-ash-free (*daf*) coal) volume and the pore volume, is constant. Therefore, there is a trade-off between the pore and solid volumes: The pore volume increases as the solid is consumed. On the other hand, if the ash compressibility is

considered non-zero, the rock volume varies with time, and the bulk volume should remain constant, leading to changes in the volumetric heat capacity of the rock material and in the temperature distribution.

5.3.1 Homogeneous Reversible Reactions

The rate of the homogeneous reversible reaction in the gas phase is usually calculated in UCG modeling using equilibrium constants and a power law model. The general form of the gas phase reversible reaction can be defined as in equation (5-7), where k_{fj} and k_{bj} are the forward and backward reaction constants, respectively, according to the Arrhenius relationship.

$$\sum_{i=1}^{i=n_c} \nu_{ij} M_i \overset{k_{fj},\ k_{bj}}{\longleftrightarrow} \sum_{i=1}^{i=n_c} \upsilon'_{ij} M_i \tag{5-7}$$

Applying the thermodynamics definition of Gibbs free energy and the fugacity concept, the partial pressure based equilibrium constant of the j^{th} reaction can be derived as shown in equation (5-8), where ΔG_j^o is the standard Gibbs-energy change of the reaction, which depends only on temperature.

$$K_{pj} = \prod_{i=1}^{i=n_c} \left(\frac{\hat{f_i}}{f_i^o}\right)^{\xi_{ij}} = exp\left(\frac{-\Delta G_j^o}{RT}\right) \tag{5-8}$$

Where k_f and k_b are forward and backward reaction constants, respectively. f_i^o and $\hat{f_i}$ are fugacity coefficients of component i at standard reference and at current pressure and temperature. ξ_{ij}, K_p, and ΔG_j^o are algebraic stoichiometric coefficient of i^{th} reactant or product in reaction j, partial-pressure based equilibrium constant, and standard Gibbs-energy change of reaction j in *J/gmol*, respectively.

ξ_{ij} is the algebraic stoichiometric coefficient of the species in the j^{th} reaction, such that it is negative for reactants and positive for products. As a result, the equilibrium constant is a function of temperature only. Assuming ideal gas behavior and that the fugacity coefficient for a pure component at ideal state is one, the composition-based equilibrium constant can be defined as in equation (5-9) (Smith et al. 2001).

$$K_{Cj} = \prod_{i=1}^{i=n_c} y_i^{\xi_{ij}} = K_{pj} \left(\frac{p}{p^o}\right)^{-\upsilon_j}, \quad \upsilon_j = \sum_{i=1}^{i=n_c} \xi_{ij} \tag{5-9}$$

Where K_C, p^o, and υ_j are composition-based equilibrium constant, standard-state pressure (101.325 *kPa*), and algebraic summation of stoichiometric coefficients of reactants and products in reaction *j*, respectively.

The reaction rate at a specified pressure and temperature can be determined using the equilibrium constant and kinetics of the exothermic direction (e.g., forward direction) based on equation (5-10).

$$r_j = k_{fj} \left(\prod_{i=1}^{i=n_c} y_i^{\upsilon_{ij}} - \left(\frac{1}{K_{Cj}}\right) \prod_{i=1}^{i=n_c} y_i^{\upsilon'_{ij}} \right) \tag{5-10}$$

As described in the previous section, all kinds of reactions are treated in the same manner in the porous medium model, as shown equation (5-2). For this reason, two reactions are used to model a reversible reaction: one for the forward reaction and the other for the backward reaction. Moreover, separate kinetics has to be used for each of these reactions. Therefore, a method is proposed to obtain the kinetics of the endothermic direction for a given pressure, temperature and kinetics of the exothermic direction using equilibrium constants.

At the equilibrium condition (i.e., the net rate of the reaction is zero), the composition-based equilibrium constant, K_{Cj}, can be defined as the ratio of the forward reaction constant to the backward reaction constant. Reaction constants are only a function of temperature, implying that, at a specified pressure, K_{Cj} is only an exponential function of temperature. Therefore, with the equilibrium constant of the j^{th} reaction, K_{pj}, as a function of temperature and setting the pressure, an exponential function can be fitted on K_{Cj} data versus temperature, equation (5-11a). Using equations (5-11b) and (5-11c), the frequency factor and activation energy for the endothermic direction can then be obtained as $A_{0bj} = \left(\frac{A_{0fj}}{A_{0ej}}\right)$ and $E_{abj} = E_{afj} - E_{aej}$.

$$K_{Cj} = \frac{k_{fj}}{k_{bj}} = f_j(T) = A_{0ej}.\exp\left(\frac{-E_{aej}}{RT}\right) \tag{5-11a}$$

$$k_{fj} = A_{0fj}.exp\left(\frac{-E_{afj}}{RT}\right) \tag{5-11b}$$

$$k_{bj} = A_{0bj}.exp\left(\frac{-E_{abj}}{RT}\right) = \left(\frac{A_{0fj}}{A_{0ej}}\right).exp\left(\frac{-\left(E_{afj} - E_{aej}\right)}{RT}\right) \quad (5\text{-}11c)$$

Where subscripts b, e, and f represent backward direction, equilibrium condition, and forward direction, respectively.

In the porous medium model, the primary variables are the pressure, temperature, gas mole fractions, and pore volume concentration of solid components. Due to oxidant injection, the producer bottom-hole pressure setting and the generation and consumption of gaseous components as a result of the reactions, the pressure in the whole domain is variable. However, the pressure has to be set to a single value for the calculation of K_{Cj} in equation (5-9).

The water-gas shift (WGS) and methane-steam reforming (MSR) reactions, **Table 5-1**, are the two important homogeneous reversible reactions in the UCG process. Since the value of υ_j becomes zero in a WGS reaction, K_{Cj} remains the same as K_{pj}, which implies that pressure does not affect this reaction. On the other hand, the value of υ_j becomes two for an MSR reaction, indicating the existence of a pressure term in K_{Cj}.

Homogeneous reactions are most likely to take place in a cavity and linking channel, due to their high permeability and the low permeability of the original coal seam. Moreover, operating conditions are set so that the cavity pressure remains lower than the hydrostatic pressure, in order to avoid the escape of syngas from cavity, working to support the goal for production that has the least negative impact on the environment. Practically, the cavity pressure is kept at about 90 % of the hydrostatic pressure; therefore, to obtain the kinetics of the endothermic direction, the pressure in equation (5-9) is set as 90 % of hydrostatic pressure at the average depth of the flat coal seam or at the depth of injection point (Huq 2013).

Figs. 5-2 and **5-3** illustrate the cumulative production and the rate of production of various species for two cross-sectional models, respectively. Physical and thermal properties of coal seam and solid components and operating conditions of production and injection wells are summarized in **Table 5-2**. The activation energy of the homogeneous reversible reactions for these models were determined according to the proposed method and that of Nourozieh et al. (Nourozieh et al. 2010), in which the activation energy is assumed to be the same for both the forward and backward directions, as shown in **Table 5-3**. As can be seen, the proposed method

had a higher production of methane (CH_4), but carbon monoxide (CO) and H_2 were produced in lower amounts. The higher activation energy of the backward direction of the WGS reactions and the forward direction of the MSR reactions prevents the conversion of CH_4 and CO. Therefore, using the proposed method, the MSR reaction has less effect on the conversion of CH_4 into CO and H_2. The produced amounts of nitrogen (N_2) and CO_2 were nearly the same. UCG is a complex process, which can be significantly influenced by parameters such as the type and composition of the coal, porosity, moisture and volatile matter content, rate and type of the injected oxidant, and the rate and distance of the retraction of the injection point. Changes to these parameters dramatically affect the rate and composition of the produced syngas. For this reason, a precisely tuned and consistent simulation model is required to accurately replicate a real UCG process. Therefore, the composition of the syngas produced by the above-mentioned test models may not follow the trend of a typical UCG process because the main purpose of the investigation was to determine the effect of kinetics using two methods.

Table 5-2: Physical and thermal properties of coal seam and solid components and operating conditions of injection and production wells

	Property	Value	Unit
Physical Properties of Coal Seam	Porosity	8.6	*%*
	Permeability	1.0	*md*
	Depth	1370.0	*m*
Initial Properties of Coal Seam	Pressure	11.5	*MPa*
	Temperature	60.0	*°C*
	Water Saturation	70.0	*%*
	Methane Mole Fraction	100.0	*%*
Thermal Properties	Volumetric Heat Capacity of Bulk of Coal	3.00E+06	*J/m^3-°C*
	Thermal Conductivity of Ash	2.00E+05	*J/m-day-°C*
	Thermal Conductivity of Water	4.84E+04	*J/m-day-°C*
	Thermal Conductivity of Solid (Coal and Char)	4.50E+05	*J/m-day-°C*
	Thermal Conductivity of Gas Mixture	4.00E+03	*J/m-day-°C*
	Heat Capacity of Coal and Char	17.0	*J/gmol-°C*
Physical Properties of Solid Components	Coal Molecular Weight	14.323	*kg/gmol*
	Char Molecular Weight	12.0	*kg/gmol*
	Coal Solid Density	1365.0	*kg/m^3*
	Char Solid Density	1700.0	*kg/m^3*
Operating Conditions	Injected Oxidant	Pure Oxygen	
	Injection Rate	0.3	*sm^3/day*
	Producer Bottom-Hole Pressure	11.2	*MPa*

Table 5-3: Applied activation energy for reversible homogeneous reactions

Method	Reaction Direction	E_a, *kJ/gmol*	
		WGS Reaction	MSR Reaction
Proposed Method	Forward	12.6	236.0
	Backward	53.6	30.0
Nourozieh et al.	Forward	12.6	30.0
	Backward	12.6	30.0

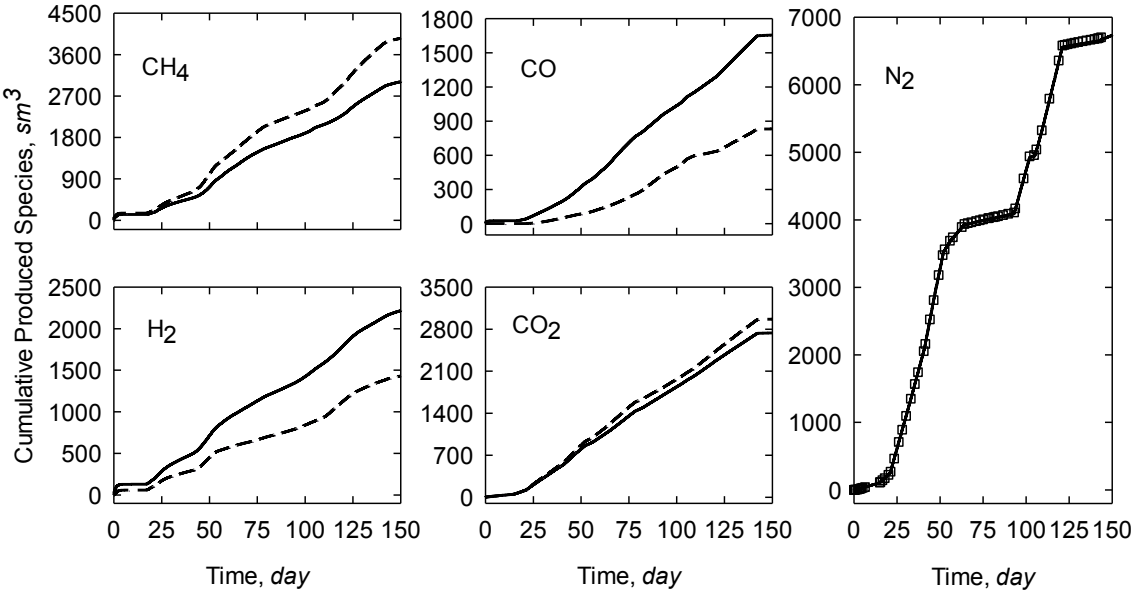

Fig. 5-2: Comparison of cumulative production of species using the proposed (symbol or dashed-lines) and Nourozieh et al. (solid-lines) method

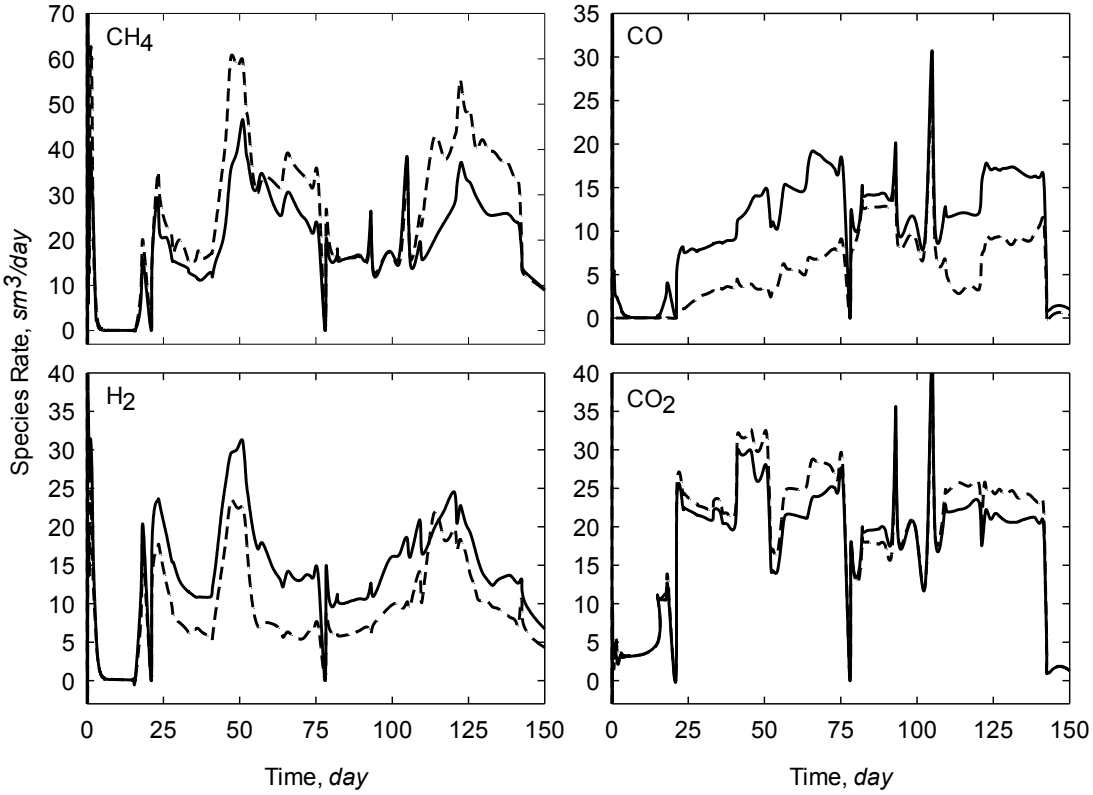

Fig. 5-3: Comparison of production rate of species using the proposed (dashed-lines) and Nourozieh et al. (solid-lines) methods

5.3.2 Heterogeneous Reactions

Heterogeneous reactions of char with gaseous components are the main source of heat generation/consumption in UCG, indeed in any coal gasification processes. Therefore, using the fundamentally reliable kinetics of these reactions in UCG modeling is crucial, particularly when there are no experimental results for the kinetics of these reactions and the composition of the produced syngas, such as in the generic modeling of a specified coal. One approach is the application of the kinetics of these heterogeneous reactions from the literature, which are generally in the form of equation (5-12) (Perkins 2005). In this form, the rates of the reactions are calculated per square meter of a specific surface area of the solid material; however, the porous medium model computes the rates of reactions per cubic meter of bulk volume, as in equation (5-2).

$$r_j\left(\frac{kg\ Char}{sec.m^2}\right) = A'_{0j}.exp\left(\frac{-E_{aj}}{RT}\right)P_i^{e_{ij}} \quad (5\text{-}12)$$

A method is, therefore, proposed to convert the kinetics to the format of the porous medium model. γ_i in equation (5-2) can be considered either as partial pressure or bulk volume concentration of gaseous components. Applying the former option, equation (5-12) can be converted into equation (5-13a), in which the activation energy is the same as the value in the literature, but the frequency factor can be obtained according to equation (5-13b). Parameter *S* is the surface area of the char, which is variable with time; however, the frequency factor has to be a constant value.

$$r_j\left(\frac{gmol\ char}{day.m^3 bulk\ volume}\right) = A_{0j}.exp\left(\frac{-E_{aj}}{RT}\right)C_{char}.P_i^{e_{ij}} \quad (5\text{-}13a)$$

$$A_{0j} = 8.64E5\frac{S.A'_{0j}}{P_o^{e_{ij}}}, \quad P_o = 101.325kPa \quad (5\text{-}13b)$$

Where *S* and C_{char} are reactive surface area in m^2/gr and bulk volume concentration of char in $gmol/m^3$, respectively.

Fig. 5-4 illustrates the variation of the specific surface area as a function of char conversion, X_C, according to equation (5-14), which is the result of a random pore model. The pore structure parameter, ψ, is assumed to be 5 for UCG modeling of bituminous coal (Liu et al 2000; Perkins 2005). Therefore, with the initial surface area, S_0, and the average of the specific surface area, $\overline{S/S_0(\psi = 5)} = 0.88787$, *S* and, hence, the frequency factor can be determined.

$$S = S_0(1 - X_C)\sqrt{1 - \psi.ln(1 - X_C)} \quad (5\text{-}14)$$

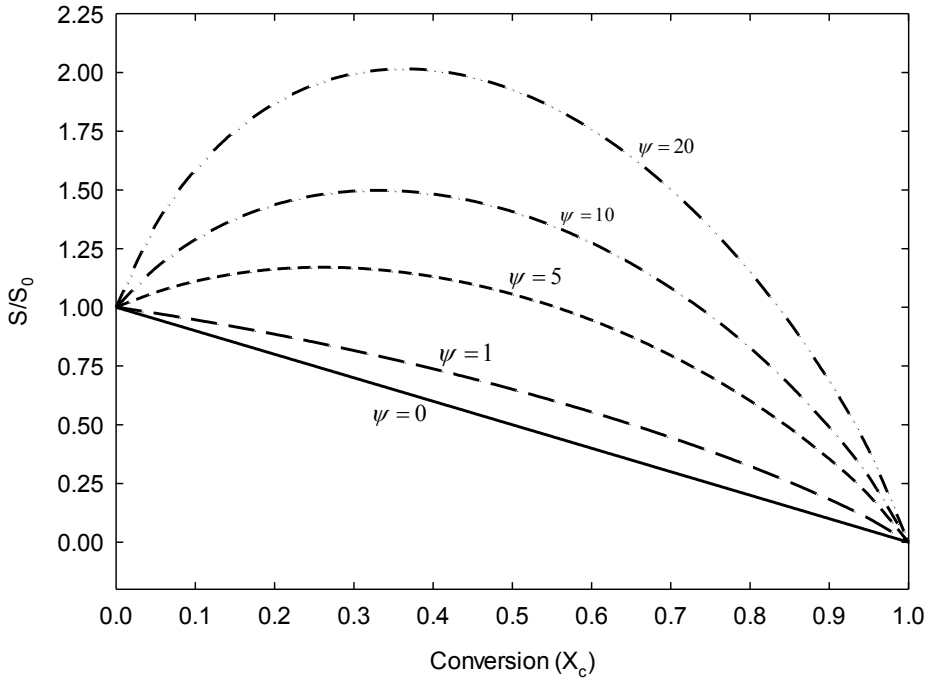

Fig. 5-4: Specific surface area for various pore structure parameters

If γ_i is, however, considered as the concentration of gaseous components per bulk volume, equation (5-12) can be converted into the form in equation (5-15a). In this case, an extra term is introduced into the frequency factor, which is strongly time-dependent due to the temperature, fluid porosity, and gas saturation. Consequently, the former approach, where γ_i is partial pressure, is proposed to be used for the application of the kinetics of heterogeneous reactions in the porous medium model.

$$r_j\left(\frac{gmole\ char}{day.m^3 bulk\ volume}\right) = A_{0j} exp\left(\frac{-E_{aj}}{RT}\right) C_{char}.C_i^{e_{ij}} \tag{5-15a}$$

$$A_{0j} = \left(\frac{RT}{1000\phi_f S_g}\right)^{e_{ij}} \left(\frac{8.64E5\ S.A'_{0j}}{P_o^{e_{ij}}}\right) \tag{5-15b}$$

Typical frequency factor values for heterogeneous reactions using the proposed method and considering γ_i as partial pressure of gaseous components are summarized in **Table 5-4**. The char density, char molecular weight, and average surface area (N_2 based, daf basis) were assumed to be 9 m^2/gr, 12.01 $kg/gmol$, and 1200 kg/m^3, respectively, which are typical values for Ardley and Judy Creek coal formations in Alberta, Canada (Parkash and Chakrabartty 1986; Richardson and CanZealand 2010). The estimated values of the frequency factors are in the same order of magnitude as those obtained by Nourozieh et al. for the Boudouard and steam gasification

reactions. In their work, the concentration of the gaseous components per bulk volume was assumed to be γ_i and the values of the frequency factors were estimated by applying optimization methods. For this reason, there are significant discrepancies for the oxidation and methanation reactions.

Table 5-4: Frequency factors of heterogeneous reactions for porous medium approach of underground coal gasification simulation

Reaction	Frequency Factor, A'_{0j} *kg-char/m^2-sec-[atm]^{ei}*	Pressure Order, e_{ij} []	Frequency Factor, A_{0j}	
			Proposed Method *1/day-[kPa]^{ei}*	Nourozieh et al. [*Variable*]
Oxidation	3.050E+03	1.0	2.494E+14	1.80E+06
Boudouard	3.000E+00	0.5	2.469E+12	5.67E+14
Steam Gasification	3.000E+01	0.5	2.469E+13	1.61E+12
Methanation	2.848E-05	1.0	2.329E+06	1.56E+19

5.3.3 Pyrolysis Reaction

Pyrolysis is a complex process that takes place when coal is heated in the absence of oxygen. Various gas components evolve in their own temperature ranges and at their individual rates of evolution. The onset temperature of evolution for each species is also different (Tsang 1980). However, in the porous medium approach, pyrolysis is modeled using a single-step decomposition method. Therefore, all components are considered to begin to evolve at the same temperature and in the same temperature range. Although the rate of evolution is specific for each component, it is influenced only by the final contribution of that component in the entire pyrolysis process.

Coal loses about 40-50 % of its weight during pyrolysis, which causes a significant increase in porosity and permeability of the domain (Campbell 1976). Furthermore, char is the main reactant of heterogeneous reactions and one of the major products of pyrolysis. As a result, precise prediction of pyrolysis using only a single reaction is necessary. Unrealistic predictions may cause either the extinction of combustion or gasification, due to lack of char or abnormal composition of syngas resulting from a fast pyrolysis process. In the following paragraphs, a

method is suggested for the determination of the kinetics of a pyrolysis process for UCG simulation.

The general form of the pyrolysis reaction can be defined as in equation (5-16), in which it is assumed that five gas components evolve during pyrolysis. Moreover, the pyrolysis rate in the porous medium model is obtained with equation (5-17), in which C_{coal} is the molar amount of coal per cubic meter of bulk volume.

$$\boldsymbol{Coal(daf)} \rightarrow \alpha_1 \boldsymbol{Char} + \alpha_2 \boldsymbol{CO} + \alpha_3 \boldsymbol{CO_2} + \alpha_4 \boldsymbol{N_2} + \alpha_5 \boldsymbol{H_2} + \alpha_6 \boldsymbol{CH_4} \tag{5-16}$$

$$r = A_0 . exp\left(\frac{-E_a}{RT}\right) C_{coal} \tag{5-17}$$

Equation (5-17) can be written in the form of equation (5-18), in which m is the current mass of daf coal during the devolatilization of coal. It is also assumed that the temperature varies linearly with time at a linear heating rate, $T = \beta t + T_0$ in which β is the heating rate in $°C/min$ and t is time in *min*.

$$\frac{dm}{dT} = \frac{-A_0}{\beta} . exp\left(\frac{-E_a}{RT}\right) m \tag{5-18}$$

Applying the approximation as in equation (5-19) for integration of the exponential term in equation (5-18), the total amount of remaining coal and the rate of weight loss at time t can be obtained with equations (5-20) and (5-21), respectively.

$$\int_0^T exp\left(\frac{-E_a}{RT}\right) dT \cong \left(\frac{RT^2}{E_a}\right) exp\left(\frac{-E_a}{RT}\right) \tag{5-19}$$

$$m = m_0 . exp\left(\frac{-A_0 RT^2}{\beta E_a} . exp\left(\frac{-E_a}{RT}\right)\right) \tag{5-20}$$

$$\frac{dm}{dT} = \left(\frac{-m_0 A_0 R}{\beta E_a}\right) . \left(2T + \frac{E_a}{R}\right) . exp\left(-\frac{E_a}{RT} - \frac{A_0 RT^2}{\beta E_a} . exp\left(\frac{-E_a}{RT}\right)\right) \tag{5-21}$$

Using equation (5-21), a set of graphs can be generated for specified activation energy. These plots illustrate the correlation between the frequency factor and the activation energy for the pyrolysis reaction. **Fig. 5-5** shows the rate of weight loss for activation energy of 150 *kJ/gmol* at various frequency factors, assuming that the initial amount of coal and heating rate are 1 *gr* and 5 $°C/min$, respectively. It can be seen that, in the range of pyrolysis temperatures from 350 to 900

°*C*, the temperature range, maximum rate, and onset temperature of evolution changed, as the value of frequency factor increased. This implies that both the activation energy and the frequency factor control the evolution of volatile matters in the single-step decomposition method. Consequently, such plots can be developed for various activation energies and frequency factors. Moreover, if the weight loss rate has been measured experimentally, as shown in **Fig. 5-6** for a coal sample of the upper part of Leopold coal seam from Thulin UCG pilot test (Mostade 2012), this result can be simulated to obtain a set of kinetics for the pyrolysis process using equation (5-21). Since ash is separated from coal in the porous medium model and the predominant driving force in this approach is viscous force, the obtained kinetics from simulating experimental data may not be the appropriate kinetics of pyrolysis. Therefore, simulations should be conducted for several sets of kinetics obtained from the above methods. A set of kinetics that produces realistic pyrolysis length (the distance from a fire front on the surface of a cavity to the coal seam with non-zero char concentration), less than one meter, can be considered as pyrolysis kinetics.

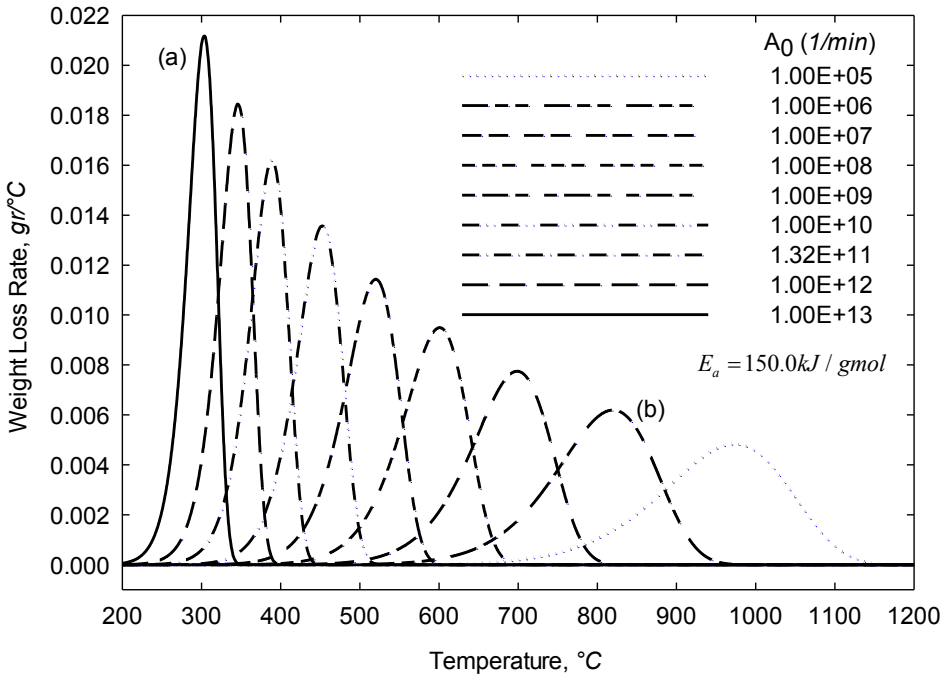

Fig. 5-5: Weight loss rate for activation energy of 150 *kJ/gmol* at various frequency factors

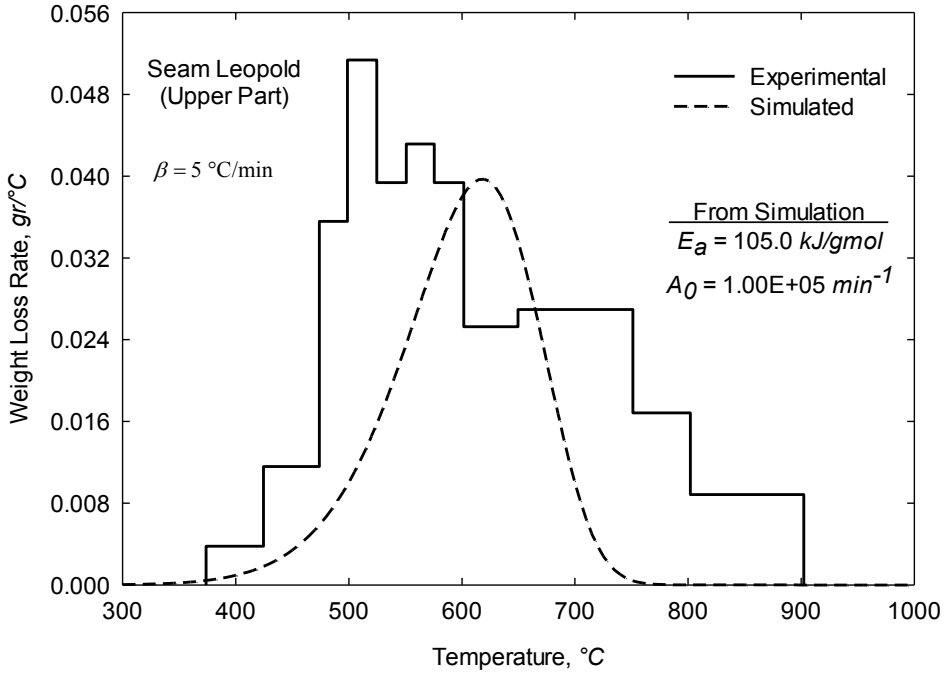

Fig. 5-6: Total degassing curve

Fig. 5-7 shows the coal and char concentration profiles at various times for two one-dimensional simulation models using different frequency factors for the pyrolysis reaction. The length of the models is 5 *m* and injection and production wells are located at the beginning and at the end of the domain, respectively, i.e. linked vertical well configuration. The abscissa indicates the distance between injection and production points such that the location of injector and producer correspond to the distance of zero (left side of the plots) and the distance of 5 m (right side of the plots), respectively. The activation energy for both models was 150 *kJ/gmol*. The applied frequency factors were 1.00E+06 min^{-1} and 1.00E+13 min^{-1} for the fast and slow pyrolysis models, respectively. Consequently, the rate of evolution of volatile matters using single-step decomposition model can be illustrated as plots (a) and (b) in **Fig. 5-5** for fast and slow pyrolysis, respectively. The thermal conductivity of solid flammable components was assumed to be 0.29 *J/m-sec-°C*. Other physical and thermal properties of the models are according to **Table 5-2**. As can be seen in **Fig. 5-7**, the whole domain was completely pyrolyzed for the fast-pyrolysis case before a time of 2.5 *days*, due to a lower onset temperature, narrow

temperature range, and higher rate of evolution. For the slow-pyrolysis case, approximately the first half meter of the domain was partially pyrolyzed.

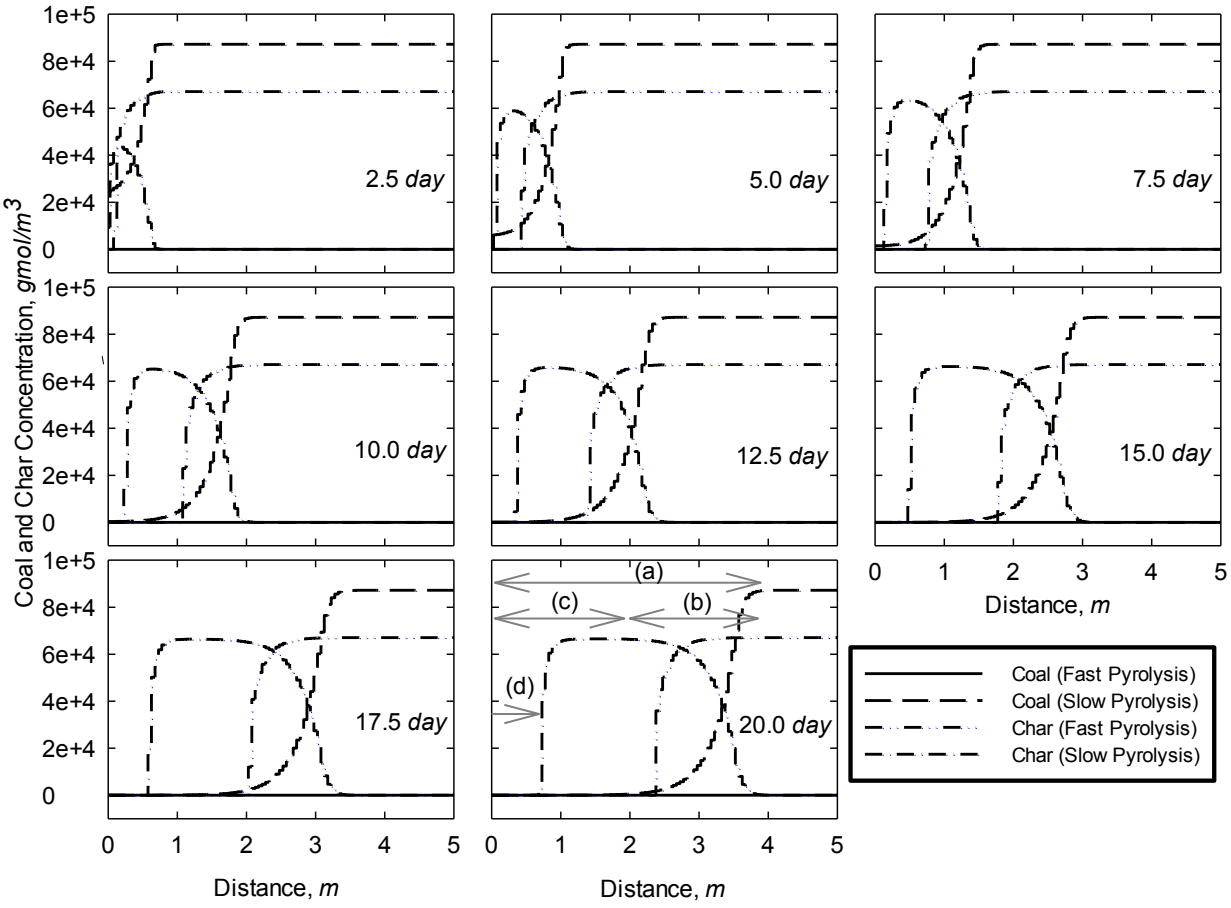

Fig. 5-7: Coal and char concentrations (*gmol/m^3-of-pore-volume*) at various times for fast and slow pyrolysis models. At time 20 *days*, for slow pyrolysis case, in region (a) coal concentration is lower than initial amount which is the indication of pyrolysis-affected zone, (b) coal concentration is not zero which indicates that pyrolysis process is still active in this zone, (c) coal concentration is zero which implies the completion of pyrolysis process in this region, and (d) char concentration is zero which indicates that all solid components have been gasified and combusted up to this point starting from injection point (distance of zero)

Moreover, since the pyrolysis process is slow and other heterogeneous reactions that consume char compete with the pyrolysis reaction, the region with maximum char concentration for the slow-pyrolysis case can be seen at a time between 10 *days* to 12.5 *days*. Afterwards, the length of the region with the maximum char amount increased, due to the predominance of the oxidation

reaction, more heat conduction, and possibly a lower rate of char consumption by the heterogeneous reactions. However, the length of the currently active pyrolysis region in the slow-pyrolysis case is about one meter, determined from zero to the maximum value of coal concentration, which indicates that the applied kinetics for slow pyrolysis can be considered as more reliable kinetics for pyrolysis of the specified coal.

Fig. 5-8 illustrates the coal and char concentrations at different initial coal seam permeabilities for a slow pyrolysis case at time 12.5 *days*. As can be seen, the rate of advancement of the pyrolysis front and the amount of unconsumed char increased at higher permeabilities, due to greater convective heat transfer by hot produced syngas ahead of the fire front. Moreover, since heat conduction is predominant, rather than convective heat transfer, in a UCG process, permeability variation at higher ranges is less effective. On the other hand, gas species cannot be transported easily at lower permeabilities; therefore, the availability of gaseous reactants for endothermic reactions lowers the heat conduction ahead of the fire front and, hence, a reduced pyrolysis process.

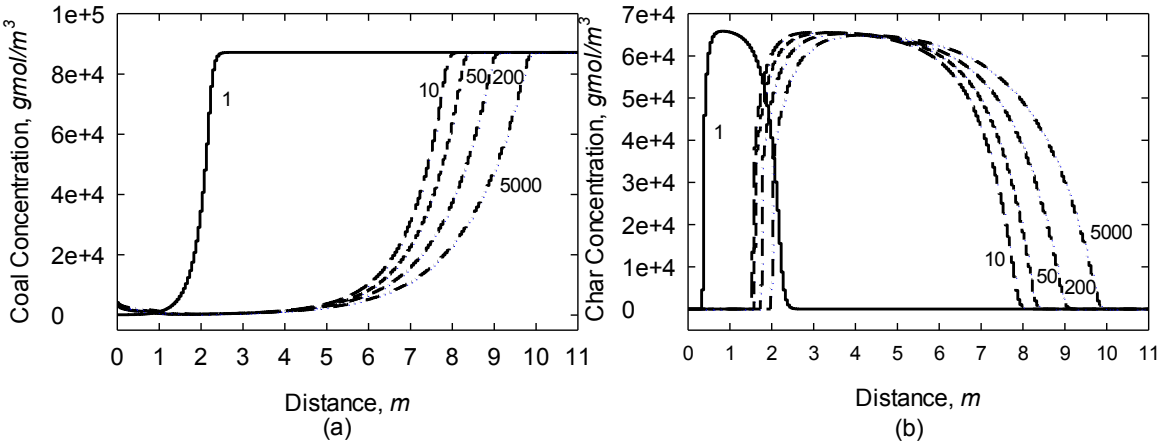

Fig. 5-8: Coal and char concentrations at different initial permeabilities (*md*) of coal seams at time 12.5 *days*

The thermal conductivities of coal and char are considered to be the same in the porous medium approach of UCG simulation. As shown in **Fig. 5-9**, although the rate of advancement of the pyrolysis front decreased with increased thermal conductivity of solid flammable components, the effect of this parameter was not significant. As the thermal conductivity declined, more heat was available ahead of the fire front for the pyrolysis process.

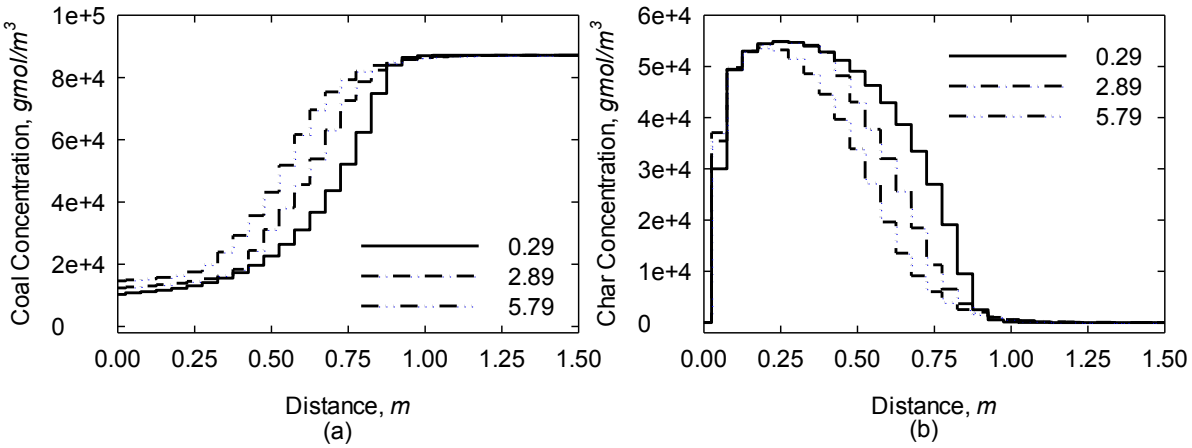

Fig. 5-9: Coal and char concentrations for different thermal conductivities (*J/m-sec-°C*) of coal and char at 4.0 *days*

5.4 Discussion

Field scale simulation of heavy oil in-situ combustion requires a large grid block size to reduce computation expense. In addition, access to consistent and fundamentally reasonable data is crucial for the design of pilot tests in order to obtain reliable insights into the results of the test. For this purpose, a lab-scale experiment called the combustion tube test is conducted to investigate various operational parameters such as maximum temperature, amount of coke deposition, required air and/or water, rate of fire front movement, and the rate and composition of the produced gas for the specified operating conditions. Performing simulations and matching the results of the combustion tube test allow us to determine the most effective reactions and their kinetics, which can be applied to large-scale simulations.

Large-scale simulations of UCG processes can be conducted in the same manner as heavy oil in-situ combustion simulations. However, UCG processes suffer from a lack of lab tests, which consider the effect of the pyrolysis process and all of the other homogeneous and heterogeneous reactions simultaneously in a small scale. These tests would provide reliable information on the reactions taking place during combustion and gasification of the specified coal at underground conditions during the UCG process. Furthermore, current UCG models have primarily applied complex reaction rate expressions in an attempt to separately capture the effects of major possible phenomena such as bulk diffusion, gas film, intra-particle diffusion, and intrinsic

reactivity. On the other hand, current porous medium simulators apply the power law method to model reaction rates, which combines the effect of the above-mentioned phenomena in one set of kinetics. As a result, the methods proposed in this study can provide fundamentally reliable kinetics for the different reactions in a UCG process within an acceptable range. Subsequently, they can be tuned to produce physically and chemically reasonable results and used to investigate the effect of different parameters and operating conditions on the process. The developed simulation model can be optimized to match the result of the pilot test by tuning individual parameters such as the kinetics of the reactions. Moreover, the information obtained will provide a possible range of the kinetics so that they can be considered in matching the results of the simulation model and field tests and we will be able to constrain the values of the kinetics of the reactions during the optimization process.

The proposed method to obtain Arrhenius constants with experimental data may result in multiple choices for each of the pre-exponential factors and activation energies. Thus the prediction ability of porous medium simulation models for UCG applying the obtained kinetics may be limited in the tuning range. To increase the reliability of the simulation models, the real data of a UCG process can be divided into two categories: The first category is used to initiate the simulation model and conduct a sensitivity analysis to distinguish the effective parameters including the most effective reactions and their kinetics. Then the effective parameters can be optimized to match this set of data. The second set of data can be used to verify the predictive capability of the optimized model and make more possible tuning of the parameters.

5.5 Conclusions

This paper proposes methods to obtain fundamentally reliable kinetics for the endothermic direction of homogeneous reversible reactions, heterogeneous reactions, and pyrolysis for the simulation of UCG process using the porous medium approach. The intended use is to expand our fundamental knowledge of the UCG process and hence advance the environmentally sound use of this process of coal energy production. The proposed procedures were investigated using one- and two-dimensional numerical models. It can be concluded that, with the kinetics of the exothermic direction of homogeneous reversible reactions and the equilibrium constant as a function of temperature, the kinetics of the endothermic direction can be obtained, which may result in a negative value of the activation energy only for computational purposes. Also, the rate

of evolution of volatile matters was strongly influenced by the frequency factor, activation energy and initial permeability of the coal seam, while the thermal conductivity of the solid materials did not have a significant effect. Therefore, in order to determine the kinetics of pyrolysis reactions, simulations should be conducted for each set of obtained kinetics using the proposed method, to make sure the length of the pyrolysis active zone is realistic.

The obtained kinetics will be used to initiate the simulation of a UCG process for the specified coal so that the entire data set of the model is consistent. They can also provide a possible range of variation of the kinetic parameters during optimization of the model by applying field results. Having an optimized model, a variety of scenarios can be conducted by simulation to investigate the composition of produced syngas, size and shape of the cavities, and prediction of environmental effect of a UCG test such as possible subsidence and heave when these models coupled with a geomechanics module. The obtained information might be used to design gas-treatment surface facilities and carbon capture and storage techniques such as storage of CO_2 in developed in-situ cavities.

5.6 Nomenclature

A_{0j} = Frequency factor of reaction *j*, *variable unit*

c_i = Pore volume concentration of solid component *i*, *gmol/m^3 pore volume*

C_i = Bulk volume concentration of component *i*, *gmol/m^3 bulk volume*

C_{coal} = Bulk volume concentration of coal, *gmol coal/m^3 bulk volume*

C_{char} = Bulk volume concentration of char, *gmol char/m^3 bulk volume*

C_p = Isothermal expansion coefficient, *1/kPa*

C_T = Isobaric expansion coefficient, *1/K*

e_{ij} = Order of reaction to component *i* in reaction *j*

E_{aj} = Activation energy of reaction *j*, *J/gmol*

$\hat{f_i}$ = Fugacity coefficient of component *i* in mixture at current *P* and *T*

f_i^o = Fugacity coefficient of component *i* in mixture at standard reference

k_{fj} = Forward reaction constant of reaction *j*, *variable unit*

k_{bj} = Backward reaction constant of reaction *j*, *variable unit*

K_{pj} = Partial-pressure based equilibrium constant

K_{Cj} = Composition based equilibrium constant

m = Remaining mass of coal during pyrolysis process, *gr*

M = Component's name

n_c = Number of components in a reaction

n_r = Number of reactions

n_s = Number of solid components

p = Pressure, *kPa*

p^o = Standard-state pressure, *101.325 kPa*

R = Universal gas constant, *8.314 J/gmol-K*

r_j = Rate of reaction *j*, *gmol/day-m^3-bulk-volume*

S = Reactive surface area, *m^2/gr*

S_g = Gas phase saturation

t = Time, *min*

T = Temperature, *K*

V_b = Bulk volume, *m^3*

V_r = Rock volume, *m^3*

V_v = Void volume, *m^3*

X_C = Char conversion factor

y_i = Mole fraction of *i^{th}* gas component

ΔG_j^o = Standard Gibbs-energy change of reaction *j*, *J/gmol*

ΔH_j = Heat of reaction *j*, *J/gmol*

Greek Letters

α = Stoichiometric coefficient of volatile matter during pyrolysis process

β = Heating rate, *°C/min*

γ_i = Partial pressure or bulk volume concentration of *i^{th}* component

ξ_{ij} = Algebraic stoichiometric coefficient of *i^{th}* reactant or product in reaction *j*

ρ_i = Solid density of solid component *i*, *gmol/m^3*

ρ_g = Gas phase density, $gmol/m^3$

ϕ_f = Fluid porosity

ϕ_{ref} = Reference void porosity at p_{ref} and T_{ref}

ϕ_v = Void porosity

ν_{ij} = Stoichiometric coefficient of reactant *i* in reaction *j*

υ'_{ij} = Stoichiometric coefficient of product *i* in reaction *j*

υ_j = Algebraic summation of stoichiometric coefficients of reactants and products in reaction *j*

ψ = Pore structure parameter

Subscripts

b = Backward direction, bulk volume

e = Equilibrium condition

f = Fluid phase, forward direction

g = Gas phase

i = i^{th} component

j = j^{th} reaction

5.7 Appendix 5-A: Proof of Equations (5-20) and (5-21)

Assuming an initial amount of coal, m_0, undergoes pyrolysis process with linear heating rate, β, $T = \beta t + T_o$, the coal will lose its weight due to the evolution of volatile matters. It was also assumed that the weight loss rate of the coal is proportional to the current mass of the coal and can be described as a first-order reaction with proportionality parameter as Arrhenius type reaction constant, equation (5-A.1), where m is the current amount mass of coal during pyrolysis process.

$$\frac{dm}{dt} = -A_0 exp\left[-\frac{E_a}{RT}\right] m \qquad (5\text{-A.1})$$

Since $\frac{dT}{dt} = \beta$, equation (5-A.1) can be rewritten as equation (5-A.2) which can be integrated as shown in equations (5-A.3) and (5-A.4).

$$\frac{dm}{dT} = -\frac{A_0}{\beta} exp\left[-\frac{E_a}{RT}\right] m \tag{5-A.2}$$

$$\int_{m_0}^{m} \frac{d\omega}{\omega} = -\frac{A_0}{\beta} \int_{T_0}^{T} exp\left[-\frac{E_a}{R\theta}\right] d\theta \tag{5-A.3}$$

$$ln\left(\frac{m}{m_0}\right) = -\frac{A_0}{\beta} \int_{T_0}^{T} exp\left[-\frac{E_a}{R\theta}\right] d\theta \tag{5-A.4}$$

Applying the estimation of (5-A.5) for the right hand side integral of equation (5-A.4) will obtain the current mass of the coal at time *t* with temperature *T*, equation (5-A.6).

$$\int_{T_0}^{T} exp\left[-\frac{E_a}{R\theta}\right] d\theta \cong \left(\frac{RT^2}{E_a}\right) exp\left[-\frac{E_a}{RT}\right] \tag{5-A.5}$$

$$m = m_0 . exp\left(-\frac{A_0 RT^2}{\beta E_a} . exp\left(-\frac{E_a}{RT}\right)\right) \tag{5-A.6}$$

The rate of weight loss can be obtained by taking the derivative of equation (5-A.6) with respect to temperature, equation (5-A.7).

$$\frac{dm}{dT} = -\frac{m_0 A_0 R}{\beta E_a}\left(2T + \frac{E_a}{R}\right) . exp\left(-\frac{E_a}{RT} - \frac{A_0 RT^2}{\beta E_a} . exp\left(-\frac{E_a}{RT}\right)\right) \tag{5-A.7}$$

Chapter 6 Large Scale Simulation of UCG Process Applying Porous Medium Approach[5]

6.1 Abstract

Underground coal gasification (UCG) has significant advantages and can be categorized as a clean coal technology to produce syngas *in-situ*. However, it suffers from lack of a comprehensive understanding of the process because it takes place deep underground and consists of multi-phenomena. It is paramount to anticipate the process behavior prior to a pilot design and technology selection and it is critical to employ a UCG model while considering different aspects of this process. While small scale processes can be mechanistically informative, large scale processes may behave quite differently.

In this work, detailed 3D simulation modeling of three widely applied UCG technologies was conducted for the Ardley coal formation (Alberta, Canada) in order to compare the performance of different technologies in field scale. The results of these comparisons can be helpful for selecting the right technology for a desired UCG pilot test. The results show that in spite of higher heating value of produced syngas from P-CRIP (parallel controlled retracting injection point) method over L-CRIP (linear controlled retracting injection point) method, the volumetric rate and sweep efficiency of these methods are comparable. Moreover, we conducted 2D cross-sectional modeling of the Thulin test as the earliest UCG process at great depth and in tight coal seams to address modeling issues. Several possible approaches, such as geomechanical modeling, are presented to resolve the issues of UCG modeling in tight coal seams. The modeling results are analyzed and compared with the field results. Comparison shows an engineering match for the composition of the produced syngas. Computer Modeling Group's STARS software was used in this study as the porous medium modeling approach.

[5] M. Seifi, Z. Chen, and J. Abedi 2014. Large Scale Simulation of UCG Process Applying Porous Medium Approach. *The Canadian Journal of Chemical Engineering*. CJCE-14-0521.R1. Accepted.

Keywords CRIP Methods, Geomechanics, Pressurization, Retraction Strategy, Tight Coal Seams, UCG Technologies

6.2 Introduction

Underground coal gasification (UCG) is a potential method for economically recovering stored energy in coal formations, especially from coal deposits that cannot be mined using conventional methods. A well-developed UCG technology has the potential to increase the exploitation of the world's coal resources substantially. While UCG may cause surface subsidence in shallow tests, overall it presents fewer negative environmental effects. A basic UCG process consists of two boreholes drilled into a coal seam some distance apart, one for the injection of oxidants and the other for the production of synthetic gas (syngas). Depending on the deliverability of the coal seam mainly to gas flow, the distance between the wells may need human interference to increase the connectivity of the injection and production points. This can be done using well-developed methods from the oil and gas industry, such as directional drilling, hydraulic fracturing, and reverse combustion (Perkins 2005; Couch 2009; Shafirovich and Varma 2009; Richardson and CanZealand 2010; Richardson 2011; Synfuels:SwanHill 2012).

Generally, underground coal gasification can be conducted on a field scale as a sequence of well pairs that divide the entire gasification region into *gasification modules*. Each module is intended to be combusted and gasified by a well pair. The configuration of these wells in each module proposes a number of technologies, such as steeply dipping seams, linked vertical wells (LVW), and linear and parallel controlled retracting injection points (L-CRIP, P-CRIP), all of which are widely used in the UCG industry. Other recovery techniques include the use of man-made underground tunnels from abandoned coal mines in China and εUCG Technology by Ergo-Exergy in Canada. The LVW technology uses two vertical wells as the producer and injector in each gasification module. In CRIP methods, appropriate for nearly horizontal coal seams, the injector is always horizontal. Initially, it is close to the production point and over time it is retracted to access fresh coal. L-CRIP and P-CRIP utilize vertical and horizontal producers, respectively. Therefore, the location of the production point in the L-CRIP method will remain the same in each gasification module. In the P-CRIP technique, the horizontal producer will be retracted at almost the same rate as the injector during the gasification of the module. In steeply dipping seams, a slanted injection well is drilled into the bottom of the coal bed and the vertical

producer is located above the injector a short distance away. In highly dipped coal deposits, the location of the injection and possibly production points will be displaced in order to access fresh coal and reduce the effects of deposited ash and rubble over the injection point (Perkins 2005; Couch 2009; Shafirovich and Varma 2009).

More than fifty years of UCG tests have provided a vast amount of information on different aspects of the process. However, since UCG takes place at great depths and involves multi-disciplinary phenomena, it still requires a comprehensive integration of knowledge from exploration, geology, hydrogeology, drilling, and the chemistry and thermodynamics of gasification reactions in cavities in a coal seam. Consequently, one still lacks a detailed understanding and ability to accurately predict the complicated UCG process. On the other hand, UCG modeling in small and large scales can provide more accurate information about the different phenomena that take place during the UCG process. The information obtained from small scale modeling can be used to mechanistically analyze UCG processes and can be scaled-up for use in large scale simulations. A variety of small scale UCG models are found in the literature (Perkins 2005; Magnani 1973; Winslow 1977; Tsang 1980; Massaquoi 1981; Britten and Thorsness 1988; Shirsat 1989; Batenburg 1992; Biezen 1996; Yang 2005; Yonggang et al 2009; Seifi et al 2013). However, large scale tests behave quite differently than lab scale experiments. This is particularly true in UCG because of the necessity of generating a large cavity, tolerating overburden loads, and the thermo-mechanical variation of the solid materials. There are a few large scale models in the literature some of which were applied only for specific tests (Hong 1984; Nourozieh et al 2010; Seifi et al 2011).

The present work consists of two sections. In the first part, three-dimensional large scale simulations of the most common UCG technologies (LVW, L-CRIP, and P-CRIP) are explained in great detail applying the porous medium approach. The Ardley coal formation in Alberta, Canada is used as the candidate for a UCG process modeled in this section. The simulation results are compared to provide information for technology selection depending on the intended usage of the produced syngas. In the second part, we present a 2D cross-sectional model of the Thulin UCG test. This test was the deepest UCG trial in tight coal seams prior to the SwanHills UCG pilot in Alberta, Canada (Chandelle et al 1993; Mostade 2012; Synfuels:SwanHills 2012). The modeling issues that arose as a result of the tightness of the coal seams and the approaches taken to resolve it, including geomechanical modeling, will be explained. The comparison of

knowledge obtained from the Thulin simulation and the field results will improve our understanding of the UCG process.

6.3 Comparison of Technologies

6.3.1 Model Structure and Well Configurations

The dimensions of the gasification module (simulation model) are assumed to be $70.5 \times 65.5 \times 12.0\, m$. The three-dimensional domain was discretized using the finite difference method (FDM) into cubic grid blocks with the size of 0.5 m in each direction, which is optimal for temperature distribution and computation time. This gridding method generated 443,304 simulation grid blocks and 24 simulation layers. According to the grid sensitivity test described by Seifi et al. (2011), decreasing the size of the grid blocks may increase the accuracy and resolution of the temperature distribution slightly, but would exponentially increase the total number of grid blocks and the runtime of the simulations. The production and injection points in all of the models were placed in layer 22, one meter from the bottom of the coal seam. **Fig. 6-1** illustrates the layout and the extension of the injector and producer and the distance between the injection and production points at the initial time for the LVW, L-CRIP, and P-CRIP methods. The dimensions of the simulation domain and grid block sizes are the same for all of the models. However, the location of the perforated zones, the distance between injection and production wells, and the well operating conditions vary for each model. The Ardley coal seam with sub-bituminous coal is located at a depth of 550 m and has an average thickness of 12 m (Huq 2013). The diagonal section of the P-CRIP method creates an approximate angle of 35° with the horizontal section (Huq 2012). However, in this work it was assumed to be 45°, since a lower angle requires either a larger initial distance between the injection and production points at the constant domain dimensions or larger domain dimensions with the same distance between the injection and production points.

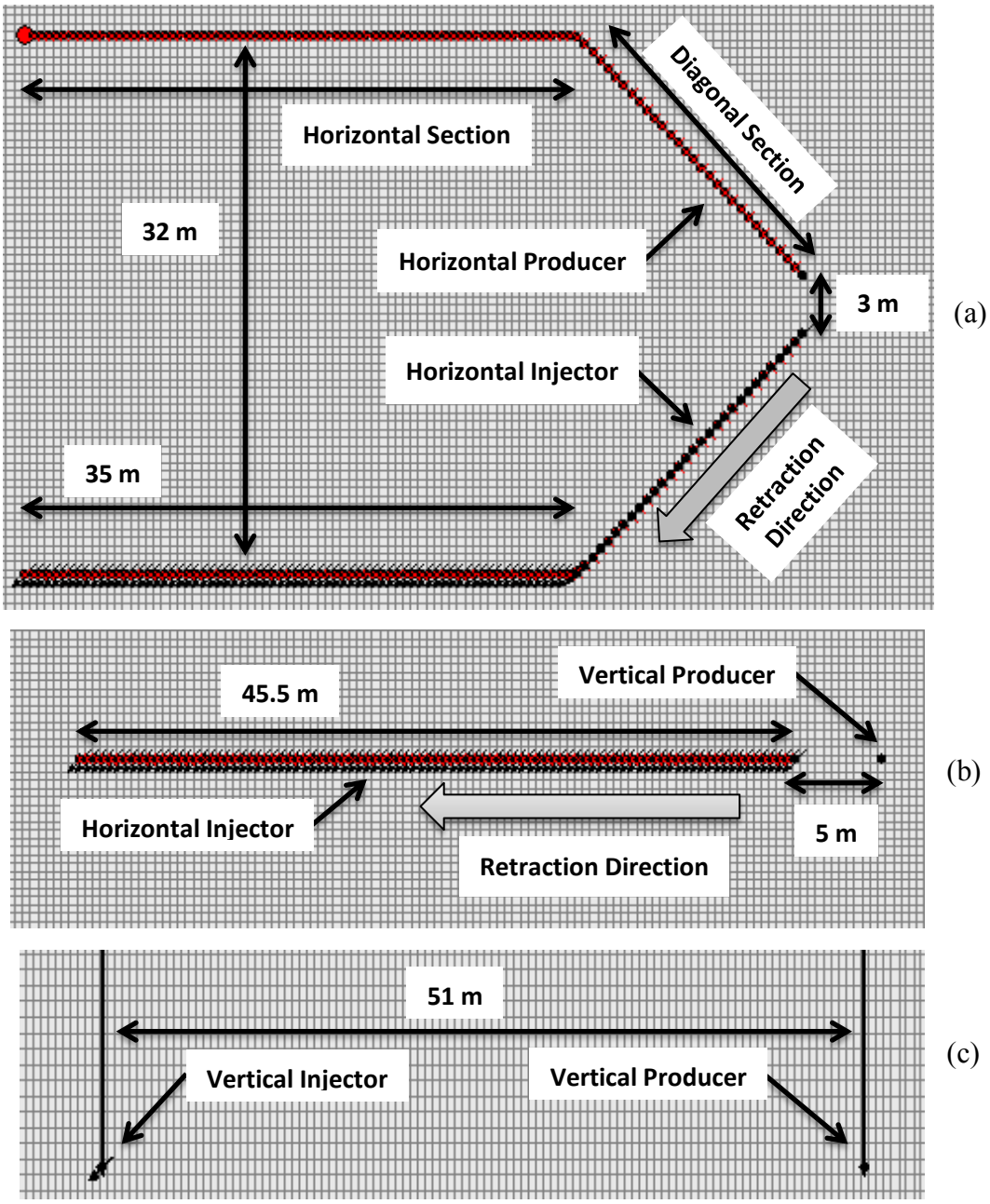

Fig. 6-1: Well configurations (a) P-CRIP, (b) L-CRIP, and (c) LVW

The permeability of the coal seam is assumed to be an exponential function of the fluid porosity, equation (6-1). The consumption and generation of solid components and the variation in the void porosity both affect the fluid porosity, equation (6-2). Since the geomechanical effect has been ignored, void porosity is simply a linear function of pressure and temperature, equation (6-3). However, due to lack of information on the isobaric and isothermal expansion coefficients of the rock (ash), the void porosity was assumed to remain constant at the initial value of 66.34 %. The permeability multiplier, K_{mul}, in equation (6-1) is assumed to be 4 in all directions. A greater permeability multiplier under the same operating conditions increases the speed of gas production and markedly reduces the residence time of the reactions. On the other hand, a smaller value of K_{mul} lowers the syngas production and pressurizes the coal seam, which may cause the gas components to escape from a cavity to the surrounding formations (CMG: STARS Technical Manual 2013).

$$K = K_0 . exp\left[K_{mul} . \left(\frac{\phi_f - \phi_{f0}}{1 - \phi_{f0}}\right)\right] \tag{6-1}$$

$$\phi_f = \phi_v \left(1 - \sum_{i=1}^{n_s} \left(\frac{c_{s_i}}{\rho_{s_i}}\right)\right) \tag{6-2}$$

$$\phi_v = \phi_{vr} \left(1 + C_p(P - P_r) - C_T(T - T_r)\right) \tag{6-3}$$

Figs. 6-2a and **6-2b** illustrate the variation of coal seam permeability versus fluid porosity for different values of the exponential multiplier and initial permeability, K_0, of the coal seam, respectively. The orders of magnitude of permeability at higher fluid porosities are the same, but the variation of permeability with the initial permeability at lower fluid porosity is very significant. This observation is useful in cases with much lower initial permeability resulting in pressurization of the domain.

6.3.2 Component Properties

Since all models are of equal size and applied to the same coal formation, the properties and initial quantity of fluid and solid components and the properties of the rock network will remain the same. The proximate and ultimate analyses for the *Lower Ardley B* coal formation are shown in **Table 6-1**. The average values of the coal analyses are used for property evaluation purposes.

The results of the ultimate analysis were normalized for elimination of the sulfur element to reduce the number of stoichiometric coefficients in the pyrolysis reaction (H_2S was ignored from the volatile matters of the pyrolysis process). The initial static pressure of the water and gas prior to injection/production/gasification was calculated as hydrostatic pressure assuming a water density of 1,000 kg/m^3 and using $\rho_w g d$ where d is the depth of the coal seam. The molecular weight of the coal, coal solid density, and initial coal concentration were calculated using the procedure explained by Seifi et al. (2013). Other physical properties are assumed to be the average and typical values of this formation. **Table 6-2** summarizes the physical properties of the coal layer, fluid, and solid components.

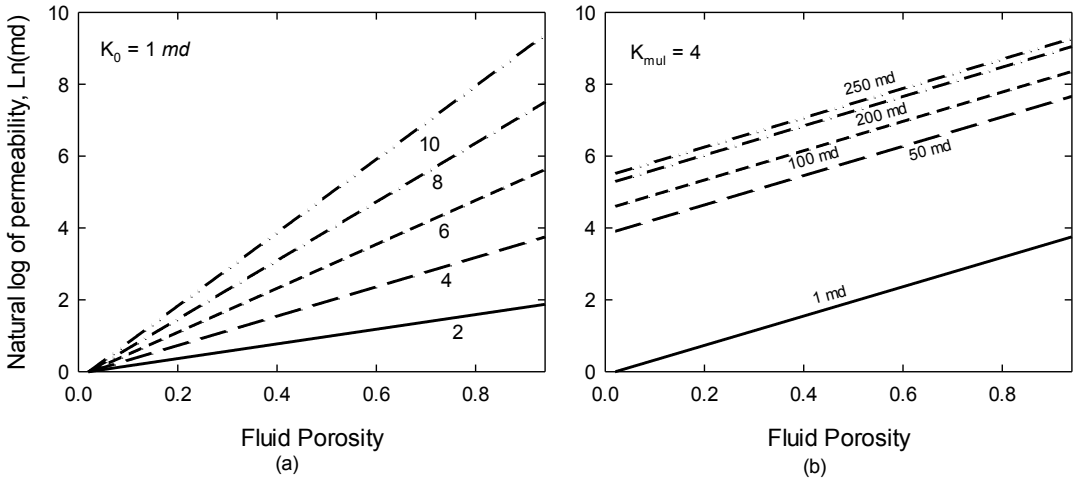

Fig. 6-2: Variation of permeability with, (a) exponential multiplier, K_{mul} , and (b) initial permeability of coal seam, K_0

The gas phase viscosity, approximately 0.01 *cp*, is usually much smaller than the liquid phase viscosity. In the porous medium approach to UCG simulation, the viscosity of the gas phase is a linear function of the temperature, $\mu_g = 0.0136 + 3.8E - 5T$, in which temperature is in $°C$ and viscosity is measured in *cp*. This indicates that the gas viscosity is only dependent on temperature, and not on composition or pressure. This simplified equation is quite sufficient in most cases (CMG: STARS Technical Manual 2013). The comprehensive description of the property evaluation procedures is explained by Seifi et al. (2013).

Table 6-1: Proximate and elemental analyses of Lower Ardley B coal seam

Ultimate Analysis (wt %, daf)				Proximate Analysis (wt%, ar)			
	Ref[1]	Ref[2]	Average		Ref[1]	Ref[2]	Average
Carbon	75.7	75.2	75.5	**Moisture**	19.3	21.1	20.2
Hydrogen	4.1	5.0	4.6	**Ash**	16.1	19.2	17.7
Nitrogen	1.2	1.0	1.1	**Fixed Carbon**	39.4	36.1	37.8
Sulfur	0.5	0.3	0.4	**Volatile Matter**	25.2	23.6	24.4
Oxygen	18.5	18.5	18.5				
Total	**100.0**	**100.0**	**100.0**		**100.0**	**100.0**	**100.0**

[1] Shafirovich and Varma (2009)
[2] Shirsat (1989)

Table 6-2: Physical and thermal properties of Lower Ardley B coal seam and solid components

	Property	Value	Unit
Physical Properties of Coal Seam	Porosity	9.5 %[1]	
	Permeability	10[2]	*md*
	Permeability of Linking Channel (*Assumed*)	1000	*md*
	Depth	550[3]	*m*
Initial Properties of Coal Seam	Static Pressure (*Calculated*)	5394	*kPa*
	Temperature	25[4]	*°C*
	Coal Concentration (*Calculated*)	70900	*gmol/m^{3}PV*
	Water Saturation (*Assumed*)	70 %	
	Methane Mole Fraction (*Assumed*)	100 %	
Thermal Properties (Typical Values for Coal and Char)	Volumetric Heat Capacity of Bulk of Coal	3.00E+06	*J/m^3-°C*
	Thermal Conductivity of Ash	2.00E+05	*J/m-day-°C*
	Thermal Conductivity of Water	4.84E+04	*J/m-day-°C*
	Thermal Conductivity of Solid (Coal and Char)	3.03E+05[5]	*J/m-day-°C*
	Thermal Conductivity of Gas Mixture	4.00E+03	*J/m-day-°C*
	Heat Capacity of Coal and Char	14.779	*J/gmol-°C*
Physical Properties of Solid Components	Coal Molecular Weight (*Calculated*)	15.8437	*kg/gmol*
	Char Molecular Weight (*Carbon as char*)	12.01	*kg/gmol*
	Coal Bulk Density	1200.0[3]	*kg/m^3*
	Coal Solid Density (*Calculated*)	1311.07	*kg/m^3*
	Char Solid Density (*Assumed*)	1700	*kg/m^3*

[1] Parkash and Chakrabartty (1086)
[2] Synfuels: SwanHills (2012)
[3] Huq (2013)
[4] Bachu and Burwash (2008)
[5] Herrin and Deming (1996)

6.3.3 Reactions

Common homogeneous and heterogeneous reactions in a UCG process include vaporization (drying zone), pyrolysis, and combustion and gasification of char and combustible gas components. Detailed descriptions of these reactions can be found in reference by Seifi et al. (2014). In this study, the stoichiometric coefficients of the pyrolysis reaction were calculated using the elemental balance and assuming that 50% of total hydrogen (H) content of the coal is released as methane and the rest as hydrogen molecules (H_2). This assumption was necessary in order to maintain a positive value for all of the coefficients. It was also assumed that only five gas species were evolved during the pyrolysis process. The kinetics of pyrolysis reaction ($A_0 = 1.44E9\ day^{-1}, E_a = 150\ kJ/gmol$) was selected using the procedure explained by Seifi et al. (2014). The single-step decomposition pyrolysis method was applied, equation (6-4).

$$\boldsymbol{Coal(daf)} \rightarrow 0.802994529\boldsymbol{C} + 0.006247059\boldsymbol{N_2} + 0.076737890\boldsymbol{CO_2} + 0.029526621\boldsymbol{CO} + 0.181481919\boldsymbol{H_2} + 0.090740960\boldsymbol{CH_4} \quad (6\text{-}4)$$

Other common heterogeneous and homogeneous reactions applied in the models are summarized in **Table 6-3**.

Table 6-3: Applied heterogeneous and homogeneous reactions in the models

Reaction	A_0	E_a (kJ/gmol)	ΔH (kJ/gmol)
$C + O_2 \rightarrow CO_2$	1.8E+06	100.0	393.0
$C + CO_2 \rightarrow 2CO$	3.2E+10	249.0	-172.0
$C + H_2O \rightarrow H_2 + CO$	4.7E+07	156.0	-131.0
$C + 2H_2 \rightarrow CH_4$	1.5E+14	200.0	75.0
$CO + H_2O \rightarrow CO_2 + H_2$	2.4E+05	12.6	41.0
$CO_2 + H_2 \rightarrow CO + H_2O$	2.4E+03	53.6	-41.0
$CH_4 + H_2O \rightarrow CO + 3H_2$	2.7E+07	236.0	-206.0
$CO + 3H_2 \rightarrow CH_4 + H_2O$	2.7E+08	30.0	206.0

In the drying zone, the surface water in the wet coal is vaporized at temperatures above the saturation temperature of the seam water at the current pressure, making the coal more porous. In the porous medium approach, the moisture content of the coal (from proximate analysis) is

assumed to be equal to the initial water saturation of the domain. The possible addition of pore space, due to evaporation, is added at the beginning (Campbell 1976; Seifi et al 2013). The liquid water is vaporized according to the K-value obtained from equation (6-5) at the current gas phase pressure and temperature. The mole fraction of the water vapor in the gas phase is equal to the K-value (CMG: STARS Technical Manual 2013). This vaporization allows more space for the gas phase in the seam. The porous medium model does not consider thermo-mechanical change in the coal as a result of drying.

$$K_w(P,T) = \left(\frac{k_{v1}}{P} + k_{v2}P + k_{v3}\right).exp\left[\frac{k_{v4}}{(T - k_{v5})}\right] \quad (6\text{-}5)$$

6.3.4 Well Operating Conditions and CRIP Retraction Strategy

Enriched air was injected as the oxidant in all of the simulation models so that the concentration of oxygen and nitrogen was 95% and 5%, respectively. The bottom-hole-pressure (BHP) of the production wells was set at 4,900 *kPa* which represents a pressure drop of approximately 500 *kPa* for the flow of the gas phase to the producers. This assumption was made to ensure that the residence time was adequate for the gaseous species to contribute to the reactions. When burning is initiated, there is not enough room for the injected gas components, so the initial injection rate was assumed to be small, 400 sm^3/day (520 *kg/day*). **Fig. 6-3** depicts the oxidant injection rate based on the P-CRIP method for the remainder of the simulation time. This injection strategy is designed according to the size of the developed cavity. There is no oxidant injection during the warm-up stage, due to a very small pore volume at the beginning. As the size of the cavity increases with time around the injection point and the diagonal section of the horizontal injector, the injection rate increases linearly. At the third stage, when the evolution of the cavity is around the horizontal section of the injection well, the injection rate remains constant (Huq 2013). For the purpose of comparing the different technologies, the same operating conditions were used for all of the simulation models. The injection temperature is assumed to be equal to the initial temperature of 25 *°C*.

The retraction strategy of the injection and production points for the CRIP methods in the UCG simulation using the porous medium approach can be accomplished by either automatic or manual retractions. In general, all of the possible perforations of the wellbores are defined from

the beginning of the simulation in a closed state and will be opened to production or injection during the simulation when some of the constraints are satisfied. In automatic retraction, which is currently only possible for production wells, all of the perforations of the horizontal producer are replaced with a vertical well that is perforated at the same location. Initially, all of the vertical wells are closed except for one nearest the injection point. However, by setting the temperature and oxygen mole fraction constraints at the bottom of each vertical well, they can be opened or closed. For instance, if the temperature at the bottom of the current open vertical well is greater than 500 °C and/or if the oxygen mole fraction is greater than 6%, it might be an indication of an approaching fire front to the producer. Therefore, the current vertical well would be closed and the next one would be automatically opened for production. This scenario could be applied to a horizontal injector if the heating value of the produced syngas were used as its constraint. In the manual retraction strategy, the retraction of the injection and production points is determined by trial and error, i.e., running different simulation models and analyzing the behavior of the fire front and cavity growth rate. In the latter approach, applying a slower retraction rate during the early stage of the simulation may result in immediate consumption of the char between the production and the injection points, significantly increasing the permeability of the linking channel. This may cause an early breakthrough of the injected oxidant and extinction of the combustion. This study focuses on the manual retraction method. The applied retraction rate was 5 cm/day on average, faster at the beginning in order to prevent a breakthrough and slower as time progressed to encourage greater coverage of the domain.

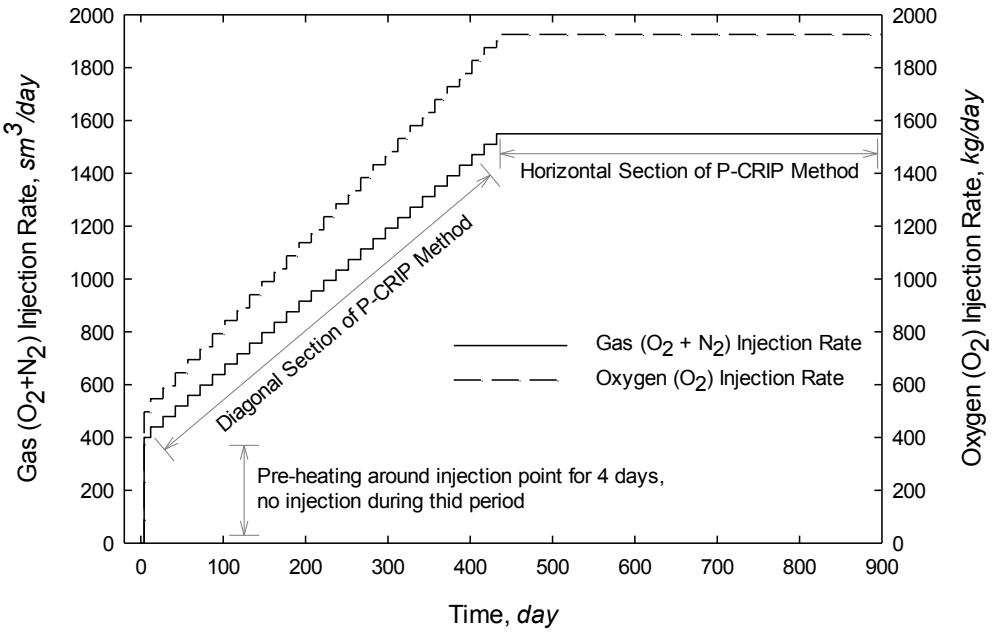

Fig. 6-3: Gas injection rate for P-CRIP method

6.3.5 Results and Discussion on Technology Comparison

In this section, three-dimensional cavity shapes, temperature distribution, and the cumulative production of syngas and gas components will be presented and analyzed in detail.

Fig. 6-4 illustrates the 3D cavity shapes for different well configurations at time 408 *days*. In all cases, the cavities grow along the injection well; however, the cavity extends significantly in the vertical direction for the LVW technique but mostly evolves laterally and longitudinally in the CRIP methods. Since the distance between the injection and production points (gasification module length) in the LVW is fixed and larger than that in the CRIP methods, the deliverability of the produced syngas from the injection point towards the production point is reduced, particularly at the early times. As mentioned above, the amount of the injected oxidant is the same for all techniques. The cavity tends to grow faster in the vertical direction in the LVW, which can be controlled by applying larger horizontal permeability. However, in order to compare the different technologies, the permeabilities in all directions for all simulation models were assumed to be the same in this study. The vertical dominancy of the cavity growth in the LVW causes more heat loss to the overburden and hence a smaller cavity. On the other hand, in the CRIP methods the initial injection point is much closer to the production point, which

increases the deliverability of hot gases within the coal seam and greater heat distribution. In this study, the same pressure drop, $P - P_{wf}$, is imposed between the injection and production points and the distance between them is different. As a result, the pressure gradient is larger for the CRIP methods than for the LVW. Thus the initial deliverability of the CRIP methods will be larger than that of the LVW. Larger deliverability means that the injected oxidant can be distributed faster and more easily in the coal seam and can access fresh coal, which will increase the reaction activities. However, larger deliverability may not increase the volumetric rate of the produced syngas. The tear-shape of the cavities in the CRIP methods is controlled by the retraction distance, the time interval of injection at each injection point, the pressure drop along the length of the gasification module, and the permeability of the domain. Moreover, since the viscous force (combination of pressure drop and permeability) is the main mechanism of gas transportation in the porous medium approach, the injected oxidant tends to flow on the path of least resistance (or larger value of $\frac{K.(P-P_{\mathrm{wf}})}{\Delta L}$) towards the production point. This is the reason that the cavity grows around the injection well in the P-CRIP rather than sweeping the entire region between the two horizontal wells. Allowing a larger time interval for each injection point in the P-CRIP may cause a breakthrough of oxidant rather than increasing the volumetric sweep efficiency. The addition of other transportation mechanisms, such as diffusion of gas species, may improve the sweep efficiency of the P-CRIP method but would require larger realistic diffusion data for a multi-component gas mixture, more precise modeling of diffusion rather than simple Fick's first law, and the inclusion of the effect of diffusion in the kinetics of the reactions. Moreover, it will introduce more non-linearity into the model and more potential numerical issues. Diffusion of gas components was ignored in this work, due to the lack of diffusion data at high pressures and temperatures in multi-component syngas. A more screening analysis, beyond the scope of this work, is required to determine the effect of the initial permeability of the domain, permeability function, retraction rate, and initial distance between the injection and production points on the shape of the cavities.

Fig. 6-5 depicts the temperature profile for different techniques at time 408 *days,* which is also an indication of the areal extension of the cavities. This figure illustrates that the fire front, the highest temperature region, is located around the injection point in all methods. The oxidation reaction takes place in these zones and produces hot carbon dioxide, which causes more activity

in the form of Boudouard reactions. The produced hot gases flow away from these regions due to the pressure drop and cause the pyrolysis of solid coal and gasification of the produced char. At the injection point, the temperature is equal to the injection temperature at 25 $°C$. In a field test, several gasification modules may function simultaneously; therefore, influence each other due to mass and heat transfer. In this study, the simulation models consider one isolated gasification module and as a result the boundary effect may not be modeled correctly. Thus it is necessary to create a larger model so that the effect of the boundary can be ignored. Unfortunately this will be very expensive. Since several endothermic and exothermic reactions take place simultaneously in a UCG process, a detailed analysis of the reaction kinetics is required to predict a more precise temperature profile.

Fig. 6-6 shows the comparison of cumulative produced dry syngas and gas species (CH_4, H_2, CO_2, and CO) for the different technologies. As shown, the LVW produces more syngas, mainly due to greater carbon dioxide and methane production. Although the cavity size is smallest in the LVW, the residence time is longest because of the lowest deliverability of the hot gases. Therefore, the carbon monoxide generated by the Boudouard reaction is used to produce more methane and carbon dioxide through water-gas-shift and methane-steam-reforming reactions. This lowers the production of hydrogen and carbon monoxide. On the other hand, the total syngas produced by the two CRIP methods is similar, due to the similar size of the created cavities and the retracting nature of the injection point, which increases the deliverability of the hot gases within the coal seam. Since the time-scale of the reactions is much smaller than mass transfer in a porous medium, even a small change in the residence time may cause a significant effect on the composition of the syngas. While the same retraction strategy has been used for both CRIP methods, the grid orientation effect may increase the residence time for hydrogen and carbon monoxide in the P-CRIP method. This will lower the production of these species and increase their storage in the cavity and possible conversion of them into methane. More analysis is required to determine the effect of grid orientation on the residence time and the composition of the produced syngas.

Table 6-4 summarizes the performance comparison of the LVW, L-CRIP, and P-CRIP at time 408 *days*. While each of the three simulation models had the same domain size, the most effective module in-seam length in the P-CRIP method is smaller, due to the specific design of the well configuration. This lowers the volumetric sweep efficiency of the P-CRIP method per

module. However, for the purpose of the coal conversion comparison, the mass of the initial coal in the entire model, 55,406,000 *kg*, has been used for all cases. There is no breakthrough of the oxygen in the LVW due to lower deliverability. The CRIP methods also produce a small amount of oxygen. Since the producer is retracted with the same retraction strategy as the injector in the P-CRIP, the amount of oxygen produced is lower. This could be due to the grid orientation effect. The greater methane production in the P-CRIP method could be due to the increased residence time as a result of the larger distance between the injection and production points and possibly the grid orientation. This will cause the hydrogen and carbon monoxide to be converted into methane. Since the heating value of methane is much greater than that of hydrogen and carbon monoxide, the heating value of the produced syngas in the P-CRIP is greater than in the L-CRIP, even though the coal conversion efficiency is almost identical. As previously explained, large methane production in the LVW increases the heating value of the syngas. The average coal conversion efficiency is defined based on the mass of carbon in the produced syngas. Due to the boundary effect in the LVW and the greater heat conduction beyond the cavity surface, most of the carbon is produced as a result of the pyrolysis rather than combustion and gasification. Therefore, in spite of the higher conversion efficiency, the size of the true cavity (without char inside) is smaller in the LVW method.

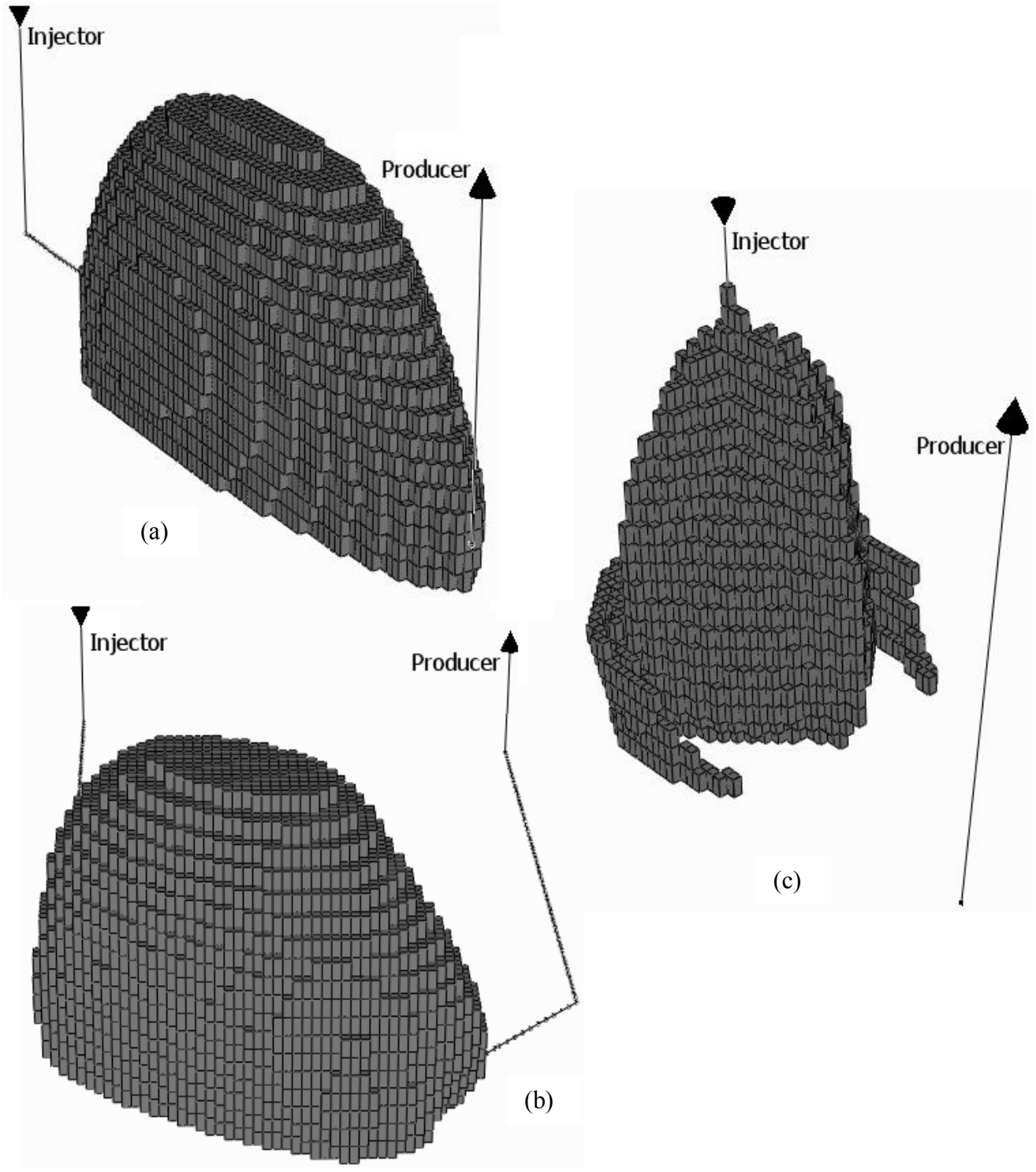

Fig. 6-4: 3D cavity shape at time 408 *days* for, (a) L-CRP, (b) P-CRIP, and (c) LVW

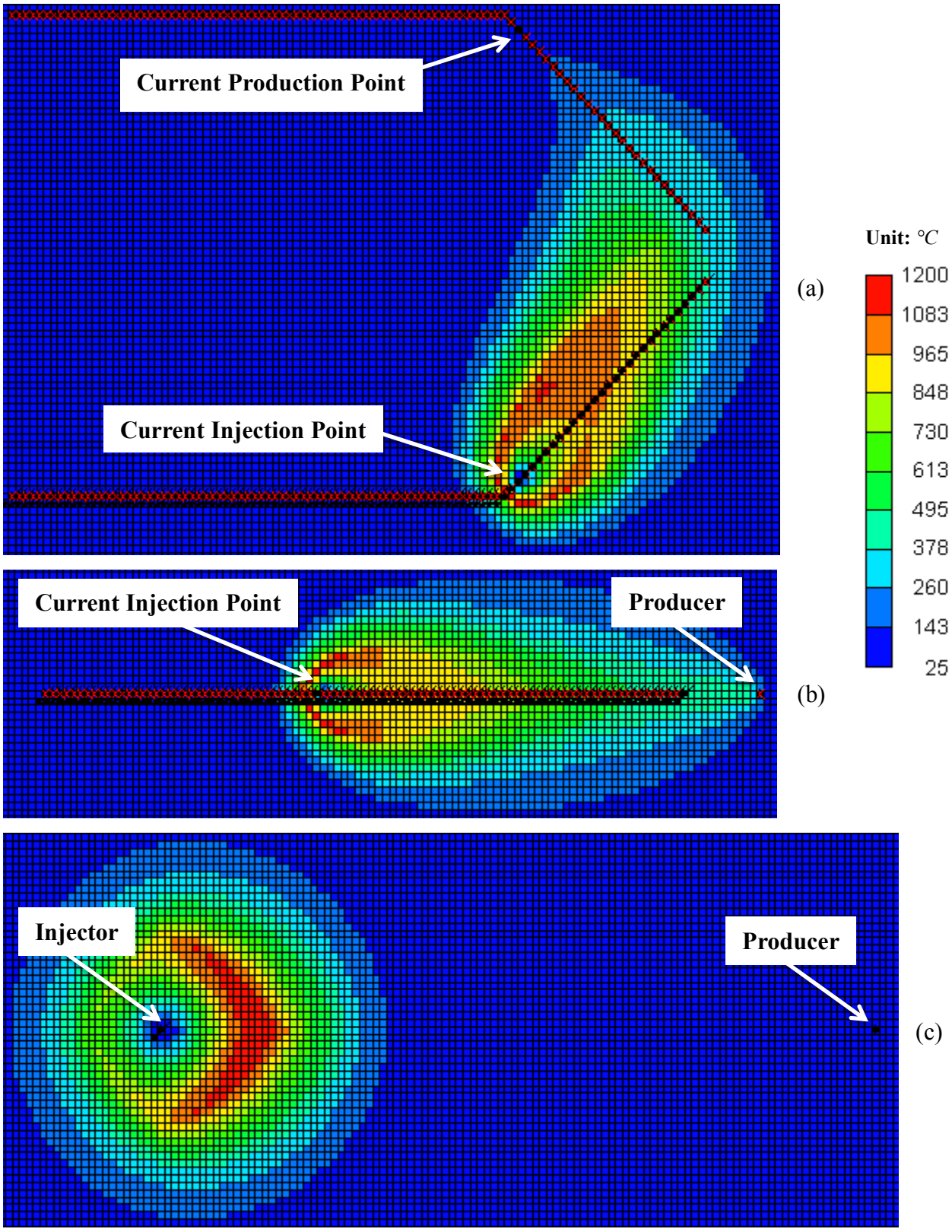

Fig. 6-5: Plan view of temperature profile at time 408 *days* for, (a) P-CRIP, (b) L-CRIP, and (c) LVW

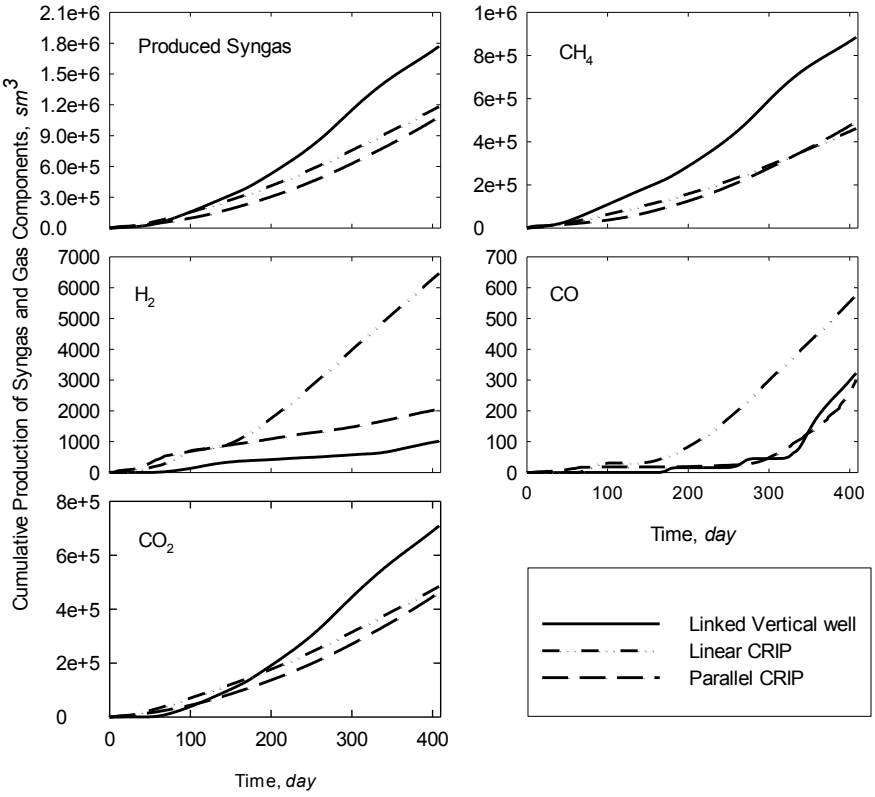

Fig. 6-6: Comparison of cumulative production of syngas and gas species for different technologies by time 408 *days*

Table 6-4: Comparison of different technologies at time 408 *days*

Parameter \ Technology	P-CRIP	L-CRIP	LVW
Coal Seam	Ardley	Ardley	Ardley
Module in-seam Length (*m*)	32	51	51
Avg. Syngas Flow Rate at Wellhead per Module (*Nm^3/day*)	2675	2903	4343
Dry Syngas Composition (dry gas basis)			
CH4	45.42	39.06	50.00
CO	0.03	0.05	0.02
CO2	42.60	40.91	40.06
H2	0.19	0.55	0.06
N2	11.45	14.06	9.86
O2	0.32	5.38	0.00
Total Carbon Initially in Place (*kg*)	55,406,000	55,406,000	55,406,000
Avg. Coal Conversion Efficiency (%) [1]	0.851	0.840	1.414
Avg. HHV of Syngas (*MJ/Nm^3*)	17.12	14.77	18.83

[1] Defined as 100 (kg of Carbon in produced syngas) / (kg of Total Carbon Initially in Place)

6.4 Tight Coal Seam (Thulin Test)

6.4.1 Model Structure and Well Configurations

The Thulin test includes two coal seams, Leopold at the top and Charles at the bottom with an approximate dipping angle of 25°. Leopold is located at a depth of 857 *m* on the shallow side (the right-hand side of **Fig. 6-7**). Each coal seam consists of several staggered and varying-thickness anthracite coal and shale beds. There are three coal layers and three shale layers in the Leopold coal seam while the Charles coal seam consists of two thicker coal layers and one shale layer. Since there was no comprehensive geological information to build a precise static model of the Thulin test, the geological profile proposed by Chandelle et al. (1993) was applied, **Fig. 6-7**. **Table 6-5** summarizes the thickness of the layers on the left- and right-hand sides of the applied geological profile (digitized from Chandelle et al.). The dimensions of the 2D cross-sectional model are $35 \times 0.18 \times 11\ m$. This domain was discretized into grid blocks with an approximate size of 18 cm using FDM, which generated $194 \times 1 \times 60$ grid blocks in the x-, y-, and z-directions, respectively. The block size of 18 *cm* was selected to capture the minimum layer thickness, the right-hand side of shale layer 1. Since permeability of the coal and shale layers (0.0078 *md* and 0.00034 *md*, respectively) in Thulin test are in the order of micro- and nano-Darcy, these coal formations can be categorized as tight coal seams (Chandelle et al 1993; Mostade 2012).

Table 6-5: Thickness of layers on the left and right side of the cross-sectional model, see Fig. 6-7

Layers	Thickness of Layers (*m*) on	
	Left-Side	Right-Side
Upper Leopold Coal Bed	1.36	1.46
Shale Layer 1 in Leopold	0.47	0.18
Middle Leopold Coal Bed	0.71	0.85
Shale Layer 2 in Leopold	0.37[1]	0.24
Lower Leopold Coal Bed	0	0.51
Shale Layer 2+3 in Leopold	0.94	0.57
Upper Charles Coal Bed	1.65	1.41
Shale Layer 4 in Charles	0.75	2.72
Lower Charles Coal Bed	1.18	1.18

[1] This thickness for the middle of the domain where shale layers 2 and 3 meet together

The production well, Thulin 2, is a vertical well, completed and perforated in the upper coal bed and in shale layer 4 in the Charles coal seam. The injection well, Thulin 1, was drilled using

directional drilling through shale layer 4 towards the producer such that the distance between the end of the open channel and the perforated zone of the producer is approximately 1.5 *m*. This distance was hydraulically fractured to establish communication between the two wells (Chandelle et al 1993; Mostade 2012). As shown in **Fig. 6-7**, the hydraulically fractured zone and open hole were considered the same to simplify the initial static model. The injection point is located in the upper coal bed of the Charles coal seam at a distance of 19 *m* from the production well without any retraction during the life of the project. Since the wellbore modeling was not included in this study, the directional injection well was replaced with a vertical injector perforated at the bottom.

6.4.2 Component Properties

Assuming the same coal type for both the Leopold and Charles coal seams, the proximate and ultimate analyses of the coal in the Thulin test are summarized in **Table 6-6**. The results of the ultimate analysis were normalized for the sulfur element to reduce the number of volatile matters evolving through the pyrolysis process. The wet coal bulk density was 1493 kg/m^3. Assuming an initial water saturation of 70% in all layers and the solid density of ash at 2500 kg/m^3, the molecular structure of the coal is $CH_{0.553777}O_{0.017656}N_{0.012098}$. An initial fluid porosity of 1.77% was calculated for the shale and coal layers. Applying the procedure explained by Seifi et al. (2011), the coal molecular weight, coal solid density, and initial coal concentration were calculated. We estimate the other physical properties as the typical values for the same type of coal. **Table 6-7** summarizes the physical properties of the coal layers, fluids, and solid components (Mostade 2012).

Table 6-6: Proximate and elemental anaylses applied in evaluation of the physical properties of the coal seams in Thulin test

Proximate Analysis (*wt %, ar*)		**Elemental Analysis (*wt %, daf*)**	
Moisture	0.83	C	91.44
Ash	9.25	H	4.25
Volatile Matter	12.20	O	2.15
Fixed Carbon	77.72	N	1.29
		S	0.87
Total	**100**	**Total**	**100**

6.4.3 Reactions

The pyrolysis process was modeled using the single-step decomposition method. The stoichiometric coefficients of the pyrolysis reaction were calculated using the elemental balance and the results of a weight loss test (Mostade 2012). The evolution of methane and hydrogen was measured during the weight loss test in which a specific sample of coal from the upper Leopold coal bed was heated at a heating rate of 5 $°C/min$. Comparing the amount of fixed carbon from the proximate analysis (assuming that the fixed carbon is a pure carbon) and the amount of carbon in the volatile matters evolved through the weight loss test indicates that other gas components were released while the coal was being heated. To satisfy the results of the elemental analysis, nitrogen, carbon monoxide, and carbon dioxide were assumed to be released during the pyrolysis process. Equation (6-6) shows the final stoichiometric coefficients of the pyrolysis reaction applied in the present work. The kinetics of the pyrolysis reaction ($A_0 = 1.44E8\ day^{-1}, E_a = 150\ kJ/gmol$) were selected using the procedure explained by Seifi et al. (2014). Due to the lack of information, all of the other heterogeneous and homogeneous reactions and their kinetics are assumed to be the same as in **Table 6-3**. The evaporation and condensation of the moisture content of the coal is controlled by equation (6-6).

$$\boldsymbol{Coal(daf)} \rightarrow 0.937012\ \boldsymbol{C} + 0.006048\ \boldsymbol{N_2} + 0.002148\ \boldsymbol{CO} + 0.009153\ \boldsymbol{CO_2} + 0.139796\ \boldsymbol{H_2} + 0.053089\ \boldsymbol{CH_4} \quad (6\text{-}6)$$

Table 6-7: Assumed and evaluated physical properties of the coal seam and solid components

	Property	Value	Unit
Initial Properties of Coal Seam	Static Pressure	8300	*kPa*
	Temperature	31.0	*°C*
	Coal Concentration (*Calculated*)	120367	*gmol /m^{3}PV*
	Water Saturation (*Assumed*)	70.0 %	
	Methane Mole Fraction (*Assumed*)	100.0 %	
Thermal Properties	Volumetric Heat Capacity of Bulk of Coal	2.65E+06	*J/m^3-°C*
	Thermal Conductivity of Ash	1.12E+05	*J/m-day-°C*
	Thermal Conductivity of Water	4.84E+04	*J/m-day-°C*
	Thermal Conductivity of Solid (Coal and Char)	5.00E+04	*J/m-day-°C*
	Thermal Conductivity of Gas Mixture	4.00E+03	*J/m-day-°C*
	Heat Capacity of Coal and Char	17.0	*J/gmol-°C*
Physical Properties of Solid Components	Coal Molecular Weight	13.02	*kg/gmol*
	Char Molecular Weight	12.0	*kg/gmol*
	Coal Solid Density	1597.14	*kg/m^3*
	Char Solid Density	1700.0	*kg/m^3*

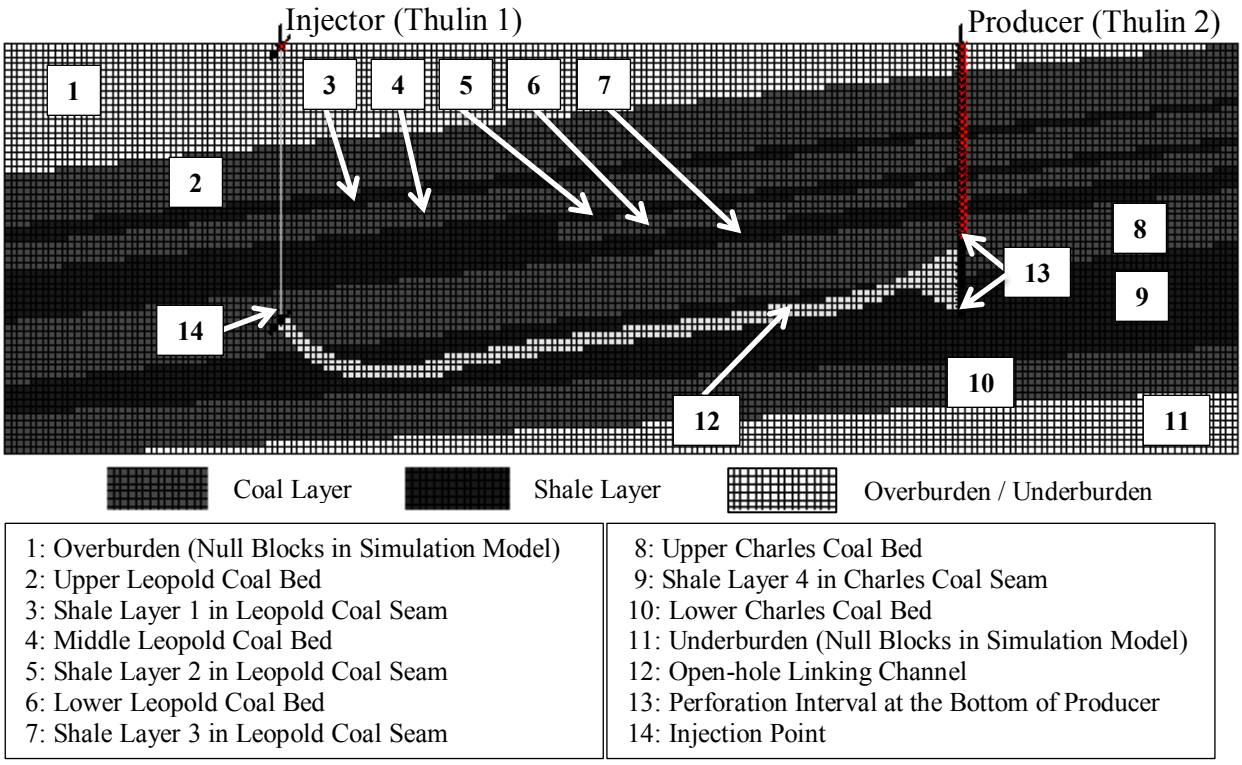

Fig. 6-7: Cross-sectional geological profile of the 2D simulation model for Thulin test

6.4.4 Well Operating Conditions

Air, enriched air, nitrogen (for cooling down the cavity and as a carrier gas), and cold water are used as injected materials during the Thulin test. The type of the injected oxidants applied in the simulation model is the same as in the real field test. The rate of injection of all of the injected materials was multiplied by a correction factor of 1/67 because the 2D model is much smaller than the real test and cannot tolerate the same field injection rate. Applying the mass and volume balances allowed us to estimate the lateral extension of the created cavity during the Thulin test at approximately 12 *m* (Mostade 2012). In this work, the width (y-direction) of the 2D model is assumed to be 18 *cm,* which implies that the lateral extension of the cavity in the model will be a maximum of 18 *cm*. The correction factor was obtained by dividing the lateral extension of the cavity from the model by the real field test. Basically, the correction factor is the ratio of the cavity volumes in the model and in reality. **Fig. 6-8** illustrates the variation of the volumetric injection rate and the bottom-hole pressure of the producer applied in the simulation

model. In summary, the rate and BHP constraints are applied for the injection and production wells, respectively. There was no retraction of the injection point in the Thulin test. The bottom of the injection well was heated for 2 *days* without any injection to resemble the initiation of the combustion in the real test. The injection temperature was assumed to be equal to the initial temperature, 31 *°C*, (Mostade 2012).

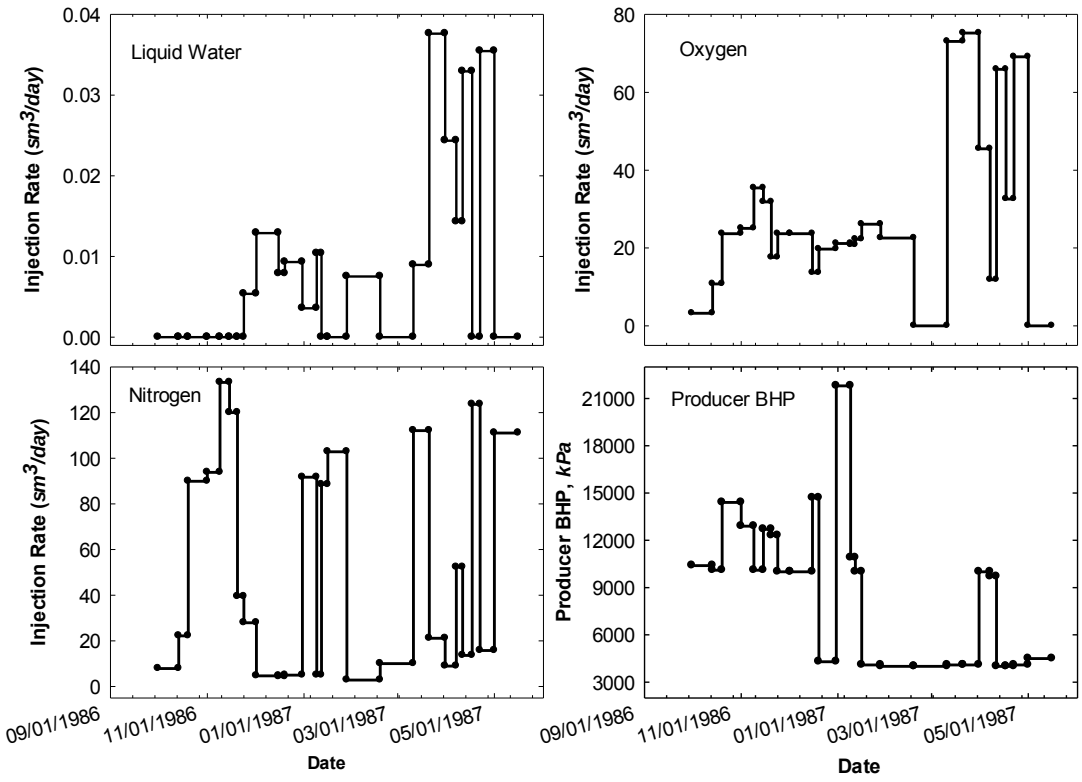

Fig. 6-8: Rate of the injected materials and the producer BHP applied in 2D Thulin simulation model

6.4.5 Results and Discussion on Thulin Test

The simulations were conducted using the developed 2D cross-sectional model using different permeability values between 10 *md* to 7,000 *md* for the open channel. However, the numerical behavior of the runs showed that because of the pressurization of certain grid blocks around the injection point, all of the runs crashed at the first time-step. **Fig. 6-9a** illustrates three simulation grid blocks, which were initially composed of ash, coal, and pore space. We assume that for a specific initial time-step, e.g., 1.0E-6 *day*, a small portion of the middle block is converted into char and some volatile matters, due to the pyrolysis reaction. This will add a little pore space to

the grid block and produce large amount of gas species. Since the permeability of the neighbouring grid blocks is very small, in the order of micro- and nano-Darcy, the produced gases cannot be transported through the surrounding grid blocks in a reasonable amount of time and will result in the pressurization of the middle grid block. The large pressure change in the first time-step results in non-convergence of the solution and cuts the time-step such that it tends to zero at very high pressurization, terminating the simulation run. Even increasing the number of Newton iterations per time-step did not solve the issue. On the other hand, the distribution and transportation of the produced gas components in the coal seam in a reasonable time scale can lower the pressurization and time-step cuts.

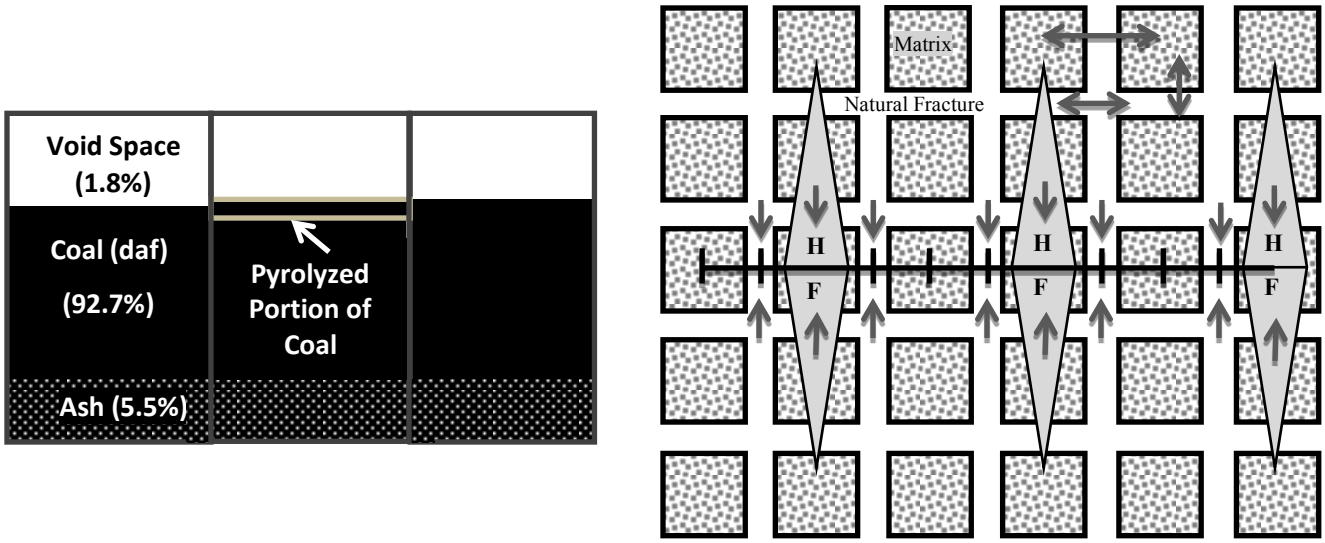

(a) (b)

Fig. 6-9: (a) Three simulation grid-blocks initially composed of ash (rock), coal (flammable solid), and void space (filled with water and methane), and (b) Schematic of a dual-permeability and hydraulic fracture model (HF: Hydraulic Fracture)

A parameter sensitivity analysis revealed that the thermal conductivity of the solid components, fluid porosity, and permeability are the parameters that are the most influential on pressurization. Large thermal conductivity increases the rate of heat diffusion in the coal seam and activates the pyrolysis process in a wider area, which can result in the production of a large amount of gas in the coal seam and greater pressurization. Fluid porosity is an indication of the fraction of pore space; the larger the porosity, the greater the pore volume and the lower the pressurization. Permeability is a measure of the ease of transportation of fluid in the coal seam; the larger the permeability, the lower the pressurization. Scenarios were investigated to reduce

the pressurization and simulation crashes: (1) increasing the initial fluid porosity and the solid density of the coal to maintain the same initial coal concentration; (2) lowering the rate of the pyrolysis reaction to reduce the amount of gas produced by pyrolysis per time-step; (3) applying the dual-permeability fracture model as utilized for the simulation of large scale shale gas reservoirs; (4) increasing the initial permeability of the entire domain and using the single-porosity model; and (5) applying different porosity functions by including geomechanical modeling. Only the last two approaches resolved the issue. The linking channel was removed from the model because even when a permeability of 1 *md* was assumed for the channel, it produced all of the injected oxidants as soon as a connection between the injection point and the channel was established and extinguished the combustion and gasification processes.

6.4.5.1 Fracture (Dual-Porosity/dual-Permeability) Modeling Approach

Fracture modeling, such as dual-porosity, dual-porosity/dual-permeability, and hydraulic fracturing, is a simulation technique for tight and/or fractured reservoirs, e.g., shale gas reservoirs. Dual-porosity/dual-permeability modeling includes matrix-matrix, matrix-fracture, and fracture-fracture mass and heat flow communication, whereas dual-porosity models do not include matrix-matrix mass and heat flow communication. Dual-porosity/dual-permeability fracture modeling is the most appropriate model because UCG is a thermal process. Natural fractures in shale gas reservoirs do not have significant flow conductivity so a series of hydraulic fractures along a horizontal well are induced in the reservoir to enable economical production, **Fig. 6-9b**. During gas production from shale gas reservoirs, adsorbed gas components are desorbed from the surface of solid materials in the matrix blocks, and then the desorbed gas components diffuse into the natural and/or hydraulic fractures which are transferred towards the producer. The time scale of desorption and mass diffusion in shale gas reservoirs are close enough that they do not pressurize the matrix blocks. On the other hand, heat diffusion and reactions are the main process of producing gas components in the matrix blocks in a UCG process. These reactions are much faster than mass diffusion and result in pressurization of the matrix blocks. Consequently, the application of fracture modeling in coal seams with micro- or nano-Darcy permeability was not successful (Warren and Root 1963; Rubin 2010; CMG: STARS Technical Manual 2013).

6.4.5.2 Effective Absolute Permeability Approach

A large initial permeability was applied in this approach instead of a micro- and nano-Darcy range. This can be interpreted as the *effective absolute permeability* of the initial fissures, cleats, and coal matrices in the coal seam. Moreover, fractures might be created in the coal seam during the UCG process as a result of the thermo-mechanical behavior of the coal and char, thus increasing the permeability of the domain. The value of the effective absolute permeability can be obtained by matching the results of the simulation model and the field test. However, since a 2D model was used in this study, it was not possible to match the entire field test. Thus the initial permeability of 250 *md* was used as a result of a sensitivity analysis on permeability. In fact, 250 *md* was the lowest permeability that prevented the simulation crash. It is worth noting that the value of the effective permeability should be selected carefully as it will change the convection heat transfer and residence time of the gas species and may alter the composition of the produced syngas and the temperature distribution within and around a cavity.

6.4.5.3 Geomechanical Modeling Approach

In general, permeability is a strong function of the fluid porosity. However, an application of empirical permeability-porosity relationships such as the exponential function and the Carmon-Kozeny relationship did not initially result in a large enough permeability to prevent the pressurization even with larger permeability variation parameters. This was because the porosity change at the first time-step is not significant and the initial porosity is too small (1.77%). Since the permeability-porosity function should be smooth, imposing an arbitrary table of permeability versus porosity for the initial state of the model may produce unacceptable results and problematic numerical behavior. Moreover, it was observed that very large stress distribution is induced in the model as a result of high pressure. To utilize the change in pressure/stress to increase the permeability of the domain and reduce the pressurization, a relationship between pressure/stress and permeability is required. This is particularly true in cases where the pressure is the main parameter that changes significantly. This situation is similar to the hydraulic fracturing of boreholes where the porous medium is fractured as a result of a pressure increase around the wells. However, in the Thulin case, slight cracking may occur everywhere at higher

pressures. To ensure the best outcome, the geomechanical modeling should be coupled with the flow simulation.

Flow and geomechanics calculations may be coupled one-way, two-ways, iteratively, or fully. In general, the current pressure, current temperature, and initial porosity are transferred to the geomechanics module during the coupling process. Reversely, the stress and strain volume distributions are passed to the flow simulation after the geomechanics calculation. However, there is no stream of information from geomechanics to the flow simulation in one-way coupling; therefore, stress variation is not captured and utilized in the flow simulation in this method. This makes it impractical for use with the Thulin model. Two-way coupling is accomplished following the convergence of the flow solution in the current time-step. Alternatively, iterative coupling takes place following each Newton iteration. In fully coupling method, all geomechanical equations (stress equilibrium solution) are solved simultaneously with flow equations at each Newton iteration. As a result, the iterative and fully coupling approaches are very expensive. For these reasons, the two-way coupling was chosen to capture the effect of geomechanics in the flow simulation in this study. The details of geomechanical modeling and its coupling with reservoir flow simulation are often referenced in the literature, such as (Gutierrez 1998; Settari and Mourits 1998; Dean et al 2003; Tran et al 2005).

In two-way coupling, the void porosity of the porous medium is obtained using equation (6-6), instead of equation (6-3), in which $C_0^{(n)}$ and $C_1^{(n)}$ are the porosity coefficients as a function of temperature, pressure, and mean total stress (MTS) at the previous time-step (*n-level*). Moreover, permeability is determined by applying equation (6-7), in which $f_{K,g}^{(n)}$ is the geomechanical permeability multiplier (GPM) as a function of MTS at the previous time-step and $f_{K,C}^{(k)}$ is the chemical permeability multiplier (CPM) at the previous Newton iteration (*k-level*) of the current time-step. The permeability multipliers are the ratio of the new permeability to the initial permeability. In the present work, $f_{K,g}^{(n)}$ is obtained via table lookup using the table of the permeability ratio versus MTS, **Table 6-8**, and $f_{K,C}^{(k)}$ is obtained from equations (6-1) and (6-2) (Tran et al 2005; Tran et al 2008; Tran et al 2009; CMG: STARS Technical Manual 2013).

Calculating permeability using this new approach is of paramount importance for a UCG process in tight coal seams. The exponential form of $f_{K,C}^{(k)}$ causes the effect of CPM to be more

pronounced in areas with greater fluid porosity as a result of solid component consumption. In these areas (mainly within the cavity), there are small pressure and stress changes. Therefore, the value of $f_{K,g}^{(k)}$ is close to one and has a negligible geomechanics effect on the permeability. However, in regions close to the fire and pyrolysis fronts with active pyrolysis, heterogeneous reactions, and fast production of gas components, there is a considerable change in pressure (more than 40,000 *kPa*) and stress. Thus $f_{K,g}^{(k)}$ is more effective in these zones. Since the solid consumption is lower in these areas, the fluid porosity change is small and $f_{K,C}^{(k)}$ is negligible compared to $f_{K,g}^{(k)}$, **Fig. 6-10**. Consequently, the main effect of **Table 6-8** is in locations that exhibit a greater pressure change. The precise relationship between MTS and GPM should be determined experimentally. However, due to the lack of data, a rough estimate has been used, **Table 6-8**. Positive MTS means compression. The estimated values in **Table 6-8** were obtained according to the simulation results using the *effective absolute permeability* approach and the amount of pressurization in the original model. **Table 6-8** was used to determine the GPM in all directions. Due to complex relationship between MTS and GPM in a UCG process, $f_{K,g}^{(k)}$ can be considered as the matching parameter such as relative permeability curves in hydrocarbon reservoir simulation.

$$\emptyset_V^{(k+1)} = \emptyset_V^{(n)} + C_0^{(n)}\left(P^{(k)} - P^{(n)}\right) + C_1^{(n)}\left(T^{(k)} - T^{(n)}\right) \quad (6\text{-}6)$$

$$K^{(k+1)} = f_{K,C}^{(k)} \cdot f_{K,g}^{(n)} \cdot K_0 \quad (6\text{-}7)$$

Table 6-8: Variation of geomechanical permeability multiplier of porous medium with mean total stress

$\Delta\sigma_m$, kPa	K/K_0	$\Delta\sigma_m$, kPa	K/K_0
-14000	0.72	1000	5000.00
-13000	0.74	2000	10000.00
-12000	0.76	3000	15000.00
-11000	0.78	4000	20000.00
-10000	0.80	5000	25000.00
-9000	0.82	6000	30000.00
-8000	0.84	7000	35000.00
-7000	0.86	8000	40000.00
-6000	0.88	9000	45000.00
-5000	0.90	10000	50000.00
-4000	0.92	11000	55000.00
-3000	0.94	12000	60000.00
-2000	0.96	13000	65000.00
-1000	0.98	14000	70000.00
0	1.00		

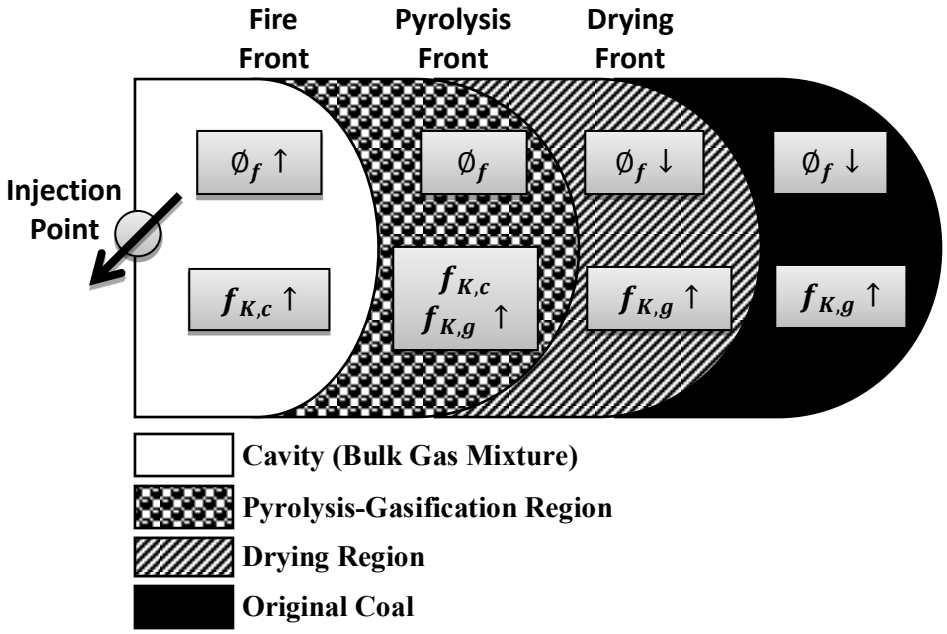

Fig. 6-10: Illustrative sketch of various regions in a typical UCG process and the variation of fluid porosity and chemical and geomechanical permeability multipliers in these regions

The Mohr-Coulomb formulation was used as a mechanical constitutive model in this study. The cohesion property of all of the solid materials constituting the rock matrix was chosen such that it was large enough to force the material to behave elastically. **Table 6-9** summarizes all of the geomechanical properties applied in the Thulin simulation model (Fjaer et al 1992).

Table 6-9: Geomechanical properties of solid components applied in Thulin simulation model

Property	Unit	Rock (ash)	Coal (daf) and Char
Young's Elastic Modulus	*kPa*	3.0E+7	5.0E+6
Poisson's Ratio	-	0.30	0.30
Cohesion	*kPa*	1.0E+10	1.0E+10
Biot's Coefficient		1.0	1.0
Internal Friction Angle	*degrees*	60	35
Dilation Angle	*degrees*	0.0	0.0
Thermal Expansion Coefficient	*1/°C*	1.5E-5	9.0E-6

To simplify the simulation model, geomechanics grid blocks are collocated with reservoir grid blocks such that the bottom of the reservoir is prevented from moving vertically and the lateral sides of the reservoir can only be displaced vertically rather than horizontally. However, there are no displacement constraints at the top of the reservoir. Precise geomechanical modeling requires the geomechanics domain to be extended to the side-burdens to include the effect of lateral formations and to the overburden up to the surface to predict the subsidence. However, as the main purpose of including geomechanical modeling in this study is to establish the flow within the tight coal seam, the geomechanical domain is limited to the coal seams (reservoir domain). The effect of the overburden has been included as an initial stress (confining pressure) of 1,625 *kPa* acting over the top of the upper Leopold coal bed.

6.4.5.4 Simulation Results

Only two of the proposed methods were able to successfully run the Thulin test simulation model with tight coal seams. These methods were the effective absolute permeability approach (EAPA) and the geomechanics approach (GEOA). The two methods differ in their permeability calculation methodology during the UCG process. In this work, the permeability parameters of these methods (the effective initial permeability and the permeability-stress relationship) were chosen in order to run the model successfully. **Figs. 6-11** and **6-12** illustrate the temperature profile, true cavity size, trend, and the amount of produced syngas and gas species, which are similar for these methods. Therefore, depending on data availability, particularly geomechanical data, either of these methods can be used for 3D simulation of the Thulin test and to match the field results. However, GEOA is able to predict the subsidence, heave, and other geomechanical behavior of the coal seams. Finally, both approaches could be used simultaneously.

The field results determined that hydrogen and carbon monoxide were produced at the lowest rate, while carbon dioxide and methane have larger production rates (Mostade 2012). **Fig. 6-11** illustrates the cumulative and rate of production of syngas and gas components for the 2D simulation model of the Thulin test applying the GEOA and EAPA methods. In both approaches, there is no oxygen or water breakthrough and hydrogen production is minimal. Carbon monoxide production was greater than carbon dioxide production, which implies that the kinetics of the Boudouard and water-gas-shift reactions may require more adjustment, as they are primarily responsible for the conversion of carbon dioxide to carbon monoxide. Additionally, the model

responded reasonably to the operating conditions, e.g., over the time interval of 160 to 200 *days*, the water injection rate increased resulting in an increase in the production of carbon monoxide and methane due to water-gas-shift and methane-steam-reforming reactions.

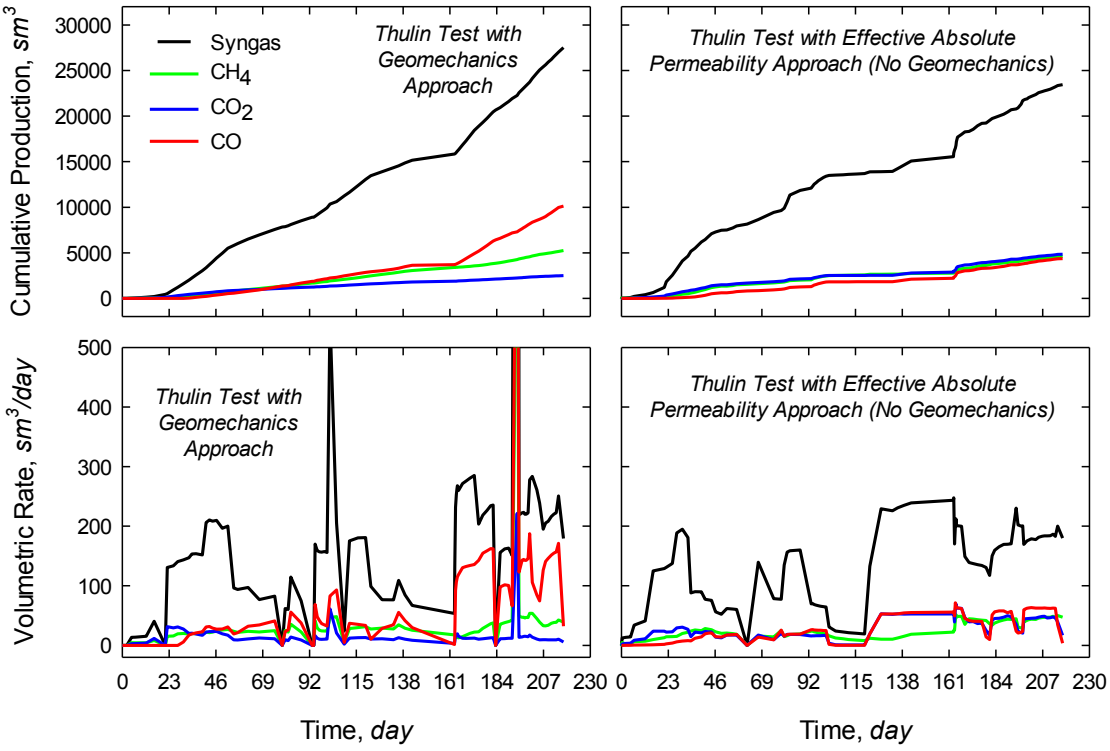

Fig. 6-11: Volumetric rate and cumulative production of syngas and gas species for 2D cross-sectional model of Thulin test applying geomechanics and effective absolute permeability approaches

Fig. 6-12 illustrates the comparison of char concentration, temperature profile, and fluid porosity for the above-mentioned methods. In the GEOA method, the cavity tends to grow vertically. This may be due to the periodic subsidence of the coal layers. The vertical extension of the true cavity in the EAPA method is smaller. Since hot gases migrate to the top side of the inclined coal layers, higher temperatures are seen in the Leopold layers. The injected cold water flows to the bottom of the Charles layers, due to gravity, and absorbs the heat of the domain in these regions to be vaporized. As a result, a wide low temperature region forms around the injection point. **Figs. 6-12e** and **6-12f** show the variation of the fluid porosity at the end of the run (229 *days*). The maximum porosity is the indication of complete pyrolysis, combustion, and

gasification of the char in these areas. Consequently, this zone is assumed to represent the size and shape of the true cavity. In EAPA, the largest attainable porosity at the end of the simulation (when all coal and char have been consumed and only ash remains) is 0.9448. However, in the GEOA method, the porosity may exceed that value or even be lower than the initial value, due to the effect of geomechanics and displacement (subsidence and heave).

Figs. 6-13 and **6-14** depict the variation of pressure, stress, temperature, permeability, solid component concentration, and vertical displacement for two specific coaly and shale grid blocks. Effective mean stress is obtained according to $\sigma_m^{eff} = \sigma_m - \alpha P$. As **Figs. 6-13a** and **6-13b** show, MTS is a function of pressure and temperature such that a significant increase in pressure and/or temperature results in a considerable change in MTS. Over the time interval of 160 to 200 *days*, temperature increases to the maximum which is the indication of fire front in this area. Therefore, both GPM and CPM are effective in this block and cause a significant increase in permeability. However, only GPM influences the permeability of the shale block. This finding can also be concluded from the concentration of the solid components. There is large quantity of solid material by time 170 *days*; however, since combustion and gasification become more active after this time, the effect of CPM on permeability is considerable. Displacement along the z-axis illustrates a periodic subsidence and heave in the location of the coaly block. This is primarily due to the pressure change over time. Moreover, the fluid porosity of the coaly block is a stronger function of the solid content than the geomechanics effect; see **Fig. 6-13b**. However, in the shale grid block, the fluid porosity is only influenced by geomechanics. There is an intermittent decline and increase in the fluid porosity of the shale layers as a result of subsidence and heave, respectively, **Fig. 6-14b**.

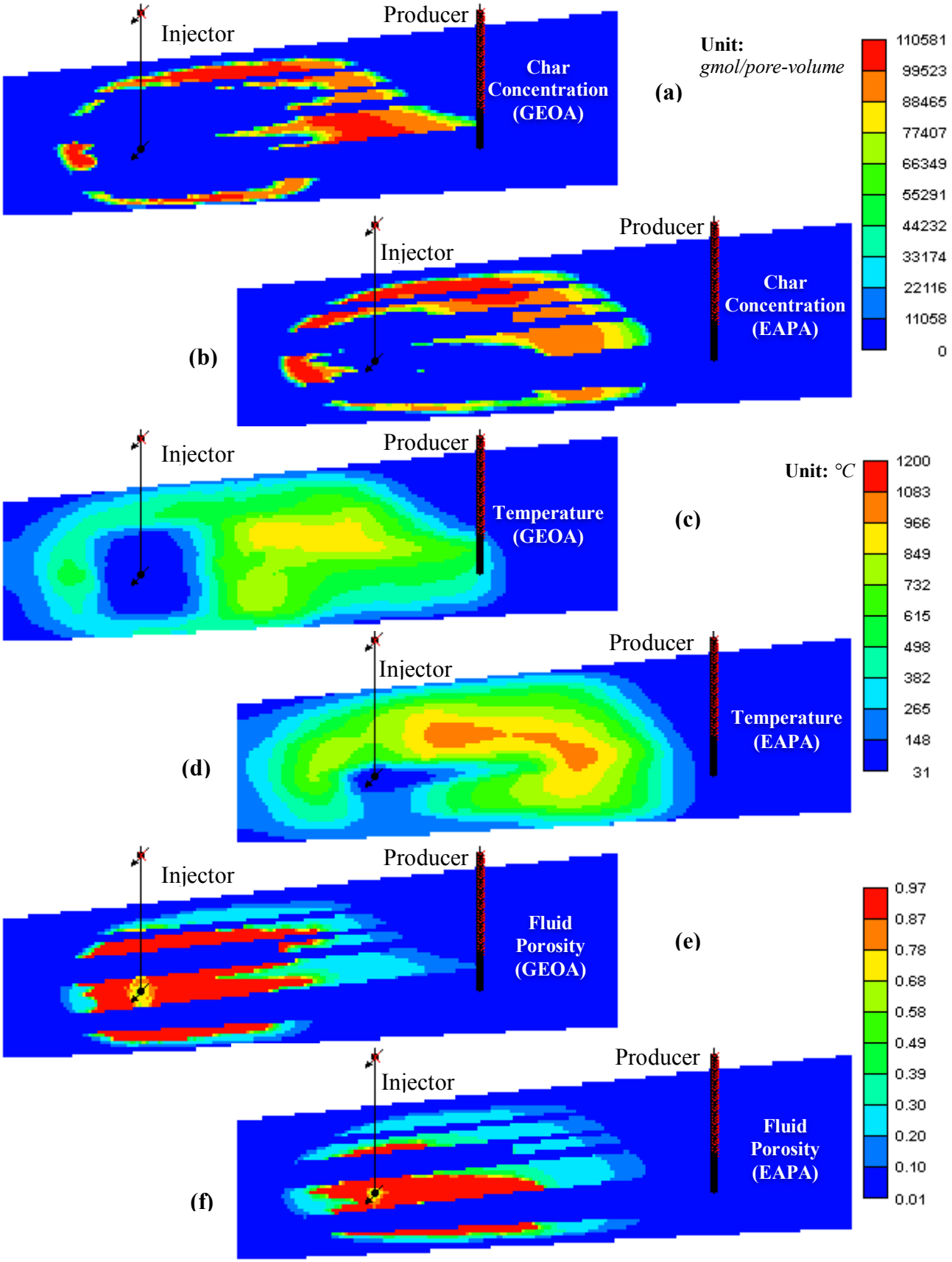

Fig. 6-12: Comparison of coal concentration, temperature, and fluid porosity for geomechanics approach (GEOA) and effective absolute permeability approach (EAPA)

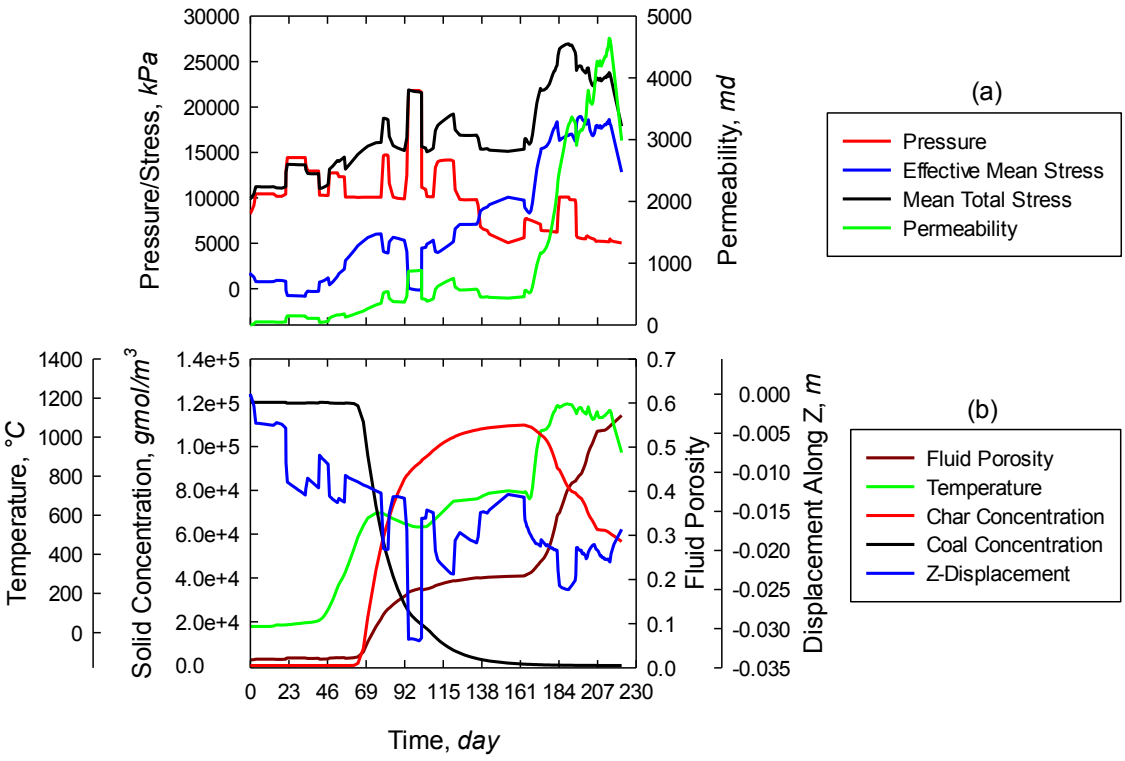

Fig. 6-13: Variation of several parameters with time for a coaly grid block of (83,1,37) using geomechanics approach, (a) pressure, stress, and permeability, and (b) fluid porosity, temperature, solid component concentrations, and displacement along z-axis (subsidence or heave)

Fig. 6-15 is a comparison of the average composition from the simulation model and field results over the entire life of the project. This figure also shows the temperature variation at different locations of the producing interval and the temperature profile between the injection and production points at different times. **Fig. 6-15a** illustrates an engineering match for CH_4, H_2, and N_2 productions. However, CO production is higher and CO_2 amount is lower in the simulation results. The thinness of the cross-sectional model compared to the field dimension means that heat distribution occurs over a smaller region in the simulation than in the field model resulting in increased temperature. As a result, more activity of the Boudouard reaction converts more CO_2 into CO. Although tuning the rate of Boudouard reaction may fix this discrepancy, however, 3D modeling of Thulin test, beyond the scope of this work, can resolve this issue by allowing wider distribution of the generated heat. Furthermore, removal of the linking channel in the simulation model increases the residence time causing O_2 production to decline and a fraction

of CO to be converted into CH_4 through the methane-steam-reforming reaction. This results in increased production of CH_4 in the simulation results. The maximum temperature at the bottom of the producer is approximately 500 °*C* which corresponds to the field measurements, **Fig. 6-15b**, (Kempka 2010). In **Fig. 6-15c**, the injection and production points correspond to the left- and right-hand sides of this figure, respectively. As shown, the temperature around the injection point decreases to the injection temperature, whereas the temperature around the production point increases as the fire front approaches the producer. In this simulation layer (corresponding to the middle of the lower Leopold coal bed), the fire front with a temperature of ~1,150 °*C* is located ~5 m from the injection point.

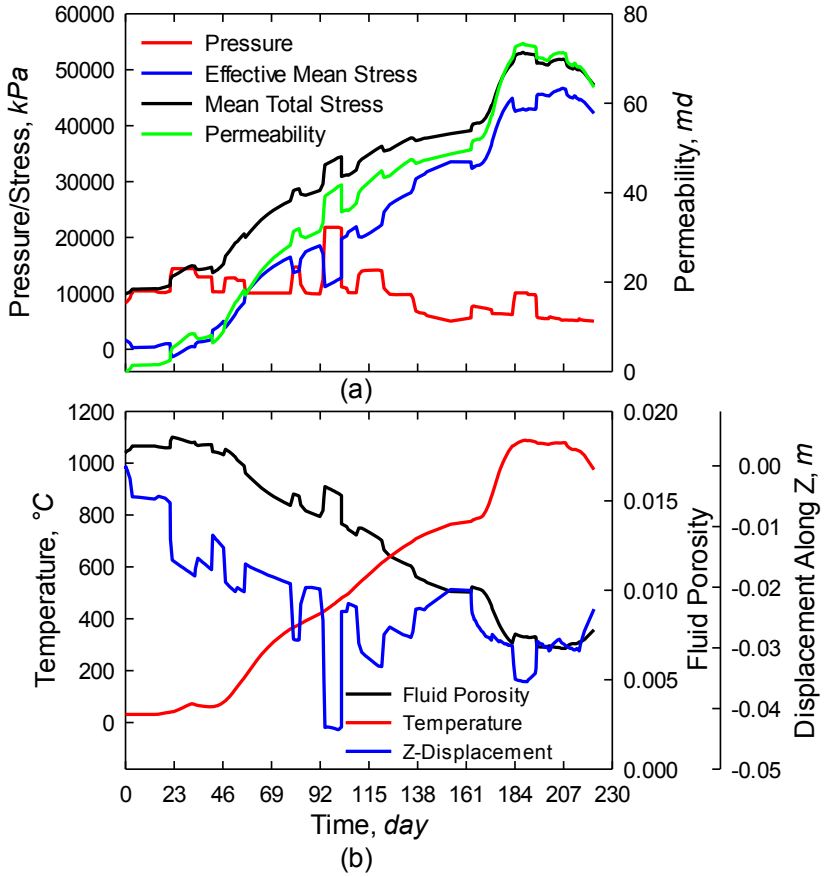

Fig. 6-14: Variation of several parameters with time for a shale grid block of (83,1,32) using geomechanics approach, (a) pressure, stress, and permeability, and (b) fluid porosity, temperature, and displacement along z-axis (subsidence or heave)

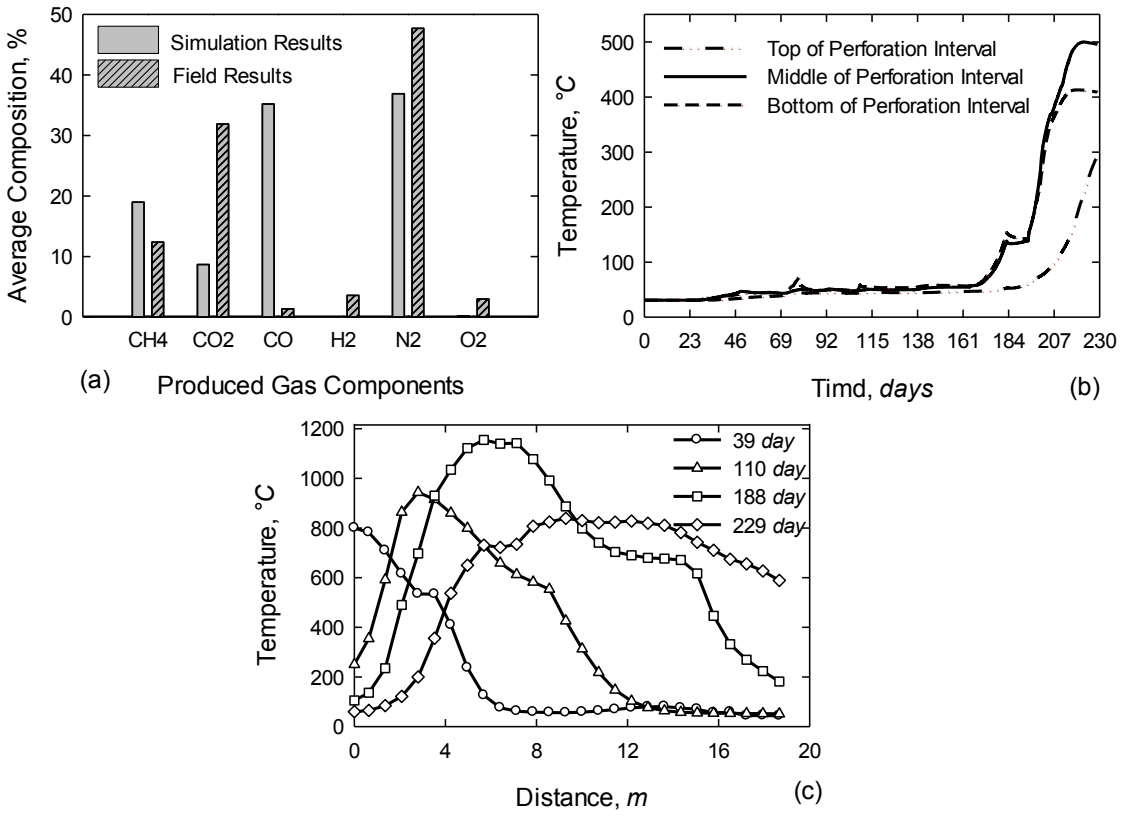

Fig. 6-15: Results of Thulin simulation model, (a) comparison of the average composition of the 2D model and field test during the entire life of project, (b) variation of temperature at different locations of the perforation interval of producer, and (c) temperature profile between injection and production points at different times in the simulation layer corresponding to the middle of the producing interval

6.5 Conclusions

In this study, three important technologies of UCG processes (LVW, L-CRIP, and P-CRIP) were explained in detail and simulation models were conducted to compare their performance for the Ardley coal seam in Alberta, Canada. Comparison and analysis of the simulation results lead to the conclusion that the evolution of the cavity in the P-CRIP technique is mainly around the injection point rather than sweeping the entire region between the two wells. Therefore, we conclude that the P-CRIP method will not increase the volumetric sweep efficiency over the L-CRIP. This could also be due to the lower in-seam module length of the P-CRIP method. Volumetric syngas production of the L-CRIP and P-CRIP were approximately the same, but the

heating value of the P-CRIP produced syngas was larger. Automatic retraction was preferred over manual retraction provided that it is done for both the injection and production points and controlled by the heating value of the produced syngas, temperature, and oxygen mole fraction at the bottom of producer because this is the case in the field test. The LVW may produce high heating value syngas at the early stage. However, after exposing the overburden to the cavity, the heat loss to the surrounding material will reduce the quality of the produced syngas.

Cross-sectional simulation of the Thulin test with tight coal seams was conducted. It was concluded that dual-porosity/dual-permeability fracture modeling should not be used to simulate UCG processes. Since coal seams in a UCG process include significant flammable solid components, fluid porosity and the permeability of the coal layers are strong functions of solid content (the higher the solid content, potentially the more permeability and porosity) rather than the geomechanics effect. However, modeling permeability as a function of fluid porosity is not sufficient to simulate a UCG process with tight coal seams. This is because the fluid porosity increases following the consumption of solid materials, which in turn requires accessibility of the oxidants. As a result, the injection of oxidants and produced hot gases from the pyrolysis process pressurize the domain. Therefore, a pressure-dependent permeability model is crucial so that the permeability can be increased before combustion and gasification takes place. Applying the larger initial absolute permeability model (EAPA) with the permeability-porosity function was successful. Determination of the permeability during the process was the only issue with this model. In this work, geomechanics was used to obtain the stress distribution, which in turn was used to calculate the permeability (an indirect pressure-dependent permeability function, GEOA). The similarity of the results for the EAPA and GEOA methods implies that simple elastic models as material constitutive laws or a simple effective absolute permeability approach can be appropriate for the simulation of UCG processes in tight coal seams. It is also possible to use the variable formation compressibility table or pressure-variable permeability directly in the model instead of geomechanics. Porosity variation as a result of the mechanical behavior of the solid materials may not be significant when compared with the effects of solid component consumption. This is true for the porous medium approach, which uses a continuum domain to model geomechanics. However, for precise prediction of the thermo-mechanical behavior of coal and char in a UCG process (roof spalling and collapsing, and sidewall scratching), a discrete element method is required.

6.6 Nomenclature

A_0 = Frequency factor, *variable unit*

c_{s_i} = Solid component *i* concentration (daf basis), *mol/m³ pore volume*

E_a = Activation energy, *kJ/mol*

$f_{K,C}$ = Chemical permeability multiplier

$f_{K,g}$ = Geomechanical permeability multiplier

C_P = Isothermal compressibility of rock matrix (ash), *1/kPa*

C_T = Isobaric compressibility of rock matrix (ash), *1/°C*

K = Permeability, *md*

K_0 = Initial permeability, *md*

K_{mul} = Permeability variation parameter

K_w = Water component K-value

$k_{v1}, \ldots, k_{v4}$ = Constant values of the K-value correlation

n_s = Number of solid components

P_r = Reference pressure, *kPa*

P_{wf} = Bottom hole pressure of producer, *kPa*

T = Temperature, *K*

T_r = Reference temperature, *K*

Greek Letters

α = Biot's coefficient

σ_m = Mean total stress, *kPa*

σ_m^{eff} = Effective mean total stress, *kPa*

ρ_{s_i} = Solid density of solid component *i*, *kg/m³*

$\emptyset_f$ = Fluid porosity

$\emptyset_f^o$ = Initial fluid porosity

$\emptyset_v$ = Void porosity of the porous medium

$\emptyset_{vr}$ = Reference void porosity

μ_g = Gas phase viscosity, *cp*

Chapter 7 Conclusions and Recommendations

This dissertation focused on the simulation of an UCG process using a hydrocarbon reservoir simulator with a porous medium approach as opposed to the CFD method. Relevant conclusions were presented in detail in each chapter separately; however, the key findings are summarized here followed by a list of recommendations for future study.

7.1 Conclusions

This study explained the process of numerically simulating a UCG process with an existing 3D commercial hydrocarbon simulator. We developed and investigated various numerical models to avoid the use of a complicated CFD model and lowered costs by developing new software. The developed models can be used to investigate a syngas flow rate, gas composition, cavity shape, a cavity evolution rate, a rate of the pyrolysis front, a rate of the fire front, an effect of water influxes, and an application of different UCG technologies.

7.1.1 Analytical Channel Model

We developed an analytical model, which assumed a constant channel diameter between fixed injection and production points at a constant rate for the applied reactions in the model. In spite of this simplification, this model can be used to investigate the effect of several operational parameters on the temperature profile inside the seam as well as the composition of the produced syngas and its heating value. The applied operational parameters can include an injection rate, injection temperature, the distance between injection and production points, a molar ratio of steam to oxygen in the injected material, the kinetics of the reactions at different situations, and the properties of the applied coal, in particular thermal and physical properties. Since all UCG technologies require a linking channel between the injection and production points, this closed-form analytical model can be applied to any UCG technology.

7.1.2 Numerical Models

The main purpose of this study was to adapt a hydrocarbon reservoir simulator to model the UCG process. The major findings are summarized as follows:

- Since porous medium simulators require a rock network consisting of pores and pathways to transport the materials within the domain, it is necessary to separate the ash material for the UCG process and consider them the rock network. Therefore, ash-related phenomena such as the diffusion of gas species through ash material, fusion of ash at temperatures above the fusion temperature, and the catalytic effect of the ash minerals cannot be considered directly in the porous medium approach to UCG simulation.
- Current thermal compositional hydrocarbon simulators do not include turbulent fluid flow and instead apply Darcy's law as the momentum equation to determine fluid velocity. As a result, the porous medium approach is unable to model possible turbulent flow within the void volume of the cavities, especially large cavities.
- The single-step-decomposition approach is the most appropriate method of modeling complex pyrolysis processes in simulation of the UCG process using the porous medium simulators. The simultaneous independent reactions approach requires a large number of components and reactions, which complicates the model and increases the modeling cost.
- The proposed numerical simulation model for the pyrolysis process can be used to estimate the kinetics of the reactions using the simultaneous independent reactions approach by matching with the experimental data. This is important in cases where cracking and carbonate decomposition phenomena are dominant because analytical models do not include these phenomena.
- Viscous force, the main driving force of fluid flow in a hydrocarbon simulator, is varied by a pressure drop and the permeability of a domain. As a result, it is necessary that the difference between the permeability of the linking pathway along the injection and production points and the surrounding zones is not significant. The larger permeability variation between these regions can result in easy transportation of the syngas and/or injected materials through the linking area. This will decrease the residence time and quality of the produced syngas and result in breakthrough of the injected materials, which may extinguish combustion. In most cases, it is preferable to remove the linking channel to avoid these issues. However, this should be decided

according to the injection rate, operating pressures, initial permeability, and applied permeability model.

- As a result of viscous force in the porous medium approach, the cavity is primarily developed around the injection well in the parallel retracting injection point method rather than sweeps the entire area between the injector and producer. This may reduce the sweep efficiency of this technique.
- In general, it is preferable to disregard fracture models such as a dual-porosity/dual-permeability model in UCG process simulation using the porous medium approach over the entire domain. An application of high permeability fractures with low-permeability coal matrix can result in breakthrough of the injected materials and/or reduce the residence time of the in-situ syngas.
- Most of the solid components in a UCG process are flammable or volatile and the fluid porosity of the domain in the UCG simulation relies largely on the solid content of the domain rather than the geomechanical effects. Removal of the solid components in this approach only occurs by heterogeneous reactions. An application of geomechanics in a porous medium model may influence the permeability of the model such as in hydraulic fracturing. However, since a continuum domain is used to model the geomechanics, the precise thermo-mechanical behaviour of the coal and char cannot be predicted using the porous medium approach. This is especially true for cases in which roof spalling and collapsing or sidewall scratching phenomena are dominant.
- The performance of three widely applied technologies, LVW, L-CRIP, and P-CRIP, were compared using 3D field-scale numerical simulation models. The porous medium approach is capable of handling complex geological layering at variable depths and various well configurations, which may be difficult or impossible to model with conventional CFD approaches.
- Having a UCG simulation model prior to pilot design is a crucial step towards increasing knowledge of the behaviour of the domain during the process and the potential quality of the produced syngas. However, in most cases, there is no experimental or practical information on the kinetics of the reactions taking place. This study proposed procedures for obtaining the kinetics of the reactions required by porous medium simulators, using information from surface gasifiers operated at similar

conditions as the UCG process or by observing the behaviour of the developed simulation model. The obtained kinetics are based on fundamental and theoretical concepts so the data set of the model is nearly consistent.

- Since producing large amounts of in-situ syngas during UCG simulation in a tight coal seam causes pressurization of the domain, having a pressure- or stress-dependent permeability model is crucial to increasing the permeability before combustion and gasification take place.

7.2 Recommendations

The following is the list of recommendations for future studies.

- Because ash is treated as a fixed rock structure, it is not possible to directly include the effect of the ash phase on mass transport into a model. The temperature-dependent permeability method can be used to investigate the effect of ash fusion, since fused and condensed ash can act as a barrier to the flow of materials.
- The thermo-mechanical mechanisms of cavity growth including spalling and collapsing of the solid materials cannot be considered in this approach. Coupling the porous medium model with a discrete element geomechanical simulator can compensate for this deficiency by updating the porosity and permeability of the model based on geomechanical properties at each time step.
- Inclusion of a diffusion mechanism in the model may improve the component transportation within and surrounding the cavity. This is important in UCG processes taking place within tight coal seams where viscous flow may not be significant due to lower permeability of the domain.
- Turbulent flow can significantly influence the transportation of the oxidant materials from the injection point to the surface of the cavity. Coupling this type of flow with the conventional Darcy's approach in the porous medium simulators may predict the performance of the UCG process more realistically, particularly in cases with a larger cavity size and void volume.
- Declining quality and heating value of the produced syngas contribute to retraction of the injection and production points during the CRIP techniques. For this reason, the heating value of the produced syngas should be used as the triggering condition for

retracting the injection point during the automatic retraction process. This requires that this capability be added to the porous medium simulators because this situation does not exist in conventional oil and gas.

- The CRIP technique employs a pair of production and injection wells at different phases to gasify the gasification module such that a series of cavities are developed along the injection and/or production wells. However, depending on the size of the evolved cavities, pillars are left among them to support the overburden. We recommend that this situation be modeled using the porous medium approach. This is especially important when the thermo-mechanical properties of the coal are highly temperature-dependent, which may affect the length of the required pillars.
- In this study, the physical and thermal properties of the solid components were assumed constant. Since the UCG process takes place over a wide range of temperatures, we recommend the use of temperature-dependent properties for the solid components, particularly in cases with geomechanical modeling.
- The water component influences the performance of the UCG process in several ways. For example, large amounts of water may extinguish the process, while the right amount can increase the quality of the produced syngas. The water for the in-situ reactions comes from an aquifer, injected water, the surface water of the initial coal, and/or chemical water generated during the pyrolysis process. In this study, water was only from injection and the moisture content of the coal. Further study is suggested to explore the effects of aquifers and the chemical water vapour evolved during pyrolysis on the performance of a UCG process.

References

Bachu A and Burwash R.A. 2008. Geological atlas of the western Canada sedimentary basin-Chapter 30. Alberta Geological Survey, Edmonton.

Batenburg van, D.W. 1992. Heat and mass transfer during underground gasification of thin deep coal seams. *PhD Dissertation*. Delft University of Technology.

Biezen, E.N.J. 1996. Modeling underground coal gasification. *PhD Dissertation*. Delft University of Technology.

Britten, J.A., and Thorsness, C.B. 1988. A mechanistic model for axisymmetric cavity growth during underground coal gasification. *American Chemical Society*.

Bryden, K.M., and Ragland, K.W. 1996. Numerical modeling of a deep, fixed bed combuster. *Energy & Fuels* **10**: 269-275.

Burton, E., Friedmann, J., and Upadhye, R. 2008. Best practices in underground coal gasification. *Lawrence Livermore National Laboratory*.

Campbell, J.H. 1976. Pyrolysis of sub-bituminous coal as it relates to in-situ gasification (Part 1: Gas evolution). University of California, Livermore, California. *UCRL-52035*.

Chandelle, V., Jacquemin, C., Letolle, R., Mostade, M., Pirard, J.P., and Somers, Y. 1993. Underground coal gasification on the Thulin site: results of analysis from post-burn drilling. *Fuel Journal*. **72**: 949-963.

Computer Modeling Group 2009. STARS Technical Manual.

Computer Modeling Group (CMG) 2013. STARS Technical Manual.

Couch, G.R. 2009. Underground coal gasification. http://www.coalonline.info/site/coalonline/content/Viewer/82189/7789/778900001.html/Underground-coal-gasification.

Dean, R.H., Gai, X., Stone, C.M., and Minkoff, S.E. 2003. A comparison of techniques for coupling porous flow and geomechanics. *SPE 79709*.

Dutta, S., and Wen, C.Y. 1977. Reactivity of coal and char. 1. In carbon dioxide atmosphere. *Ind. Eng. Chem*. **16**(1): 103-114.

Fjaer, E., Holt, R.M., Raaen, A.M., Risnes, R., and Horsrud, P. 1992. Petroleum Related Rock Mechanics. Elsevier.

Forrester, R.C.III., Westmoreland, P.R. 1979. Two-dimensional pyrolysis effects during in-situ coal gasification: preliminary results. *J. Pet. Tech*. p. 571.

Furnas, C. 1936. A new method for interpreting reactivity data. *Ind. Eng. Chem*. **28**: 498-502.

Green, D.W., and Willhite, G.P. 1998. Enhanced oil recovery. Richardson, Tex., *Society of Petroleum Engineers*.

Gutierrez, M. 1998. The role of geomechanics in reservoir simulation. SPE 47392.

Herrin, J.M., and Deming, D. 1996. Thermal conductivity of U.S. coals. *Journal of Geophysical Research* **101**.

Hong, L.C. 1984. Process analysis and simulation of underground coal gasification. The University of Texas at Austin. *PhD Dissertation*.

Huq, I. 2012. Scope of work: In-situ coal gasification (ISCG) modeling and simulation. Sherritt International Corporation, Edmonton.

Huq, I. 2013. Scope of work: In-situ coal gasification (ISCG) modeling and simulation. Sherritt International Corporation, Edmonton.

Kempka, T. 2010. The Thulin underground coal gasification field test in Belgium: Summary of resources and gasification data. GFZ German Research Center for Geosciences, Potsdam.

Khadse, A.N., Mahajani, S.M., Qayyumi, M., and Aghalayam, P. 2006. Reactor model for the underground coal gasification (UCG) channel. *Indian Institute of Technology*. Bombay.

Liu, G., Benyon, P., Benfell, K.E., Bryant, G.W., Tate, A.G., Boyd, R.K., Harris, D.J., and Wall, T.F. 2000. The porous structure of bituminous coal chars and its influence on combustion and gasification under chemically controlled conditions. *Fuel Journal* **79**: 617-626

Lowry, H. 1963. Chemistry of Coal Utilization. *John Wiley and Sons Inc.* New York.

Ma, S., Hill, J.O., and Heng, S. 1991. A kinetic analysis of the pyrolysis of some Australian coals by non-isothermal thermogravimetry. *Journal of Thermal Analysis* **37:** 1161-1177.

Magnani, C.F. 1973. Mathematical foundations for the process of underground gasification of coal. *PhD* Dissertation. The Pennsylvania State University.

Massaquoi, J.G.M. 1981. Combustion in underground coal conversion. *PhD Dissertation*. West Virginia University.

Merrick, D. 1983. Mathematical models of the thermal decomposition of coal (1. The evolution of volatile matter). *Fuel Journal* **62**:534.

Monson, C.R., Germane, G.J., Blackham, A.U., and Smoot, L.D. 1995. Char oxidation at elevated pressures. *Combustion and Flame* **100**: 669-683.

Mostade, M. 2012. The Thulin underground coal gasification field test in Belgium: Summary of resources and gasification data. Most Coal Engineering, Liege.

Nourozieh, H., Kariznovi, M., Chen, Z., Abedi, J. 2010 Simulation study of underground coal gasification in Alberta reservoirs: geological structure and process modeling. *Energy Fuels* **24**: 3540-3550.

Parkash, S., Chakrabartty, S.K. 1986. Microporosity in Alberta plains coals. *International Journal of Coal Geology* **6**: 55-70.

Perkins, G. 2005. Mathematical modeling of underground coal gasification. *PhD Dissertation*. The University of New South Wales.

Reid, R.C., Prausnitz, J.M., and Poling, B.E. 1987. The properties of gases and liquids. 4th edition. *McGraw-Hill Inc.*

Richardson, R.J. 2011. Alberta's vast coal resources; an opportunity for very large scale UCG developments. *Presented at 6th International Conference On Underground Coal Gasification*. London, UK.

Richardson, R.J., and CanZealand, P.G. 2010. Alberta's 2 trillion tonnes of unrecognized coal. Alberta Innovates-Energy and Environment Solutions. http:// eipa.alberta.ca / media / 43006 / alberta_2_trillion_tonnes_coal.pdf.

Roberts, D.G., and Harris, D.J. 2000. Char gasification with O_2, CO_2, and H_2O: Effects of pressure on intrinsic reaction kinetics. *Energy & Fuels* **14**: 483-489.

Rubin, B. 2010. Accurate simulation of non-Darcy flow in stimulated fracture shale reservoirs. *SPE* 132093.

Sawyer, W.K., and Shuck, L.Z. 1976. Numerical simulation of mass and energy transfer in the longwall process of underground gasification of coal. *SPE Paper 5743*. *4th Symposium of* Numerical *Simulation of Reservoir*. Los Angeles. Calif.

Seifi, M., Abedi, J., and Chen, Z. 2013. Application of porous medium approach to simulate UCG process. *Fuel Journal* **116**: 191-200.

Seifi, M., Chen, Z., and Abedi, J. 2011. Numerical simulation study of underground coal gasification using the CRIP method. *The Canadian Journal of Chemical Engineering* **89**(6): 1528-1535.

Seifi, M., Chen, Z., and Abedi, J. 2014. Reaction rate constants in UCG simulation using porous medium approach. *Mitigation and Adaptation Strategies for Global Change*. DOI 10.1007/s11027-014-9582-3.

Settari, A., and Mourits, F.M. 1998. A coupled reservoir and geomechanical simulation system. *SPE* 50939.

Shafirovich, E., and Varma, A. 2009. Underground coal gasification: A brief review of current status. *Ind. Eng. Chem. Res.* **48**: 7865-7875.

Shirsat, V.A. 1989. Modeling of cavity growth in underground coal gasification. *MSc. Thesis*. Texas Tech University.

Smith, J.M., Van Ness, H.C., and Abbott, M.M. 2001. Introduction to chemical engineering thermodynamics. 6th edition. *The McGraw-Hill Companies*. New York.

SwanHills Synfuels Report-Final outcomes 2012. http://www.ai-ees.ca/media/6876/swan_hills.pdf.

Thorsness, C.B., and Rozsa, R.B. 1976. In-situ coal gasification: model calculations and laboratory experiments. *SPE Paper 6182. 51st annual fall technical conference and exhibition*. New Orleans. Oct. 3-6.

Tomita, A., Mahajan, O.P., and Walker, P.L.J. 1977. Reactivity of heat-treated coals in hydrogen. *Fuel Journal* **56**: 137-144.

Tran, D., Nghiem, L., Buchanan, L. 2005. An overview of iterative coupling between geomechanical deformation and reservoir flow. *SPE 97879*.

Tran, D., Nghiem, L., and Buchanan, L. 2009. Aspects of coupling between petroleum reservoir flow and geomechanics. *American Rock Mechanics Association* **89**.

Tran, D., Nghiem, L., and Buchanan, L. 2005. Improved iterative coupling of geomechanics with reservoir simulation. *SPE 93244*.

Tran, D., Nghiem, L., and Buchanan, L. 2008. Modeling thermal geomechanical effects on simulation porosity. *American Rock Mechanics Association* **87**.

Tsang, T.H.T. 1980. Modeling of heat and mass transfer during coal block gasification. *PhD Dissertation*. The University of Texas at Austin.

Vargas, J.M., and Perimutter, D.D. 1985. Interpretation of coal pyrolysis kinetics. *Ind. Eng. Chem.* **25**: 49-54.

Warren, J.E., and Root, P.J. 1963. The behavior of naturally fracture reservoirs. *SPE 426*.

Winslow, A.M. 1977. Numerical model of coal gasification in a packed bed. *Symposium (International) on Combustion* **16**: 503-513.

Yang, L. 2004. Study on the model experiment and numerical simulation for underground coal gasification. *Fuel Journal* **83**: 573-584.

Yang, L. 2008. Coal properties and system operating parameters for underground coal gasification. *Energy Sources, Part A* **30**: 516-528.

Yang, L.H. 2005. Numerical study on the underground coal gasification for inclined seams. *AIChE Journal* **51**: 3059-3071.

Yang, L., Liang, J., and Yu, L. 2003. Clean coal technology-Study on the pilot project experiment of underground coal gasification. *Energy* **28**: 1445-1460.

Yonggang, L.U.O., Coertzen, M., and Dumble S. 2009. Comparison of UCG cavity growth with CFD model predictions. *Seventh International Conference on CFD in the Minerals and Process Industries*. Australia: Melbourne: CSIRO. Dec. 9-11.

Appendix A. Copyright Permissions

Permissions

T & F Reference Number: P072514-01

7/25/2014

Mojtaba Seifi
310 Jackson PL NW
Calgary T3B2V3
Canada
mseifi@ucalgary.ca

Dear Mojtaba Seifi:

We are in receipt of your request to reproduce your article

M. Seifi, J. Abedi, Z. Chen (2013)
The Analytical Modeling of Underground Coal Gasification through the Application of a Channel Method
Energy Sources, Part A: Recovery, Utilization, and Environmental Effects 35(18): 1717-1727.

for use in your thesis

This permission is all for editions, both print and electronic.

We will be pleased to grant you permission free of charge on the condition that:

This permission is limited to non-exclusive English rights for this usage only.

This permission does not cover any third party copyrighted work which may appear in the material requested.

Full acknowledgement must be included showing article title, author, and full Journal title, reprinted by permission of Taylor & Francis LLC (http://www.tandfonline.com).

Thank you very much for your interest in Taylor & Francis publications. Should you have any questions or require further assistance, please feel free to contact me directly.

Sincerely,

Mary Ann Muller

Permissions Coordinator

Telephone: 215.606.4334

E-mail: maryann.muller@taylorandfrancis.com

530 Walnut Street, Suite 850, Philadelphia, PA 19106 • Phone: 215-625-8900 • Fax: 215-207-0050
Web: www.tandfonline.com

Title: Numerical simulation of underground coal gasification using the CRIP method

Author: Mojtaba Seifi,Zhangxin Chen,Jalal Abedi

Publication: Canadian Journal of Chemical Engineering

Publisher: John Wiley and Sons

Date: Mar 9, 2011

Order Completed

Thank you very much for your order.

This is a License Agreement between Mojtaba Seifi ("You") and John Wiley and Sons ("John Wiley and Sons"). The license consists of your order details, the terms and conditions provided by John Wiley and Sons, and the payment terms and conditions.

Get the printable license.

License Number	3430600272145
License date	Jul 16, 2014
Licensed content publisher	John Wiley and Sons
Licensed content publication	Canadian Journal of Chemical Engineering
Licensed content title	Numerical simulation of underground coal gasification using the CRIP method
Licensed copyright line	Copyright © 2011 Canadian Society for Chemical Engineering
Licensed content author	Mojtaba Seifi,Zhangxin Chen,Jalal Abedi
Licensed content date	Mar 9, 2011
Start page	1528
End page	1535
Type of use	Dissertation/Thesis
Requestor type	Author of this Wiley article
Format	Print and electronic
Portion	Full article
Will you be translating?	No
Title of your thesis / dissertation	Simulation and Modeling of Underground Coal Gasification Using Porous Medium Approach
Expected completion date	Sep 2014
Expected size (number of pages)	160
Total	0.00 USD

ORDER MORE... CLOSE WINDOW

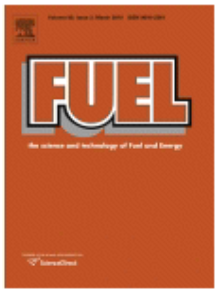

Title: Application of porous medium approach to simulate UCG process

Author: Mojtaba Seifi,Jalal Abedi,Zhangxin Chen

Publication: Fuel

Publisher: Elsevier

Date: 15 January 2014

Order Completed

Thank you very much for your order.

This is a License Agreement between Mojtaba Seifi ("You") and Elsevier ("Elsevier"). The license consists of your order details, the terms and conditions provided by Elsevier, and the payment terms and conditions.

Get the printable license.

License Number	3430590937838
License date	Jul 16, 2014
Licensed content publisher	Elsevier
Licensed content publication	Fuel
Licensed content title	Application of porous medium approach to simulate UCG process
Licensed content author	Mojtaba Seifi,Jalal Abedi,Zhangxin Chen
Licensed content date	15 January 2014
Licensed content volume number	116
Number of pages	10
Type of Use	reuse in a thesis/dissertation
Portion	full article
Format	both print and electronic
Are you the author of this Elsevier article?	Yes
Will you be translating?	No
Title of your thesis/dissertation	Simulation and Modeling of Underground Coal Gasification Using Porous Medium Approach
Expected completion date	Sep 2014
Estimated size (number of pages)	160
Elsevier VAT number	GB 494 6272 12
Permissions price	0.00 USD
VAT/Local Sales Tax	0.00 USD / 0.00 GBP
Total	0.00 USD

ORDER MORE... CLOSE WINDOW

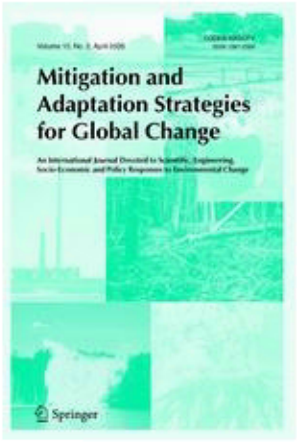

Title: Reaction rate constants in simulation of underground coal gasification using porous medium approach

Author: Mojtaba Seifi

Publication: Mitigation & Adaptation Strategies for Global Change

Publisher: Springer

Date: Jan 1, 2014

Order Completed

Thank you very much for your order.

This is a License Agreement between Mojtaba Seifi ("You") and Springer ("Springer"). The license consists of your order details, the terms and conditions provided by Springer, and the payment terms and conditions.

Get the printable license.

License Number	3430600570501
License date	Jul 16, 2014
Licensed content publisher	Springer
Licensed content publication	Mitigation & Adaptation Strategies for Global Change
Licensed content title	Reaction rate constants in simulation of underground coal gasification using porous medium approach
Licensed content author	Mojtaba Seifi
Licensed content date	Jan 1, 2014
Type of Use	Thesis/Dissertation
Portion	Full text
Number of copies	1
Author of this Springer article	Yes and you are the sole author of the new work
Title of your thesis / dissertation	Simulation and Modeling of Underground Coal Gasification Using Porous Medium Approach
Expected completion date	Sep 2014
Estimated size(pages)	160
Total	0.00 USD

CLOSE WINDOW

RE: Article Permission

Wiley Global Permissions [permissions@wiley.com]
Sent: Wednesday, September 17, 2014 2:20 AM
To: Mojtaba Seifi

Dear Mojtaba,

Thank you for your request.

Permission is granted for you to use the material requested for your thesis/dissertation subject to the usual acknowledgements (author, title of material, title of book/journal, ourselves as publisher) and on the understanding that you will reapply for permission if you wish to distribute or publish your thesis/dissertation commercially.

You should also duplicate the copyright notice that appears in the Wiley publication in your use of the Material. Permission is granted solely for use in conjunction with the thesis, and the material may not be posted online separately.

Any third party material is expressly excluded from this permission. If any material appears within the article with credit to another source, authorisation from that source must be obtained.

Kind Regards

Brian Collins | Permissions Assistant
John Wiley & Sons Ltd, The Atrium, Southern Gate, Chichester, West Sussex, PO19 8SQ

WILEY

From: Mojtaba Seifi [mailto:mseifi@ucalgary.ca]
Sent: 15 September 2014 22:52
To: Wiley Global Permissions
Subject: Article Permission

Dear Sir/Madam,

I submitted a paper titled as "Large Scale Simulation of UCG Process Applying Porous Medium Approach" with manuscript ID of CJCE-14-0521.R1.
I would like to have a permission to include this paper in my thesis.
Since it has not published yet, but accepted, I was not able to follow the copyright permission procedure online.
Your help is highly appreciated.

Regards,

-
Mojtaba Seifi